ERROR ANALYSIS AND OPTIMAL POSE SELECTION FOR *IN-SITU* FABRICATION OF MECHANISMS

A DISSERTATION
SUBMITTED TO THE DEPARTMENT OF MECHANICAL ENGINEERING
AND THE COMMITTEE ON GRADUATE STUDIES
OF STANFORD UNIVERSITY
IN PARTIAL FULFILLMENT OF THE REQUIREMENTS
FOR THE DEGREE OF
DOCTOR OF PHILOSOPHY

By
Sanjay Rajagopalan
May 2000

I certify that I have read this dissertation and that in my opinion it is fully adequate, in scope and quality, as a dissertation for the degree of Doctor of Philosophy.

Mark R. Cutkosky
(Principal Adviser)

I certify that I have read this dissertation and that in my opinion it is fully adequate, in scope and quality, as a dissertation for the degree of Doctor of Philosophy.

Friedrich B. Prinz

I certify that I have read this dissertation and that in my opinion it is fully adequate, in scope and quality, as a dissertation for the degree of Doctor of Philosophy.

Kosuke Ishii

Approved for the University Committee on Graduate Studies:

Abstract

The last decade of the millennium has seen the widespread adoption of a new "freeform" fabrication technique. Called by various names (Rapid Prototyping, Layered Manufacturing, Solid Freeform Fabrication etc.), this technology builds a part directly from its digital (CAD) representation by "slicing" the part model, and building it incrementally by selectively adding and removing material.

As an indicator of industry adoption of what, till recently, was a highly experimental technology - it has been reported that the unit sales of Rapid Prototyping (RP) equipment has increased ten-fold in the last decade. This ten-fold increase in annual sales is still small compared to its future potential, especially as new materials and capabilities are delivered with higher resolution, at a lower price. Combined with this are the parallel advances in meso-scale and micro-electomechanical system (MEMS) fabrication. It is clear today that highly integrated and finely crafted consumer devices, made with modern, high-performance materials and integrated electronics, are no longer the stuff of science-fiction, but of everyday reality. Of particular interest to the author of this thesis is the capability of these techniques to produce assemblies (i.e. parts with mating and fitting components), without requiring an explicit assembly step in the process. Within the context of the thesis, this is referred to as *in-situ* fabrication.

This thesis contributes to the growing innovations within the manufacturing and product design community by taking a new step. The goal of this research it to create a better understanding of the manner in which manufacturing errors affect the performance of mechanical devices fabricated *in-situ*. Another major motivation for this work is to inform design-support tools that feed back information to the fabrication process, enhancing manufacturability, and improving performance accuracy of mechanical devices built using the new techniques. A natural question in this regard is - is there a preferred configuration, or *pose*, in which the device should be

built in order to minimize errors? The problems of error analysis and optimal pose selection in mechanisms slated for *in-situ* fabrication are formulated and solved.

Acknowledgements

I gratefully acknowledge my advisor, Prof. Mark Cutkosky at the Stanford Center for Design Research. It was he who started me off on my doctoral journey by responding (within minutes of my sending it) to an exploratory e-mail asking if he would support me in my application to Stanford. His response was brief and to-the-point - "Your background is interesting. Call me anytime." Thank you, Mark, for picking me out from the sea of hopeful applicants, and supporting me - intellectually and financially - at every step along the way.

I would also like to acknowledge Prof. Fritz Prinz for valuable guidance and discussions about the Shape Deposition Manufacturing process, Prof. Kos Ishii and Prof. Bernard Roth for their insightful comments and suggestions on my research, Puneet Goel, Roger Goldman, Vinod Kumar, Prof. S. K. Gupta, Prof. Deba Dutta, Paul Losleben, Miguel Pinilla, Ki-Hoon Shin and Qi Tian - all of whom co-authored research papers with me, and all students and staff at the Center for Design Research and the Rapid Prototyping Laboratory at Stanford. I am also greatly indebted to the Alliance for Innovative Manufacturing at Stanford and the National Science Foundation for providing financial assistance for portions of this work.

Finally, I would like to thank my parents, my brother and all my friends - both at Stanford and outside, for providing the emotional support that helped me complete this work while living 7701 miles away from my hometown. I dedicate this thesis to all of you.

Contents

List of Tables

List of Figures

Chapter 1

Introduction

1.1 Motivation

The last decade of the millennium (1990 - 2000) has seen the widespread adoption of a new "freeform" fabrication technique. Called by various names (Rapid Prototyping, Layered Manufacturing, Solid Freeform Fabrication etc.), this technology builds a part directly from its digital (CAD) representation by "slicing" the part model, and building it incrementally by selectively adding and removing material (Beaman, 1997) (Chua and Fai, 1997) (Merz *et al*, 1994).

As an indicator of industry adoption of what, till recently, was a highly experimental technology - it has been reported (Wohlers, 1999) that the unit sales of Rapid Prototyping (RP) equipment has increased from less than 100 per year in the early 1990s to close to 1000 annually by the year 2000. This ten-fold increase in annual sales is still small compared to its future potential, especially as new materials and capabilities are delivered with higher resolution, at a lower price. Combined with this are the parallel advances in meso-scale (Stampfl *et al*, 1999) and micro-electomechanical system, or MEMS, (Maluf, 2000) (Kovacs, 1998) fabrication. It is clear today that highly integrated and finely crafted consumer devices, made with modern, high-performance materials and integrated electronics, are no longer the stuff of science-fiction, but of everyday reality. Of particular interest to the author of this thesis is the capability of these techniques to produce assemblies (i.e. parts with mating and fitting components), without requiring explicit assembly. Within the context of the thesis, this is referred to as *in-situ* fabrication. In conventional fabrication, each component of a device is individually fabricated and then assembled

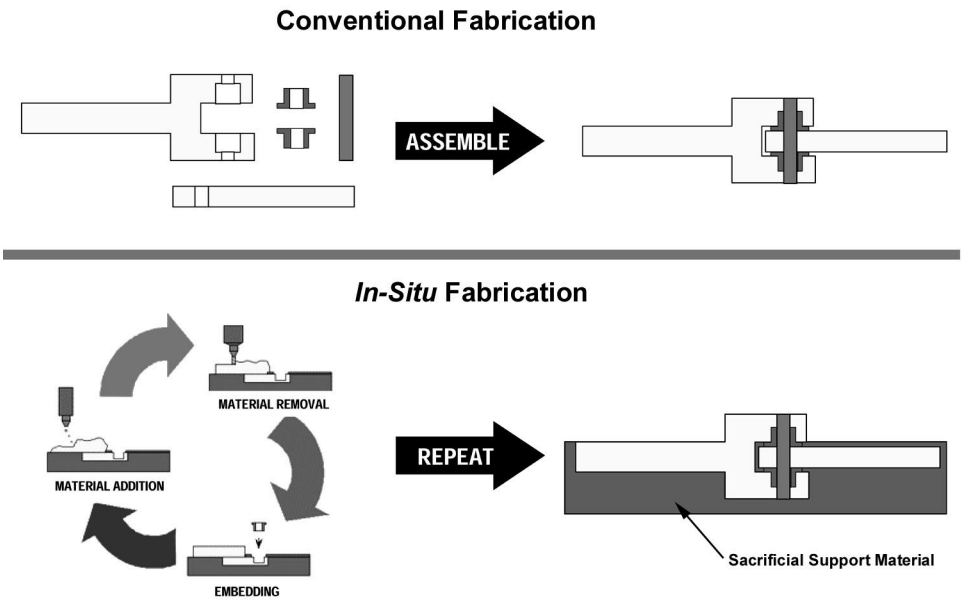

Figure 1.1: Conventional and *in-situ* fabrication.

together. A key characteristic of the *in-situ* process is that no subsequent assembly step is required after fabrication to obtain a working device (see Figure 1.1). The device is built encapsulated in a sacrificial support material. This support material is removed (by etching, melting, or dissolving it away) to yield the final part with operational mating and fitting features.

This thesis contributes to the growing innovations within the manufacturing and product design community by taking a new step. The goal of this research it to create a better understanding of the manner in which manufacturing errors affect the performance of mechanical devices fabricated *in-situ*. Another major motivation for this work is to inform design-support tools that feed back information to the fabrication process, enhancing manufacturability, and improving performance accuracy of mechanical devices built using the new techniques. A natural question in this regard is - is there a preferred configuration, or *pose*, in which the device should be built in order to minimize errors? The problems of error analysis and optimal pose selection in mechanisms slated for *in-situ* fabrication are formulated and solved.

1.2 Scope Of The Thesis

Freeform fabrication techniques are capable of producing a variety of innovative products including, for example, those with complex internal geometry, heterogeneous materials (Rajagoplan *et al*, 2000) and embedded electronics (Weiss *et al*, 1996). This thesis is restricted to the study of general (i.e. planar or spatial, open-chain or multi-loop) mechanisms, fabricated using freeform techniques.

Mechanisms are important sub-components of many devices in widespread use today. Examples can be found in automobiles, robots, aircraft, satellites, micromachines and many other mechanical and electro-mechanical products. Applications range from the mundane (e.g. table-lamps, staplers, switches and relays) to exotic and cutting-edge devices (e.g. robot hands, force-feedback displays, satellite solar panels, and high speed cameras). Sensors, actuators and sophisticated electronics are increasingly being integrated into mechanisms to produce complex "mechatronic" systems. Design and prototype-fabrication of mechanisms that perform pre-determined tasks within specified performance limits (e.g. connecting points in space, path following, function generation etc.) is a scenario that likely confronts every mechanical designer at some point. Performance requirements are also being stretched to unprecedented levels, as speed and desired accuracy of the tasks being performed continue to increase - even as allocated product development budgets and design cycle-times shrink. Consequently, development of scientific methods and analytical tools that inform the design and fabrication of accurate, robust and cost-effective mechanical devices is a challenge that has drawn a fair amount of interest in both academia and industry.

Fabrication of precise mechanism prototypes can be a complex, time-consuming and sometimes, frustrating task. It is believed that Charles Babbage's mechanical computing engine, a good example of a complex spatial mechanism, failed mainly because of the inability of its fabricators to avoid accumulated component dimensional errors in the 1800s (Morrison and Morrison, 1961). Students that have taken classes in the kinematic synthesis of mechanisms are familiar with the many difficulties experienced in fabricating even simple planar mechanisms. The problems typically occur due to inaccuracies in mechanism dimensions, poor joints, out-of-plane flexibility in links and assembly issues. These problems are further exacerbated during the construction of spatial mechanism prototypes. The integration of sensing and actuating elements into the mechanism adds another level of complexity - involving connectors

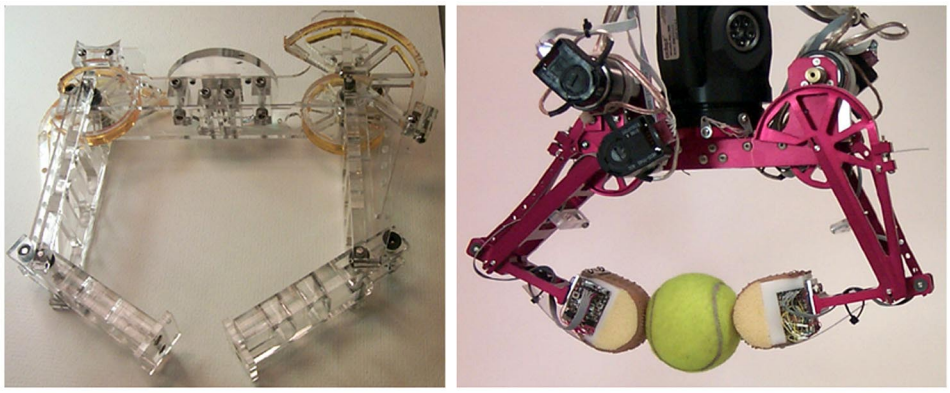

(a) Dextrous robot-hand mechanism protoyped in acrylic using conventional fabrication techniques

(b) Robot-hand operational prototype, outfitted with sensors, actuators and control electronics

Figure 1.2: A robot end-effector built using conventional prototyping and fabrication techniques, courtesy: Weston Griffin, DML, Stanford University.

and fasteners, power transmission components, wires, pneumatic hose etc. Figure 1.2 shows an example of a mechanism (a dextrous robot hand) designed, prototyped and fabricated using conventional manufacturing methods. The machining and assembly of this device took several weeks of work by a graduate student at Stanford's Dextrous Manipulation Lab.

The advent of Solid Freeform Fabrication (SFF) could revolutionize the manner in which mechanisms are prototyped and fabricated (Cham *et al*, 1999) (Weiss *et al*, 1996). *In-situ* technology allows for precision components, sensors, actuators and electronics to be directly integrated into the mechanism frame during fabrication (rather than being sequentially assembled into the mechanism). Figure 1.3 shows examples of such mechanisms recently fabricated at the Center for Design Research, and the Rapid Prototyping Laboratory at Stanford University. Most of these devices have been fabricated in under a week. Similar devices have also been seen in the realm of micromechanical systems and meso-scale manufacturing, which enable similar devices are different size-scales (see Figure 1.4).

1.3 Research Contributions

In this thesis, a general method for the error analysis and optimal pose selection for mechanisms that are fabricated *in-situ* has been developed. Conventional methods

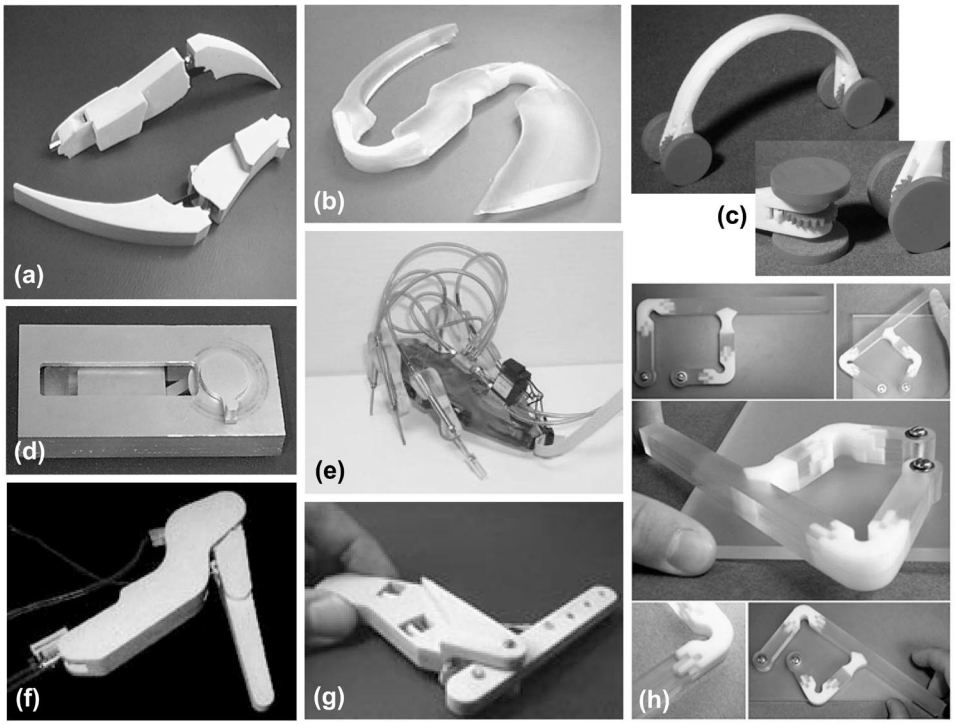

Figure 1.3: *In-situ* mechanism prototypes fabricated at Stanford University. (a) A polymer insect-leg prototype with embedded pneumatic actuator, pressure sensor and leaf-spring joint, (b) A polymer insect-leg prototype with complex surface geometry and flexible joints, (c) An "inchworm" mechanism, with integrated clutch components, (d) A slider-crank mechanism made from stainless steel, (e) A biomimetic robot with integrated sensors, actuators and electronics, (f) A polymer linkage with embedded high-precision joint and displacement sensor, (g) Another polymer linkage with embedded joint and micro-motor actuators, (h) A multi-material 5-bar insect leg prototype with graded material transition regions. Images courtesy: Fritz Prinz, Jorge Cham, Roger Goldman, Alexander Cooper, Mike Binnard, Shawn Bailey, Stanford University.

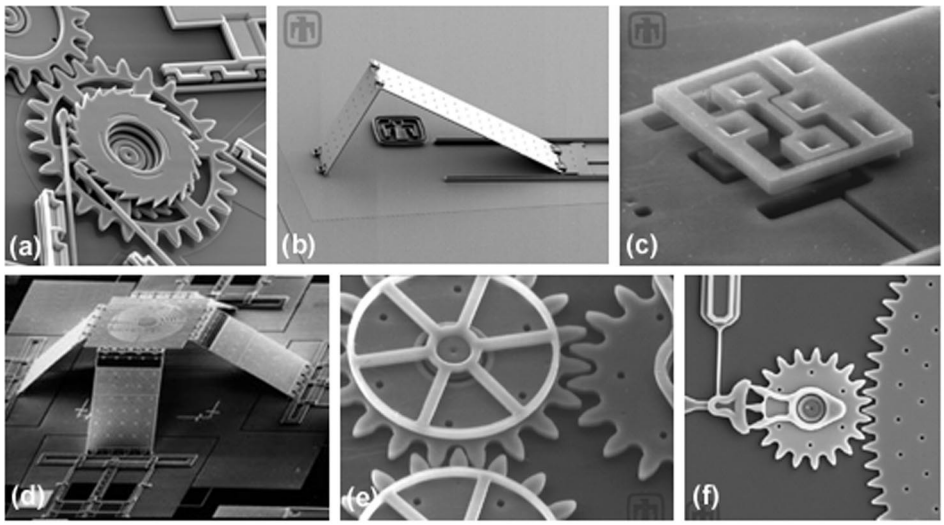

Figure 1.4: Smaller scale mechanisms and devices built using *in-situ* fabrication techniques, Courtesy: Sandia National Laboratories Intelligent Micromachine Initiative, www.mems.sandia.gov. Used with permission.

for analyzing the effects of manufacturing variations on mechanism performance are found to be either inadequate or inappropriate for *in-situ* fabrication (Chapter 3). The problem of finding the best configuration (or *pose*) in which a mechanism should be fabricated to minimize the effects of manufacturing error is also addressed (Chapter 4). The primary accomplishments of this thesis are summarized in the following sections.

1.3.1 Contributions To *In-Situ* Fabrication

- **Developed a systematic method for *in-situ* error analysis:** Conventional error analysis techniques have been extensively reviewed. The fundamental issues that make *in-situ* error analysis different from conventional approaches have been identified. Existing models have been modified or extended to address the new concerns. A concise notation and mathematical framework have been put together to assist with the systematic analysis. In addition, an intuitive understanding of the issues involved has been developed.

- **Demonstrated the application of the developed technique to the error analysis of general planar and spatial mechanisms:** The theoretical results have been illustrated using a planar 4-bar path-generating example.

The results have been validated using Monte Carlo simulation. The relevant equations for a general spatial mechanisms have been derived.

- **Developed a systematic method for reasoning about the optimal pose for the *in-situ* fabrication of mechanisms:** The optimal pose problem has been formalized. Links with the prior error analysis results have been clearly established. An intuitive understanding of the underlying drivers that yield the optimal result has been developed.

- **Demonstrated the application of the optimal pose selection methodology to a specific planar mechanism:** The solution of the optimization problem has been illustrated using a planar 4-bar path-generating mechanism.

1.3.2 Contributions To General Error Analysis

- **Provided the basis for error reasoning in the presence of correlated and dependent error factors:** The generic components of this analysis have been clearly identified.

- **Identified future directions and applications of the developed methodology in a broader context:** Alternate problems in which the results can be applied have been posed and methods for tackling the problems have been discussed. Pathways for future extensions to this work have been identified.

1.4 Document Overview

The next chapter (Chapter 2) reviews basic concepts and background literature for mechanism analysis, tolerance representation, and solid freeform fabrication. Chapter 3 is concerned with error-analysis in mechanisms. A comprehensive methodology for (deterministic or stochastic) error estimation for *in-situ* fabricated mechanisms (in general, planar or spatial, open- or closed-chain mechanisms with revolute, spherical and prismatic joints) in the presence of manufacturing variations and joint clearances is presented. Chapter 4 develops the concept of optimal build-pose selection for these mechanisms, given non-homogeneous, non-isotropic manufacturing precision, and desired performance objectives. A summary of this work, along with ideas

Symbol	Definition
C_p	process capability index
U, L	upper and lower specification tolerances
σ	process standard deviation

Table 1.1: Chapter 2 Nomenclature.

Symbol	Definition
m	number of outputs
n	number of parameters
k	number of independent driving inputs
$\mathbf{y}$	$(m \times 1)$ vector of kinematic outputs
y_i	the i^{th} output in $\mathbf{y}$
Θ	$(k \times 1)$ vector of independent driving inputs
Φ	$(n \times 1)$ vector of mechanism parameters
ϕ_i	the i^{th} parameter in Φ
$f(.)$	kinematic function
Φ^{nom}	nominal values of the parameters Φ
ϕ_i^{nom}	nominal value of the parameter ϕ_i
$\Delta_{\mathbf{y}}$	vector of output errors
Δ_{Φ}	vector of parametric variabilities
Δ_{ϕ_i}	variability of the i^{th} parameter

Table 1.2: Chapter 3 Nomenclature.

for future directions for this work concludes this thesis in Chapter 5. References and appendices are attached after the concluding chapter.

1.5 Nomenclature

For convenience of reference, the nomenclature (see Tables 1.1, 1.2, 1.3, 1.4, 1.5 and 1.6) for this thesis has been arranged largely in order of its appearance in the text. An attempt has been made to use unique, conventional and intuitive symbols as far as possible. However, some repetition was unavoidable. A symbol once defined, typically holds for the remaining portion of the thesis. In the case of repeated usage, the most recent prior definition holds.

Symbol	Definition
$\Delta_{\mathbf{y}}^{max}$	maximum permissible output error
$\phi_i^{min}, \phi_i^{max}$	worst-case values of ϕ_i
$p_{\Phi_i}(\phi_i)$	PDF of the random parameter ϕ_i
$P_{Y_i}(y_i)$	CDF of the output y_i
$\mu_{\phi_i}, \sigma_{\phi_i}^2$	mean and variance of the parameter ϕ_i
a	$f(.)$ evaluated at the mean values μ_{ϕ_i}
$\mu_{\mathbf{y}}, \sigma_{\mathbf{y}}^2$	mean and variance of the output
θ_i	link angle in the Denavit-Hartenberg (DH) representation
a_i	link length in the D-H representation
d_i	link offset in the D-H representation
α_i	skew angle in the D-H representation
l_i	additional offset in the modified D-H representation
$\mathbf{p}_i$	position vector for the i^{th} joint frame
$\mathbf{z}_i$	orientation vector for thei^{th} joint axis
$\mathbf{p}_i^{WC}, \mathbf{z}_i^{WC}$	worst-case position and orientation for the i^{th} joint
$\mathbf{Q}_i, \mathbf{Q}_i'$	Plücker coordinates for the i^{th} joint axis
$\mathbf{Q}_{ij}, \mathbf{Q}_{ij}'$	Plücker coordinates for the i^{th} common normal
$\mathcal{C}^{nom}$	nominal configuration of a mechanism
$\mathcal{C}_b$	candidate build pose for a mechanism
$\mathcal{R}$	variability region for the i^{th} joint location
$\tau(.)$	precision function
x_i	the i^{th} joint location variable
$\mu_{x_i}, \sigma_{x_i}^2$	mean and variance of the i^{th} joint location variable
ρ_{ij}	correlation coefficient for the parameter pair (ϕ_i, ϕ_j)
$\mathbf{A}_k^j$	homogeneous transform matrix between j^{th} and k^{th} frames
$\mathcal{T}(.)$	homogeneous translation matrix
$\mathcal{R}(.)$	homogeneous rotation matrix
d	shaft diameter for a pin-joint
D	flange diameter for a pin-joint
L	hole height for a pin-joint
Δ_a	axial clearance for a pin-joint
Δ_d	diametral clearance for a pin-joint
δ_{max}	maximum allowable task position variability
l_{CA}	distance from nominal center to the task location

Table 1.3: Chapter 3 Nomenclature contd.

Symbol	Definition
$\lambda_k^b(.)$	k^{th} kinematic loop equation for $\mathcal{C}_b$
θ_b	value of independent driving variables at $\mathcal{C}_b$
$\theta_b^\star$	optimal values of driving variables
D_{max}, D_{min}	extremal distances between two regions
Δ_{min}	difference between the extremal distances
$s_{\theta x}, g_{\theta x}$	general transformations operating on regions
S_θ	rigid body rotation matrix

Table 1.4: Chapter 4 Nomenclature.

Symbol	Definition
Δ_d	desired bearing clearance for a pin-joint
$\epsilon_H^{size}, \epsilon_S^{size}$	best achievable hole and shaft size precision
ϵ_C^{size}	best achievable circular feature size precision
$\varphi_S^{nom}, \varphi_H^{nom}$	nominal shaft and hole diameters
$\varphi_H^{min}, \varphi_S^{max}$	MMC sizes for hole and shaft
d_S^{nom}	nominal shaft location
$\epsilon_S^{loc}, \epsilon_H^{loc}$	shaft and hole location precision
$\varphi_H^{max}, \varphi_S^{min}$	LMC sizes for hole and shaft
$\Delta_{max}, \Delta_{min}$	maximum and minimum clearance sizes

Table 1.5: Appendix B Nomenclature.

Symbol	Definition
i	fundamental tolerance unit in thousandth of an inch
D	manufacturing feature size in inches

Table 1.6: Appendix C Nomenclature.

Chapter 2

Background

This chapter deals with some of the background concepts that set the stage for ideas and arguments presented later in the thesis. The material presented is not comprehensive, and the intent is to briefly review the most salient components from the perspective of this thesis. The interested reader is referred to other texts and research publications at the appropriate points.

2.1 Mechanisms

2.1.1 Representation and Kinematic Analysis

As with any complex system, concise representation of mechanisms precedes their systematic analysis. This calls for the development of a convenient abstraction for the mechanism, which preserves all the relevant information, and discards the irrelevant or insignificant. For the general kinematic analysis of rigid mechanisms with lower pairs only, the information that is relevant is limited to the *type*, the *connectivity*, and nominal *positions and orientations*, of all the kinematic pairs of the mechanism. In other words, for most geometric analysis of mechanisms with simple pairs, the type and relative positions of joints completely specifies the mechanism. This is an important observation in the context of this thesis - which shall be explored in more detail later (see Section 3.3.1). Given this information about the joints, it is possible to derive the values of certain independent parameters (e.g. link lengths and joint angles), which simplify the analytical formulations. In most cases, the (fixed) mechanism parameters and driving variables are assumed specified, and the

behavior of some output quantities of interest (e.g. coupler point position, velocity and acceleration) are studied. The algebraic equations that relate output position to mechanism parameters and driving variables are, in general, highly nonlinear. The (instantaneous) velocity and acceleration equations, on the other hand, are linear.

Error analysis of mechanisms is closely related to the velocity and acceleration analysis procedure (see Section 3.2.1). Kinematic analysis of general planar and spatial mechanisms is a widely studied topic, and several textbooks deal with the subject (Shigley, 1959) (Bottema and Roth, 1979) (Shigley and Uicker, 1995).

2.1.2 Performance of Mechanisms

Real mechanisms do not behave in a manner identical to their idealized abstractions. All fabrication processes are inherently inaccurate, necessarily resulting in non-ideal parts. Errors in manufactured geometry could have a multitude of contributing factors - machine-tool precision, workpiece compliance, material properties, thermal stresses, etc. It is not physically possible to control for all of them, or control any of them absolutely.

However, it is important to realize that not all manufacturing errors need contribute towards degrading a mechanism's intended behavior. Said differently, manufacturing errors can always be *tolerated* within limits. The issue that arises next is how the intended behavior of a mechanical object can be unambiguously specified. One possible method is for designers of mechanisms to specify limits on the geometric variability of the mechanism components (see Section 2.3.2). Researchers have also developed formal languages by which designers can directly specify mechanical devices in terms of intended behavior rather than by limits on geometric variability (Joskowicz and Neville, 1996). Eventually however, manufacturing processes can only be concerned with parameters that are observable and controllable during fabrication. Thus, it is important that any behavioral specifications be eventually translated to geometric tolerances on the measured dimensions of the workpiece. Examples of behavioral specifications on mechanisms are desired end-effector accuracy at a finite number of positions, nominal path to be followed by an end-effector along with maximum allowable variation from the path-profile, higher-order (i.e. velocity/acceleration) properties at a design point, etc.

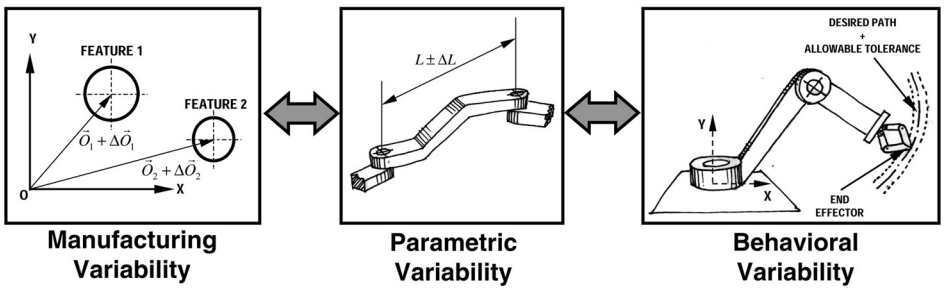

Figure 2.1: Relating behavioral specifications to the manufacturing variability.

In this thesis, the relationship between behavioral specification and manufacturing variability is studied in two stages. The first is mapping of behavioral specifications to specifications on the variability of the mechanism configuration parameters (i.e. link lengths, joint angles etc.). The second is the mapping of parametric variability to the accuracy of the manufacturing environment. Figure 2.1 illustrates this concept. Here, we make the assumptions that manufacturing variability has already been characterized, the output performance parameters are clearly defined (see Equation 3.1), and that the objective is to study the performance errors that result.

2.2 *In-Situ* Fabrication Techniques

We refer to the process of building any device with mating and fitting components, using a combination of additive/subtractive fabrication and part-embedding, as *in-situ* fabrication. The defining characteriztic of the *in-situ* process is that there is no component assembly phase of the process. Figure 2.2 compares the process flow diagrams of conventional and *in-situ* manufacturing practices. This section describes two recently developed fabrication technologies that are capable of *in-situ* fabrication of mechanisms - Solid Freeform Fabrication (SFF) and Micromachining.

2.2.1 Solid Freeform Fabrication

Solid Freeform Fabrication (SFF) is the name given to a family of recent fabrication techniques that first decompose the CAD models of parts into simple features (e.g. planar layers), and then build the part one decomposed feature at a time. It is also variously called Layered Manufacturing (LM), or Rapid Prototyping (RP). This

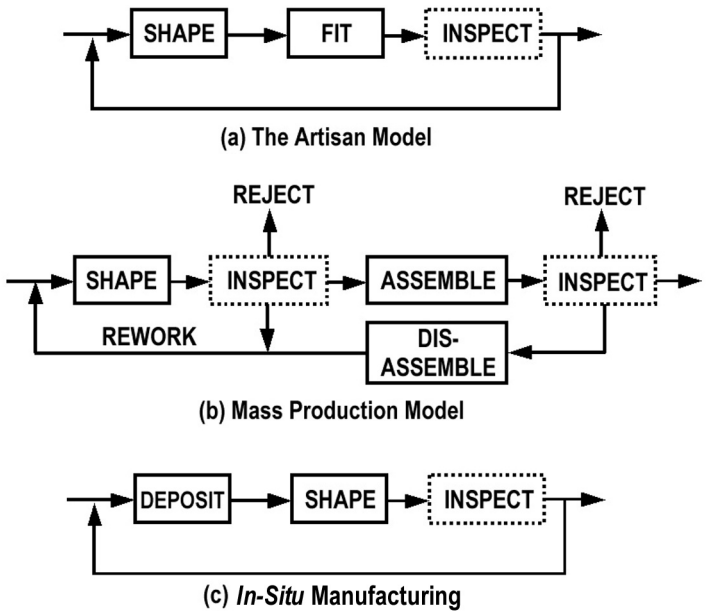

Figure 2.2: Comparing conventional and *in-situ* maufacturing methods - process flow chart.

type of fabrication is usually assumed to produce macro-scale parts (i.e. feature sizes larger than 1 cm), though mesoscopic parts (feature size from 1 mm to 1 cm) have also been demonstrated recently (Stampfl *et al*, 1999). The process is a cycle of material deposition (or part embedding), and optional material shaping. Several variants of SFF processes exist in the commercial (e.g. Stereolithography, Selective Laser Sintering, Laminated Object Manufacturing) as well as research arenas (e.g. Shape Deposition Manufacturing, 3D Printing (Merz *et al*, 1994) (Sachs, 1992)).

There are several benefits associated with SFF. Most importantly, decomposition significantly reduces the planning complexity associated with global feature interactions, which have been the bane of conventional CNC manufacturing (Gadh and Prinz, 1995). Most commercial SFF processes are "feature-blind" (i.e. they operate on purely geometric entities like lines and curves, and are blind to the existence of design features like joints, shafts, bearing-surfaces etc.). This characteristic is very attractive from the process automation point-of-view, and several efforts are underway to fully automate the interface to this technology (Sequin, 1994) (Rajagopalan *et al*, 1998) (Wright and Dornfeld, 1998). SFF also allows physical access to the entire volume of the part (not just the surfaces), thus making possible novel designs involving multiple materials, complex internal geometries or embedded components. Additionally, these processes build parts fully encapsulated in a support structure,

which makes it possible to fabricate multiple-part assemblies with bearing, mating and fitting surfaces *in-situ*. Many of the assemblies built in this manner cannot be disassembled without breakage, and typically, there is no possibility of interchanging their parts with other similar mechanisms. This feature of SFF is particularly relevant in the context of this thesis.

The indifference to feature geometry mentioned earlier is also largely responsible for restricting SFF processes to "look and feel" type of prototyping. In order to build functional engineering components that are highly integrated and precise, it is imperative that these processes allow for special handling of tolerance sensitive sub-components such as joints, sensors, actuators and electronics. Shape Deposition Manufacturing, or SDM (Merz *et al*, 1994), is a process which allows for the optional embedding of functional components during the fabrication of a layered part (Cham *et al*, 1999) (Weiss *et al*, 1996). As an example, pre-fabricated joints with precision machined shafts and bearings could be inserted automatically into the partially-built work-piece during fabrication. The process of making a mechanism with multiple links consists of insertions of joints and the layered fabrication of the link bodies and support structures that encapsulate the joints (these steps could happen in sequence, or all in parallel). Once all the joints are embedded, and the link-bodies and support structures are complete, the support structure is removed (typically by etching, melting or dissolving) to reveal a fully assembled functional mechanism with integrated joints. Figure 1.3 shows some mechanisms built using this technique. Some of the joints shown are pre-fabricated journal bearings with precision ground stainless steel shafts and teflon bushings.

2.2.2 Micromachining

Micromachining refers to the use of lithographic or other precision techniques, originally developed in the integrated-circuit industry, to carry out the fabrication of mechanisms, transducers, or planar and spatial structures (Kovacs, 1998). The feature size of these devices is typically in the order of a micrometer ($10^{-6}m$) to several millimeters ($10^{-3}m$). The devices are built on top of a single-crystal silicon substrate, using alternate additive and subtractive processes. There are many different materials that are used in this type of processing - though it is common to use polycrystalline silicon or metals as the final part material, with oxides and photo-resist making up the sacrificial support structure. The embedding of pre-fabricated parts

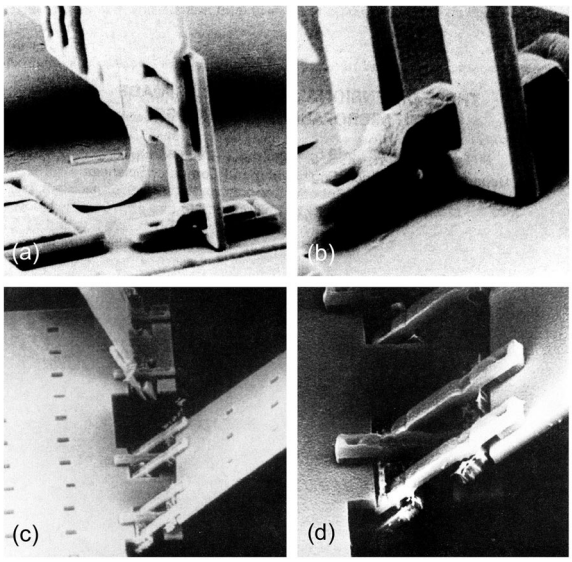

Figure 2.3: Some hinge-joints for a mechanism built using micromachining technology, Courtesy: Kristofer S. J. Pister, Associate Professor of EECS, University of California, Berkeley. Used with permission.

into the micro-machine is typically not feasible.

Two types of micromachining techniques are usually described in this context - *surface* micromachining and *bulk* micromachining. Surface machining refers to the building of devices entirely from layers of polysilicon or metals deposited on top of the substrate. This is a combination of additive and subtractive processes. Bulk machining refers to the subtractive machining of the single-crystal substrate.

Applications of micromechanical systems include micro-optics, micro-robotics, gas chromatography, micro-sensing etc. Several researchers have built mechanisms with joints and hinges in the microscopic scale (Burgett *et al*, 1992). While some physical properties (such as mass transport and surface-to-volume ratio) scale very favorably to the smaller sizes, this typically is not true for geometric properties. For example, the resolution of some of these processes typically equals the minimum feature size, resulting in clearances in joints that are comparable to the size of the shaft itself. Other scaling problems include packaging requirements and efficient heat dissipation. Figure 2.3 shows some examples of hinges and devices built using micro-machining techniques. These devices too qualify as *in-situ* mechanisms under our definition, and the techniques that are presented here, in general, apply to this realm as well.

2.3 Manufacturing Variability and Tolerancing

2.3.1 Historic Perspective

A fundamental achievement of manufacturing in the antebellum period (1820-1860) of American history was the technology to fabricate interchangeable parts. Interchangeability, which was originally advocated by the French General Jean-Baptiste de Gribeauval as early as 1765 (Hounshell, 1984) was first realized on a large scale by the arms contractors Simeon North and Eli Whitney. The driving force was the strategic advantages offered by the ability to exchange faulty musket and pistol parts with replacements recovered from other faulty arms on the battlefield. The intellectual leap that took place during this era was the conceptualization of the mechanical ideal. This ideal represented perfection (usually in the geometric sense) and every physical artifact actually built was but an imperfect copy. Methods were devised that mapped behavioral restrictions to constraints on part geometry. Functional (go, no-go) gages and process call-outs implicitly represented limits on the permissible variability from the mechanical ideal.

Other supporting technologies that made it possible to realize part interchangeability included advancements in model-making, jigs and fixturing, and metrology. Dimensioned drawings with explicit tolerances eventually replaced representational drafting practices. The first drafting and tolerancing standards were articulated in the 1930's and still continue to be refined. These major advancements in manufacturing, combined with the advent of mechanization, enabled the mass-scale production of nearly identical parts that we see to this day. A vast majority of common mass-produced devices consist of assemblies of parts that are individually and independently fabricated.

2.3.2 Tolerance Representation

It has been noted that the advent of two relatively recent phenomena, namely Computer Aided Design (CAD) and Coordinate Measuring Machine (CMM) technology, have precipitated a flurry of interest in the field of tolerance representation (Voelker, 1993). Much of the recent theoretical work in tolerancing has concentrated on one of two important problems: the mathematization of Geometric Dimensions and Tolerances (GD& T) (Requicha, 1983) (Requicha, 1993) (Walker and Srinivasan, 1993),

and the development of a "rational basis" for tolerance assignment based upon the functional requirements of a part (Srinivasan and Wood, 1995). A fair amount of thought has also gone into determining the most appropriate mechanism of associating tolerances with solid geometry. This includes representations that are CSG based (Requicha, 1984) (Requicha and Chan, 1986), Virtual Boundary Requirements based (Jayaraman and Srinivasan, 1989), or Hybrid CSG/B-rep and feature based (Turner, 1987), (Roy and Liu, 1988). Researchers have also developed data structures which make it easy to reason about over-toleranced designs and improve the efficiency of tolerance analysis on evolving designs (Tsai and Cutkosky, 1997). However, few commercial CAD systems support feature-based geometric dimensioning and tolerancing. The latest release of *AutoCAD*, for example, treats tolerances as annotations in the drafting mode. Tolerances are not directly associated with specific topological entities, making it difficult to retain (or automatically translate) the tolerance information when the model is decomposed or otherwise modified. Since SFF is closely tied to CAD (it cannot operate in the absence of an electronic representation), it suffers in the presence of any deficiencies in state-of-the-art geometric/CAD engines. It should be noted that emerging international standards for life-cycle product data representation (e.g. the ISO-10303 STEP standards, (ISO, 1994)) do seek to address these concerns.

International standards are slow at being widely adopted, however, and to this day, much of tolerancing in the manufacturing industry is seen as an art: *ad-hoc* assignments based upon the experiences of individual designers and fabricators, or traditional tolerancing practice captured in design handbooks. Recently, however, tools like statistical and geometric tolerancing have increased the expressiveness of tolerancing while simultaneously reducing the precision required from the manufacturing facility in order to ensure functional parts. Statistical tolerancing exploits the variance limiting property of the overall dimension as independent and identically distributed (IID) tolerances stack up in a tolerance chain (Evans, 1975). Geometric tolerances allow for tolerance zones with arbitrary geometry as opposed to the prismatic zones afforded by the conservative (worst-case) plus-minus tolerances (Requicha, 1983). Criteria such as the Maximum Material Condition (MMC) and Least Material Condition (LMC) allow looser positional tolerances on features based upon size measurements at the inspection stage (a larger hole can drift more from its ideal position than a smaller hole and still preserve assemblability). ANSI Y14.5M (ANSI,

1994) is a geometric dimensioning and tolerancing standard that includes specification of size, location, form, profile and run-out tolerances that has recently enjoyed wide use in industry.

It is acknowledged by researchers that surprisingly little is known about tolerancing for assemblies (Voelker, 1993). In traditional engineering practice, assembly drawings are rarely toleranced. The LMC and MMC criteria, coupled with simple one-dimensional stack-up rules, ensure satisfactory assembly of individual parts. In bearing design, for example, given the type of fit and function (e.g. clearance fit for precision machinery), standard tables in mechanical design handbooks specify allowable size tolerances on the mating shaft and hole features. Representation of feature variations using homogeneous matrix transforms has been addressed by researchers (Whitney and Gilbert, 1993). This representation facilitates statistical tolerance stack-up and error propagation analysis in sequential assemblies, particularly with a mix of linear and angular dimensions. Assembly analysis of complex parts typically requires Monte Carlo simulation (Hammersley and Handscomb, 1964). The focus of these methods is to predict the likelihood of successful assembly given allowable feature variations.

2.3.3 Machine-tool and Process Accuracy

Most commercial manufacturers of Rapid Prototyping (RP) equipment have resisted the publication of specification sheets detailing basic process accuracy. Unlike manufacturers of conventional CNC machines, who specify positioning and runout precision and repeatability numbers, RP manufacturers choose instead to provide information to potential customers about build envelope, minimum feature sizes, and material properties. This trend can be explained by the fact that the accuracy with which a layered object can be manufactured is influenced by many ill-understood phenomena (in addition to the machine-tool positioning accuracy), namely, shrinkage, warpage, stair-stepping etc. However, this has to change if these technologies are to be considered for use in building accurate functional components. At the very least, the manufacturers will need to provide dimensional (i.e. position and size) accuracy numbers for the process as a whole (which may be different from the positional accuracy of the machine tool used).

Hybrid processes like Shape Deposition have a fundamental advantage that their

dimensional accuracy is closely related to the accuracy of the material removal process used to shape the external features. In this thesis, we only consider the locational (position and orientation) accuracy with which pre-fabricated joints can be inserted into a workpiece in-process. Clearly, this will depend both on the positional accuracy of the machine-tool (robot or x-y table), and other factors such as part shrinkage, warpage etc. We assume that, in the general case, this accuracy is expressed as a precision region of arbitrary geometry around the nominal position of the joint within which the actual joint is located.

It is important to distinguish the approach adopted in this paper from those of representing geometric tolerances on traditional mechanical designs. As mentioned in the earlier section, recent work on Geometric Dimensioning and Tolerancing (GD&T) has focused on developing a rigorous mathematical foundation for the un-ambiguous representation of position, form and runout tolerances on mechanical designs. The issue of tolerance representation is also closely related to that of expressing manufacturing accuracy and process capability. However, we have chosen to use a very general model for expressing the positional accuracy of the manufacturing process for a number of reasons:

- The greatest advantage of SFF processes still remains their relative "feature blindness." Traditional notions of specifying tolerances on manufacturing features (likes holes, shafts and pockets) are largely irrelevant for SFF due to this indifference to features.

- Conventionally, given the type of fit and function (e.g. clearance fit for precision machinery), standard tables in mechanical design handbooks specify allowable size tolerances on the mating features. Tolerances that specify mate and fit quality in the conventional sense are not suitable for *in-situ* fabrication of assemblies, as gaps and clearances manifest themselves directly in the geometry of the support structure and there are no assemblability issues that can arise (Rajagopalan and Cutkosky, 1998).

- SFF is performed, in most cases, using a series of process steps (not unlike VLSI fabrication). Thus the achievable end-result accuracy is dependent on many factors and is not as easily describable as the precision of a machine tool.

2.3.4 Quality Engineering and DfM

The concept of optimizing the design and manufacturing parameters of a part in order to ensure conformance to pre-specified requirements has been extensively addressed under the ægis of Design for Manufacturability and Quality Engineering (Taguchi, 1986) (Taguchi, 1993) (Park, 1996). An important tenet of quality engineering is that of *robust design* - including parameter design and tolerance design. This is often referred to as the Taguchi approach, and is a suite of methods for optimizing the product design by choosing parameter values that are minimally influential in the degradation of product performance. This results in high-quality parts that are simultaneously cheap to produce.

In this method of analysis, a process capability index ($\mathcal{C}_p$) is defined as follows:

$$\mathcal{C}_p \equiv \frac{U - L}{6\sigma} \tag{2.1}$$

where U and L are the upper and lower specification tolerances, respectively. The quantity σ is the standard deviation of the process being described. In other words, the process capability index $\mathcal{C}_p$ is a continuous measure of process capability (and not a simple go, no-go measure of process yield). A $\mathcal{C}_p$ value of 1 indicates the 99.73% of the parts will meet the tolerance specs, and will be dispersed Normally within the entire allowable space. A recent trend in industry (dubbed the Motorola Six-Sigma Effort) requires that $\mathcal{C}_p$ be equal to 2. An comprehensive treatment of the theory and practical implementation of Six-Sigma techniques is presented in a recent textbook by Breyfogle (Breyfogle, 1999).

Process capability and other statistical methods for process control have rarely been applied to rapid prototyping (RP) processes. The primary reasons for this are that most commercial RP machines are "roughing" processes, with parts requiring post-processing in order to bring them into tolerance, and that these processes are designed for one-of prototypes rather than for mass produced parts (where statistical process control is most applicable). In this thesis, the capability of the process is defined in terms of its ability to accurately locate a mechanism feature (such as a joint) rather than its ability to deliver a certain parametric tolerance on a component. The component-centric approach is typically implicit in most DfM methodologies for tolerance design.

An interesting application area that has concerns similar to those addressed in

this thesis is that of dynamic feed-control for injection molded plastic parts (Kazmer, 1995). The gating design for an injection molding tool determines the degree of interdependence between various critically toleranced parameters of the final part. Robust tool design and dynamic feed control can be used in order to improve the quality (i.e. accuracy and yield) of plastic parts.

Chapter 3

Mechanism Error Analysis

The earliest scientific treatment of mechanism error estimation dates back to the early 1960's (Tuttle, 1960) (Knappe, 1963). In the several decades since, many alternative approaches to error analysis for mechanisms have been proposed - each with various simplifying assumptions and different levels of complexity (Hartenberg and Denavit, 1964) (Garrett and Hall, 1969) (Dhande and Chakraborty, 1973) (Lakshminarayana and Ramaiyan, 1976) (Tischler and Samuel, 1999). All approaches, however, attempt to solve the same basic problem - *to predict the nature and amount of performance deterioration in mechanisms as a result of non-ideal synthesis, fabrication, materials or componentry.*

Performance of a mechanism is usually taken to mean its accuracy in performing either a positioning, path-generation or function generation task. Clearly, there are many other quantitative and qualitative aspects to mechanism behavior that constitute "ideal" performance. These could include its dynamic behavior (including joint friction, vibration characteristics, transmission efficiency etc.), life-cycle issues (e.g. wear and fatigue resistance, serviceability and maintainability) and aesthetics. In this thesis the focus is on kinematic performance. In other words, we assume that we are always able to describe the desired task in terms of an output equation of the form:

$$\mathbf{y} = f(\Phi, \Theta) \tag{3.1}$$

where $\mathbf{y}$ denotes the $(m \times 1)$ vector of output end-effector locations, coupler-point positions or output link angles, Θ is a $(k \times 1)$ vector of known driving inputs, and Φ is a $(n \times 1)$ vector of independent mechanism variables - including deterministic or randomly distributed geometric parameters and/or dimensions. The function

$f(\cdot)$ is called the *kinematic function* of the mechanism and is, in general, assumed to be a continuous and differentiable (i.e. smooth) non-linear mapping from the mechanism parameter space to an output space (e.g. a Cartesian workspace). In the absence of higher-pairs (i.e. joints that have line and point contact, as opposed to surface contact, between their member links) and multiple-contact kinematics, the smoothness assumption generally holds true.

Conventional error analysis takes parametric variability or link dimensional tolerances as given, and estimates the resulting output deviations using worst-case or stochastic analysis methods. Alternately, in tolerance allocation problems, the sensitivity of the output function to mechanism parameters is utilized to assign allowable variability in individual component dimensions. The component-centric approach makes sense for conventional manufacturing, as the process is largely viewed as one involving sequential fabrication and assembly of (slightly faulted) components. However, these methods are inappropriate for *in-situ* fabrication due to the following reasons (discussed in more detail in Section 3.3):

- *In-situ* fabrication is blind to conventional component boundaries. Consequently, the input to the system is not the dimensional variability in links, but the absolute position and orientation variability in joints.

- Tolerance stack-up due to dimensional/parametric errors in components is not an issue for *in-situ* fabrication.

- Gaps and clearances in joints that are fabricated *in-situ* (i.e. joints that are not inserted as embedded components) are manifest directly in the geometry of the support structure. In conventional fabrication, the gap geometry is a consequence of the interaction amongst complementary mating/fitting feature geometries.

- Conventional methods of error analysis do not allow for the consideration of variable fabrication accuracy within the process workspace.

This chapter starts by reviewing conventional error analysis techniques, and builds on the prior work to formulate a general approach for the estimation of output performance errors in the *in-situ* fabrication of mechanisms.

3.1 Fundamental Error Factors

Traditionally, researchers have concerned themselves with five types of fundamental factors that result in non-ideal behavior of mechanisms. These can be broadly classified into:

- Errors due to manufacturing variability
- Errors due to play or clearance in joints
- Structural errors
- Errors due to deflection in flexible linkages
- Control errors in the independent driving variables

Each of these factors is further discussed in the following sections.

3.1.1 Manufacturing Errors

Manufacturing errors are introduced into real mechanisms due to imperfect dimensional control during the fabrication process. This typically happens due to workpiece and/or machine-tool compliance, material imperfections, residual thermal stresses, and other uncontrolled factors within the processing environment. In conventional error analysis, these variations are modeled by making dimensional parameters into interval quantities or random variables. Experimentally measured process precision values determine the extent (or moments, in the case of stochastic analysis) of these variables.

As discussed earlier, this approach is not a convenient model of manufacturing errors for *in-situ* fabrication of assemblies. In this thesis, manufacturing error is modeled as inaccuracy in the position and orientation (with respect to an absolute datum-frame) of feature-frames that are sequentially "inserted" into a 3-D workspace.

3.1.2 Clearance Errors

Clearance errors are manifest in the performance of mechanisms due to the *designed* gaps between mating parts of a mechanism. Clearances in joints are essential for smooth, low-friction operation. They also facilitate mechanism assembly and lubrication during operation. Joint clearance, however, allows small motions (i.e. *play*

or *backlash*) in directions orthogonal to the joint operational axis, thereby resulting in output errors. There is also the additional issue of manufacturing variability in the actual clearance value of joints. In most treatments, these errors are assumed to be negligible in comparison with the link dimensional errors. If needed, they can be explicitly modeled as the difference between the random mating/fitting feature sizes - for example, the hole and shaft diameters (Lee and Gilmore, 1991).

Many alternate methods have been proposed to model the actual relative position of adjacent links within a joint (see Section 3.2.2). In the stochastic analysis of errors, for example, it is typical to model the actual link position during operation as an independent random variable with a uniform distribution within the clearance space (Figure 3.1). In other words, it is assumed that the probability of finding the pin element of a revolute joint (for example) at any specific position in the clearance space between the shaft and and race, is constant for all possible pin positions. While this assumption is convenient for analysis, it is not always entirely accurate. For example, in a given linkage with revolute joints, the pin positions at any two adjacent joints are correlated if both pins share the same link (see Figure 3.2). Additionally, for a spatial revolute joint with both radial and axial clearances, it has been shown (Lakshminarayana and Ramaiyan, 1976) (Wang and Roth, 1989) that the joint will typically rest in one of four possible *contact modes*, assuming frictionless contacts and static equilibrium of the adjacent bodies. The specific mode depends upon the forces and moments on the joint at the operating position. For each mode, the positional error is deterministic, and analytically computed. However, the contact-mode approach is dependent on the specific geometry of the joint (e.g. different for journal, roller and thrust bearings), and also the ratios of the dimensions of the features (e.g. shaft diameter, flange diameter, shaft length etc.). Analysis using this type of model is computationally tedious to carry out, and researchers largely adopt the simpler (i.e. equiprobable position of pin within the race) model of joint clearance.

Another interesting issue in the context of *in-situ* fabrication is the difference in the way in which gaps or clearances are created. In conventional manufacturing, clearances are a result of interactions between mating or fitting assembly features (like holes and shafts). Typically, mating features are fabricated independently, and clearance values do not become apparent until the assembly is complete. In contrast, for *in-situ* manufacturing, gaps and clearances are directly manifest in the geometry

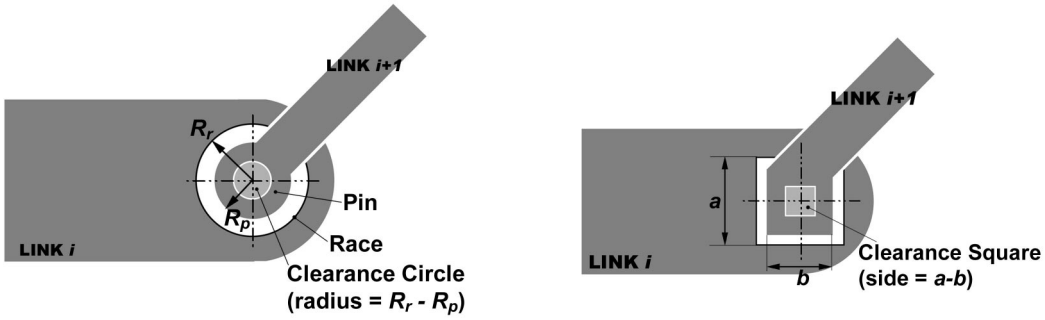

Figure 3.1: Clearance model for revolute and prismatic joints. The inner shaded circle or square represents the region within which the shaft axis can lie, and is called the Clearance Circle or Clearance Square, respectively.

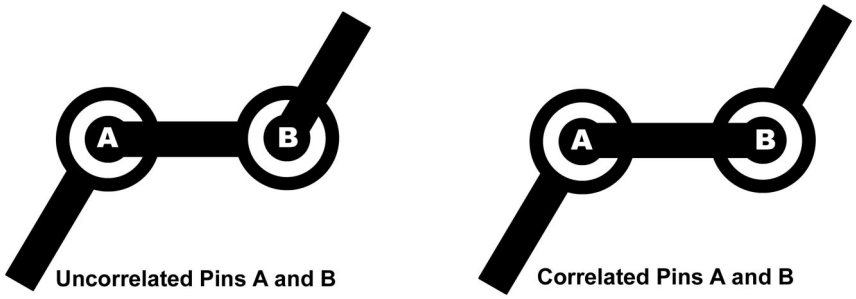

Figure 3.2: Un-correlated and correlated adjacent pins.

of the support material. Since gaps affect mechanism performance more directly than the features that produce them, *in-situ* fabrication holds some advantages over conventional manufacturing (Rajagopalan and Cutkosky, 1998). This issue is explored further in Section 3.3.5.

3.1.3 Structural Errors

Structural errors are the result of approximate synthesis of mechanisms. They would exist even if the mechanisms were built to perfection. Optimal mechanism synthesis is a procedure by which structural errors are held to a minimum, given certain performance criteria and system constraints (like number of links, joint-types etc.) (Freudenstein, 1959).

In this thesis, errors due to structural imperfection is not considered in the analysis. Structural errors are independent of the manufacturing process, and the assumption for this treatment is that the nominal mechanism parameters are an input to the system. Optimal mechanism synthesis in the presence of non-homogeneous process accuracy is an interesting problem, which could be addressed in future research that extends the work of this thesis (see Chapter 5).

3.1.4 Link Deflection Errors

Deflection errors happen due to the compliant nature of real mechanisms where rigid-body assumptions do not hold. This is true especially for links with slender or flexible constructions, or for mechanisms that experience significant stress-inducing loads during operation. The effect of link-flexibility is similar to that of dimensional variability - except for the dynamic nature of the errors. Since the emphasis of this thesis is to study mechanism errors with the intent of feeding back into the fabrication process, errors that are dependent upon operational variables (i.e. operating loads) are not considered in the analysis.

3.1.5 Control Errors

Significant mechanism configuration errors can occur due to imperfect control of the independent (or driving) variables in the device during operation. These can be eliminated to a large extent by calibration and real-time feedback control to the driving elements. Clearly, the quality of the control will depend upon the capabilities

of the sensing and actuation elements (e.g. sensitivity, resolution, range etc.). Once again, control errors in the driving elements are not considered in this analysis, since the motivation is feedback into the manufacturing process. In this thesis, it is assumed that the independent variables are held perfectly to their desired value at the position of interest. Furthermore, variants of a mechanism under consideration are always compared at the same driving input values.

3.2 Conventional Mechanism Error Analysis

Conventional error analysis deals with degradation in the performance of a mechanism as a result of parametric or dimensional variations, and play in joints. The parameters considered are typically link lengths for planar linkages, or some form of the Denavit-Hartenberg (Denavit and Hartenberg, 1955) parameters for spatial linkages. Error in the performance of known mechanisms can be estimated analytically if certain assumptions are made, rendering the underlying mathematical treatment more tractable. For example:

- Mechanism dimensions and parameters have a known, given variability characteristic - either deterministic, or stochastic.
- Dimensional/parametric variations and clearance values are significantly smaller than their nominal values.
- Individual component variations are independent, uncorrelated and identically distributed.
- The output is, at most, a weak non-linear function of the mechanism parameters at the operating configuration of interest.

As a result of these assumptions, it becomes possible to approximate the actual error by lower-order estimates with satisfactorily large confidence. Other assumptions (e.g. negligible variability of the clearance value itself, Normal or Uniform distribution of component parameters etc.), which either eliminate unnecessary model complexity or enable analytical tractability, are also commonly made.

3.2.1 Classical Sensitivity Analysis

Sensitivity analysis is based on the Taylor-series expansion of the output function. As stated in Equation 3.1, the end-effector position, coupler path or output angle of a mechanism can be expressed as:

$$\mathbf{y} = f(\Phi, \Theta) \tag{3.2}$$

where $\Theta \equiv [\theta_1, \theta_2, \cdots, \theta_k]^T$ are the k known driving inputs, and $\Phi \equiv [\phi_1, \phi_2, \cdots, \phi_n]^T$ are the n mechanism parameters (or dimensions) subject to random, or worst-case deterministic, variability. Since Θ is assumed static for a given mechanism configuration (i.e. the driving inputs are held perfectly to their nominal values), it is dropped from the equation for notational simplicity. The previous equation is re-written as:

$$\mathbf{y} = f(\Phi) \tag{3.3}$$

Expanding this function in Taylor-series around the nominal values of the mechanism parameters ($\Phi^{nom} \equiv [\phi_1^{nom}, \phi_2^{nom}, \cdots, \phi_n^{nom}]^T$), we get:

$$\begin{aligned} \mathbf{y} \;=\; & f(\Phi^{nom}) + \sum_{i=1}^{n} \frac{\partial f}{\partial \phi_i}]_{nom}(\phi_i - \phi_i^{nom}) + \frac{1}{2!}\sum_{i=1}^{n} \frac{\partial^2 f}{\partial \phi_i^2}]_{nom}(\phi_i - \phi_i^{nom})^2 \\ & + \sum_{i>j} \frac{\partial^2 f}{\partial \phi_i \partial \phi_j}]_{nom}(\phi_i - \phi_i^{nom})(\phi_j - \phi_j^{nom}) + \cdots \end{aligned} \tag{3.4}$$

or, using a more concise notation:

$$\mathbf{y} = f(\Phi^{nom}) + \frac{\partial f}{\partial \Phi}]_{nom}(\Phi - \Phi^{nom}) + \frac{1}{2!}\frac{\partial^2 f}{\partial \Phi^2}]_{nom}(\Phi - \Phi^{nom})^2 + \cdots \tag{3.5}$$

For small, independent variations about the nominal configuration, a linear approximation can be made - thereby rewriting the above equation as:

$$\mathbf{y} \approx f(\Phi^{nom}) + \frac{\partial f}{\partial \Phi}]_{nom}(\Phi - \Phi^{nom}) \tag{3.6}$$

or

$$\Delta_{\mathbf{y}} \approx \frac{\partial f}{\partial \Phi}]_{nom}\Delta_{\Phi} \tag{3.7}$$

The quantitiy $\frac{\partial f}{\partial \Phi}]_{nom}$ is known as the *sensitivity Jacobian* of the mechanism, evaluated at the nominal configuration. This Jacobian relates the component variability

(Δ_Φ) in the mechanism parameter space to the output variation ($\Delta_{\mathbf{y}}$) in Cartesian space. This is classical sensitivity analysis, where all variational effects are bundled into a simple parametric space, and all higher order effects are neglected.

Equation 3.7 is used as the basis for error analysis and tolerance allocation. For error analysis, the component variability (Δ_Φ) and sensitivity Jacobian ($\frac{\partial f}{\partial \Phi}$) are known for a given mechanism configuration. The output error ($\Delta_{\mathbf{y}}$) is then a simple calculation. The component variability can either be expressed as worst-case values, or as stochastic variations in link parameters. Each of these approaches is discussed in the next sections.

For tolerance allocation problems, the maximum permissible output error ($\Delta_{\mathbf{y}}^{max}$) and sensitivity Jacobian are known. Equation 3.7 forms the basis for the constraint equations, and the objective is to maximize the overall variability (i.e. Δ_Φ), given the constraints. Greater allowable variability typically means lower manufacturing and inspection costs, and thus, is preferred. One simple formalization of the tolerance allocation problem is as follows:

$$minimize\ Z = \sum_{i=1}^{n} \frac{1}{\Delta_\Phi} \tag{3.8}$$

subject to:

$$\begin{aligned} g(\Phi) &\equiv \Delta_{\mathbf{y}}^{max} - \frac{\partial f}{\partial \Phi}]_{nom}\Delta_\Phi \leq 0 \ \ and \\ g_i(\Phi) &\equiv \phi_i \geq 0; \ \ i = 1, 2, \ldots, n. \end{aligned} \tag{3.9}$$

Here, an assumption is made that each component variability parameter is weighted equally in the cost function, which may not always be true. Some manufacturing parameters may be easier to control accurately than others (e.g. hole size can typically be held to tighter tolerances than center-distance between holes). Additionally, zero tolerance (or close-to-zero tolerance) for some parameters, which is permissible for the above formalization, is infeasible for real manufacturing processes. Non-homogeneous manufacturing capability within the mechanism workspace is also not considered in this system.

The optimization problem can be solved using standard methods of parametric programming - Lagrange multipliers, or Powell's conjugate direction method (i.e. unconstrained optimization of a penalty function)(Fox, 1971). An example of these

optimization techniques applied to mechanism tolerance allocation can be found in (Chakraborty, 1975).

Deterministic, Worst-Case Error Estimation

In worst-case error estimation, each parameter ϕ_i is assumed to take (exclusively) one of two deterministic values ϕ_i^{min} and ϕ_i^{max}. Furthermore, it is assumed that $\phi_i^{min} \leq \phi_i^{nom} \leq \phi_i^{max}; i = 1, 2, \ldots, n$, where ϕ_i^{nom} is the nominal value of the i^{th} parameter.

The objective of this kind of error estimation is to determine the worst case envelope of the mechanism performance error. Except for applications where performance within specified limits is absolutely critical, the worst-case analysis results in conservative estimates of error (and thereby, over-design of components). The probability of the worst case combination actually occurring during fabrication is remote. Since the worst performance can occur for any combination of minimum and maximum component parameter values, the technique proceeds by exhaustive calculation of total error for each combination of individual error values. For n parameters, this leads to a search space of 2^n combinations for each mechanism configuration. If the objective is to find the worst-case performance within the entire workspace of the mechanism, then this calculation has to be repeated at each incremental driver position.

An alternative approach is to use dynamic programming techniques (Bellman, 1957) (Fenton *et al*, 1989) to estimate the maximum error without computing the total error for every possible combination. The assumption made while using this technique is that the global optimization problem can be re-stated as a multi-stage optimization problem, with the n^{th} stage solution related to the $(n-1)^{th}$ stage solution through a functional equation. While this technique results in significant reduction of the computational burden involved, it is not guaranteed to find the global optimum when the underlying monotonicity assumptions do not hold.

Stochastic Error Estimation

Statistical error estimation proceeds by assigning a probability distribution function (PDF) to each variable parameter ϕ_i. The component dimension under consideration is assumed to be a random variable, distributed according to the characteristics of its underlying PDF, denoted as $p_{\Phi_i}(\phi_i)$. The cumulative distribution function (CDF) of

the output functions can then be estimated using standard techniques for stochastic analysis. If certain assumptions can be made (e.g. linearity, independence, identical distribution etc.), the estimation of the distribution and moments of the output function is highly simplified.

The error equation (Equation 3.3) can be replaced by an equivalent equation for the stochastic estimation of each output CDF, as follows:

$$\begin{aligned} P_{Y_j}(y_j) &= \int_{-\infty}^{\phi_1} \dots \int_{-\infty}^{\phi_n} y_j . p_{\Phi_1 \dots \Phi_n}(\phi_1, \dots, \phi_n)\, d\phi_1 \dots d\phi_n \\ & \quad where \;\; j = 1, 2, \dots, m \end{aligned} \tag{3.10}$$

and for independent and uncorrelated ϕ_i

$$p_{\Phi_1 \dots \Phi_n}(\phi_1, \dots, \phi_n) = \prod_{i=1}^{n} p_{\Phi_i}(\phi_i) \tag{3.11}$$

In general, the complete analytical evaluation of the above integrals is not simple, or even tractable. However, it may not always be necessary to evaluate the error CDF. Given certain assumptions, it is possible to determine the mean and variance of the output distribution directly from the mean and variance $(\mu_{\phi_i}, \sigma^2_{\phi_i})$ of the individual components. To do this, the output (Equation 3.3) is expanded in a Taylor series about the mean values (μ_{ϕ_i}) of the component dimensions as follows:

$$\begin{aligned} \mathbf{y} &= f(\mu_{\phi_i}; i = 1, 2, \dots, n) + \sum_{i=1}^{n} \frac{\partial f}{\partial \phi_i}]_\mu (\phi_i - \mu_{\phi_i}) + \frac{1}{2!} \sum_{i=1}^{n} \frac{\partial^2 f}{\partial \phi_i^2}]_\mu (\phi_i - \mu_{\phi_i})^2 \\ & \quad + \sum_{i>j} \frac{\partial^2 f}{\partial \phi_i \partial \phi_j}]_\mu (\phi_i - \mu_{\phi_i})(\phi_j - \mu_{\phi_j}) + \cdots \end{aligned} \tag{3.12}$$

Assuming that the output is approximately linear for small variations of the random variables about their mean values, the higher-order terms in the above equation can be dropped, and the equation re-written as:

$$\mathbf{y} \approx a + \sum_{i=1}^{n} \frac{\partial f}{\partial \phi_i}]_\mu (\phi_i - \mu_{\phi_i}) \tag{3.13}$$

where $a \equiv f(\mu_{\phi_i}; i = 1, 2, \dots, n)$, and the partials are evaluated at the mean value of the parameters. Equation 3.13 can be written in terms of the proxy (difference)

variables $\Delta_{\mathbf{y}}$ and Δ_{ϕ_i} (see Equation 3.7) as:

$$\Delta_{\mathbf{y}} \approx \sum_{i=1}^{n} \frac{\partial f}{\partial \phi_i}]_{\mu} \Delta_{\phi_i} \tag{3.14}$$

where $\Delta_{\mathbf{y}}$ and Δ_{ϕ_i} are zero-mean random variables with all higher-order moments identical with $\mathbf{y}$ and Φ_i respectively. In other words, by studying the variance properties of Equation 3.14, we are in effect studying the variance properties of the original equation (i.e. Equation 3.13).

If the parameters Δ_{ϕ_i} are assumed to vary independently, then it can be shown (see *Central Limit Theorem* (Feller, 1957)) that the output $\mathbf{y}$ follows an approximately Normal distribution (for $n > 5$), with the mean and variance of the distribution given as follows:

$$\begin{aligned} \mu_{\mathbf{y}} &= a \\ \sigma^2_{\mathbf{y}} &= \sum_{i=1}^{n} (\frac{\partial f}{\partial \phi_i})^2_{\mu} \sigma^2_{\phi_i} \end{aligned} \tag{3.15}$$

where $\mu_{\mathbf{y}}$ and $\sigma^2_{\mathbf{y}}$ denote the mean and variance, respectively, of the output function.

The full derivation of Equation 3.15 is given in Appendix A, as the treatment is important for the extension of this model to the case of *in-situ* fabrication. A key assumption in this treatment - that of parametric independence - fails in the case of *in-situ* fabrication, and Equation 3.15 needs modification.

The specific probability of the output falling within a given range $\mathbf{y}_1 \leq \mathbf{y} \leq \mathbf{y}_2$ can either be estimated using the standard tables (for normal distributions), or the Chebychev inequality (for a symmetric range). Since the linearized equation approximates the output error as a weighted sum of the component variation, a normal output distribution can be assumed either when the individual component variations are each normally distributed, or when the Central Limit Theorem can be applied with Liapunov's condition (Feller, 1957) (Chakraborty, 1975). Thus, the validity of the linear approximation is a fundamental defining assumption in this type of analysis, since no simple general technique (other than numerical simulation) is available for the estimation of the probability distribution of a complex non-linear function of random variables.

In the event that the assumption of weak non-linearity of the output function does not hold, then a second order estimate of the mean a variance may yield better

results. This is given as (derivation follows from results in Appendix A):

$$\begin{aligned} \mu_{\mathbf{y}} &= a + \frac{1}{2}\sum_{i=1}^{n}(\frac{\partial^2 f}{\partial \phi_i^2})_{\mu}\sigma_{\phi_i}^2 \\ \sigma_{\mathbf{y}}^2 &= \sum_{i=1}^{n}(\frac{\partial f}{\partial \phi_i})_{\mu}^2\sigma_{\phi_i}^2 + \frac{1}{2}\sum_{i=1}^{n}(\frac{\partial^2 f}{\partial \phi_i^2})_{\mu}^2\sigma_{\phi_i}^2 + \sum_{i\neq j}(\frac{\partial^2 f}{\partial \phi_i \partial \phi_j})_{\mu}^2\sigma_{\phi_i}\sigma_{\phi_j} \end{aligned} \tag{3.16}$$

Specific Representations

The preceding sections present a generic treatment of error estimation where no assumption is made regarding specific parameter assignments to the mechanism geometry. Mechanisms could either be described using dimensions of geometric elements (e.g. link length for planar linkages) or using mechanism parameters (e.g. link length, link angle, offset and twist for spatial linkages). Typically, the assumptions made in the sensitivity calculations detailed above will fail for certain mechanism instances, depending upon the specific representation used (Hayati and Mirmirani, 1985).

A widely accepted parametric representation for spatial mechanisms is the Denavit-Hartenberg (or D-H) representation (Denavit and Hartenberg, 1955), and the extensions thereof (Suh and Radcliffe, 1978). In this representation (see Figure 3.3) a spatial mechanism is described in terms of four parameters for each link i in the linkage. These parameters are termed the link-angle (θ_i), link-length (a_i), link-offset (d_i), and twist-angle (α_i). In a mechanism with revolute, prismatic and cylindrical joints, the link-lengths and twist-angles typically remain static during operation, and the link-angles and link-offsets vary (depending upon the type of joint). The static parameters are sometimes called the *shape parameters* and the variable parameters the *joint parameters.*

Given the shape parameters of a spatial mechanism, it is possible to estimate functional variability that results from parametric variability during fabrication, using the sensitivity analysis techniques detailed in the earlier sections. However, sensitivity analysis using the D-H representation fails under some exceptional conditions. For example, small variations in the D-H parameters result in large errors in the output function when adjacent joint-axes are parallel or near-parallel, thus violating the assumptions that enable linear approximation of error. Since this is a common scenario in real mechanisms (especially in robotics), modifications have been proposed (Suh and Radcliffe, 1978) (Hayati and Mirmirani, 1985) that rectify this problem. The modified representation corrects for the problem with adjacent parallel joint

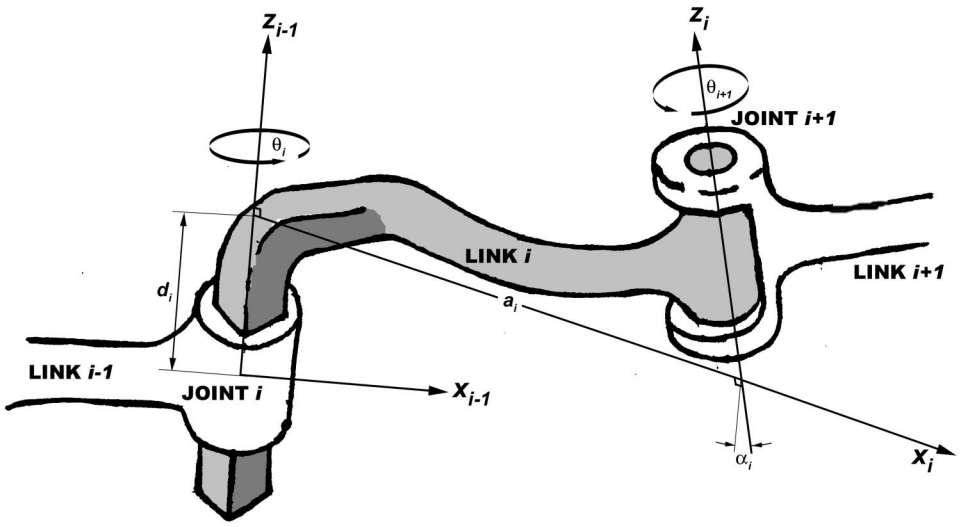

Figure 3.3: The Denavit-Hartenberg representation for spatial linkages (Denavit and Hartenberg, 1955).

axes, but introduces a similar problem for adjacent orthogonal joint axes. Thus, a combination of the two representations need to be used in order to robustly solve the general error-analysis problem for spatial mechanisms. (Lin and Chen, 1994) proposed an additional modification by introducing an extra parameter (l_i), which results in a better representation of the link shape (see Figure 3.4). It should be noted that the extra parameter does not add anything to the kinematic description of the mechanism, but it offers some practical conveniences in error analysis.

3.2.2 Clearance Models

Consideration of the effects of clearance (or gaps) in the analysis of mechanism error is a natural extension to simple error models which only consider dimensional or parametric variability. The complexity in dealing with clearance comes from the fact that it enables adjacent bodies to break contact with each other - thereby leading to unconstrained relative motion, within some geometric limits (sometimes called *multiple contact* - as opposed to *fixed contact* - kinematics). Since several mechanism analysis models use constraint equations (e.g. loop-closure equations) that are predicated upon persistent point/surface contact and non-interpenetration assumptions, they unravel in the face of joint clearances.

Various techniques have been proposed by researchers to deal with error analysis in the presence of joint clearances. Those proposed in recent years include:

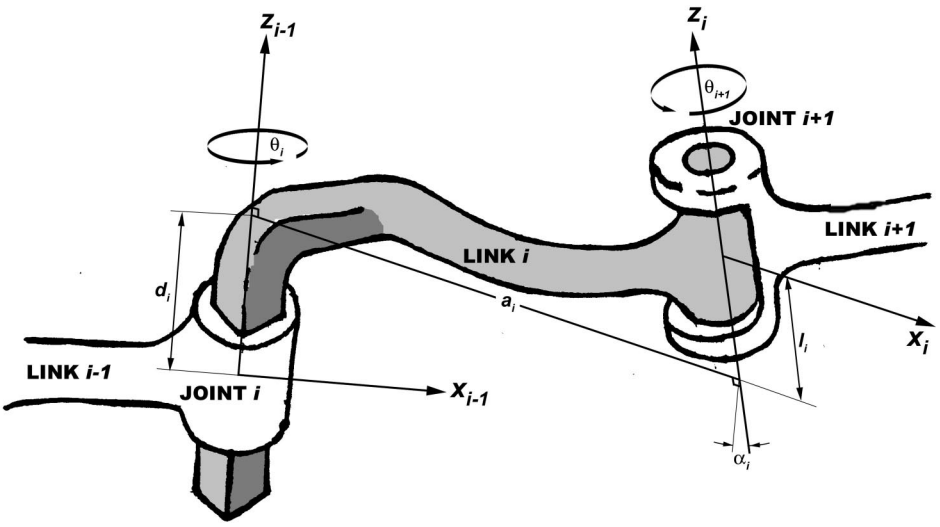

Figure 3.4: Modified Denavit-Hartenberg representation for spatial linkages (Lin and Chen, 1994).

- Equivalent linkage model (Kothalkar and Yajnik, 1970)
- Effective length model (Lee and Gilmore, 1991)
- Constrained degree-of-freedom model (Tischler and Samuel, 1999)
- Enumerated contact mode model (Wang and Roth, 1989)
- Configuration space model (Joskowicz *et al*, 1997)

Typically, the simpler clearance models (e.g. the effective length model) are inaccurate, but more generally applicable. The complex models improve prediction accuracy, but may be dependent upon specific joint geometry assumptions which do not hold generically. Clearance issues for *in-situ* fabrication are different from conventional methods (see Section 3.3.5). The conventional clearance models are discussed in more detail in the following sections.

Equivalent Linkage Model

The equivalent linkage model was originally introduced by Kothalkar and Yajnik (Kothalkar and Yajnik, 1970). The basic assumption that is made in this model of joint clearance is that the separation between the pin and race centers (due to play in the joint) is approximately constant during the operation of the mechanism.

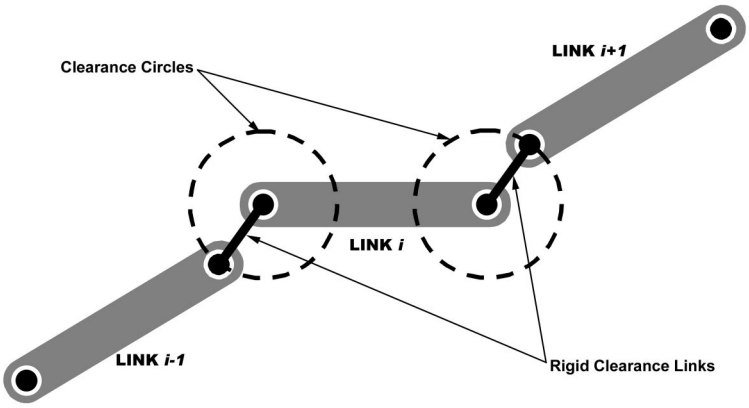

Figure 3.5: The equivalent linkage model of clearance (Kothalkar and Yajnik, 1970).

Alternately, small *clearance links* that connect the pin and race centers at each joint are added to the linkage model, and then the new mechanism is modeled assuming ideal (clearance-free) joints (see Figure 3.5).

The validity of this assumption is argued based upon the observation that mechanisms are usually transmitting forces via their links, and other than a few isolated transitory instances, pins and races of adjacent links will usually remain in contact with each other. While the model has been shown to work well for high-speed, closed-loop mechanisms (Furuhashi *et al*, 1978), it provides, in general, a conservative estimate of the error due to joint clearance, while adding significantly to the model complexity. Adding links to the mechanism results in un-actuated linkage freedoms, the values of which need to be designated at each operational point, either based upon loading conditions, or in a worst-case manner. For revolute joints, the model parameters will be different depending on which particular link ends in a pin, and which in a race - introducing multiple special-case scenarios. Furthermore, existing treatments do not extend this approach beyond revolute joints (e.g. cylindrical or prismatic) - or to general spatial mechanisms.

Once the new mechanism (with the clearance links added in) has been constructed, analysis proceeds using standard linkage modeling tools assuming ideal joints. Some general conclusions regarding the behavior of the clearance links at the extremal error positions can also be drawn (Kothalkar and Yajnik, 1970).

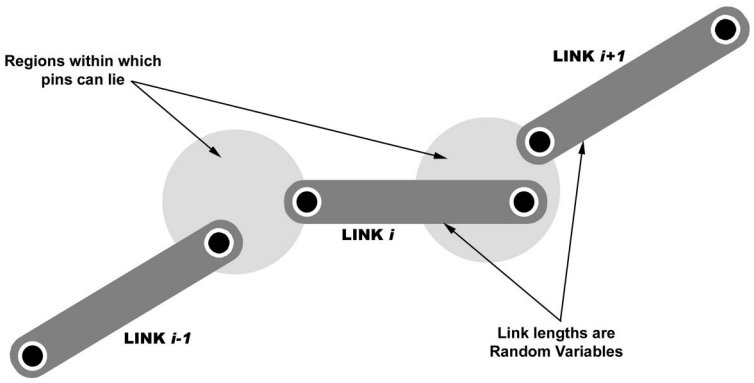

Figure 3.6: The effective length model of clearance (Lee and Gilmore, 1991).

Effective Length Model

In this model, the clearance between the components of adjacent links is effectively seen as adding length to one of the links (Lee and Gilmore, 1991). The distance between the pin and race (for a revolute joint) is not assumed to be a constant, but a random value restricted by the clearance geometry (see Figure 3.6). Thus, the effective link-length is also modeled as a random variable. By assigning a probability distribution function (typically uniform) to the position of the pin, it is possible to associate a mean and variance with the random effective length of the link.

The advantage of this model is that it treats link-length variations and clearance effects in a similar manner, resulting in a very simple error model. The analysis is also fairly independent of the specific construction of the joint, and is only dependent upon the clearance geometry. However, the model does have some limitations. For example, by considering only length variation, and not variability in joint axis orientations or in the link skew-angles, this model does not scale well to spatial linkages. The model also precludes any manner of deterministic analysis - and restricts the prediction of error to stochastic characterizations. Finally, bundling of clearance and length variability obfuscates two error-factors that can behave very differently depending upon the manufacturing scenario (e.g. when precision joints are assembled into a rough mechanism frame).

Constrained Degree-Of-Freedom Model

In the spatial analysis of mechanisms, each joint, or *kinematic pair*, is seen as restricting all but one or two degrees of relative freedom (six in all) between adjacent

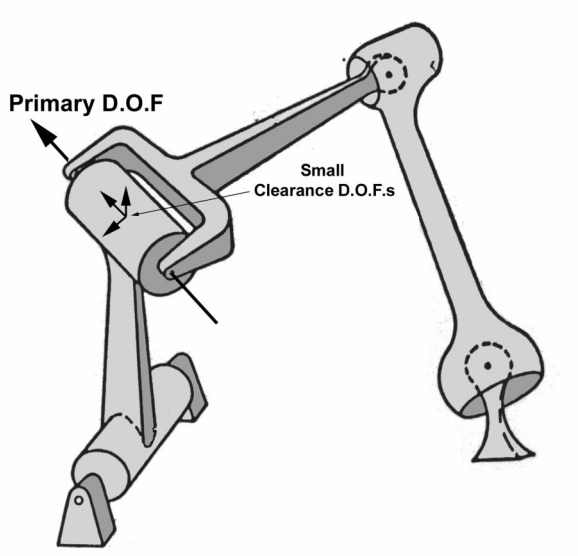

Figure 3.7: The constrained D.O.F. model of clearance (Tischler and Samuel, 1999).

bodies. In other words, depending upon the type of coupling, a joint completely restricts k relative freedoms (say), and completely allows $6 - k$ relative freedoms. There may be some range restrictions on the allowed freedoms (depending upon specific construction or linkage-type), however the allowable range is typically quite large.

In this method of modeling mechanisms, non-ideal joints with clearances can be thought of as higher-order joints that allow highly constrained (small) motions in the previously restricted freedoms. If each allowable joint freedom is mathematically represented as a *screw-motor* (i.e. a generalized, homogeneous representation of a joint axis) (Waldron and Kumar, 1979), then non-ideal joints introduce new screws into the model, with their parameter range constrained by the clearance geometry (see Figure 3.7). For very small motions, these new joint screws can be approximated as their respective instantaneous velocity screws, and velocity loop equations can be written to estimate the cumulative effect of the small perturbations. This leads to a very simple, linear model of clearance error for general spatial mechanisms. In fact, link-length variations can also be similarly modeled as additional velocity screws, thereby unifying the treatment of manufacturing variability and clearances in spatial mechanisms. Estimation of worst-case output error, subsequently, is a contrained optimization problem on the velocity model. This technique is illustrated for a specific spatial robot-finger mechanism by (Tischler and Samuel, 1999).

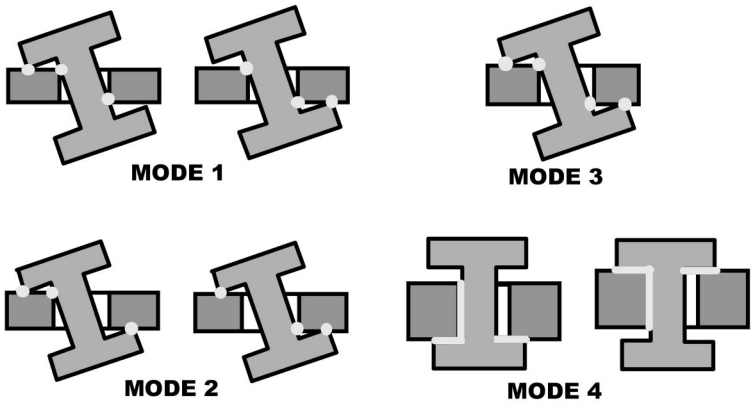

Figure 3.8: The enumerated contact-mode model of clearance (Lakshminarayana and Ramaiyan, 1976).

Enumerated Contact Mode Model

Lakshminarayana and Ramaiyan (Lakshminarayana and Ramaiyan, 1976), and later Wang and Roth (Wang and Roth, 1989), showed that with the assumption of frictionless contact and static equilibrium of the pin with the shaft, a journal bearing operates within one of four possible *contact modes* and two sub-modes (see Figure 3.8). These contact modes are classified by the type of contact (point, line or plane) and the specific contact position (journal, upper/lower rim, upper/lower thrust plate, and bearing hole). For each mode, it is possible to analytically determine the positional error (both location and orientation) of the journal within the bearing, given the axial and radial clearance values. This research also establishes an equivalence relationship between dimensional sensitivity analysis, and static (internal) force analysis on the link structure.

While this method of analysis yields very accurate, closed form solutions of the positional deviation of adjacent joint-frames, it it tedious to carry out (i.e. each contact mode would have to be examined at each candidate position) and is also very specific to the type of joint analyzed.

Configuration Space Model

Configuration space modeling of kinematic errors due to clearances and higher-pair joints was introduced under the title *kinematic tolerance analysis* by (Joskowicz *et al*, 1997). Configuration space analysis uses a graphical notation to explicitly encode the non-overlap, contact and free-motion constraints amongst mechanism components

(or more accurately, configuration parameters that proxy the components). The mechanism configuration spaces are obtained by intersecting the overlap, contact and free spaces of pairs of components. This analysis technique essentially casts kinematic analysis as a problem in computational geometry - presenting the same data from a different perspective, and thereby enabling new methods of kinematic reasoning. These techniques can predict quantitative and qualitative behaviors in non-ideal mechanisms (e.g. worst-case variability, undercutting, intereference, jamming etc.).

While this technique can be powerful in graphically illustrating the effects of component variations, it is computationally intensive. The reasoning task that is needed to fully realize the power of this technique can also be, in general, quite complex to implement in an automated fashion (akin to feature recognition in CAD).

3.3 Error Analysis for In-Situ Fabrication

This section details one of the primary original contributions of this thesis - the development of a technique for the parametric error analysis of general spatial mechanisms that are fabricated *in-situ*. The conventional error models presented in Section 3.2 cannot be directly applied to *in-situ* fabrication since this fabrication technique differs from conventional sequential shape-and-assemble fabrication techniques in some fundamental ways. Primarily, the differences are:

- Conventional error analysis starts with links as the primary components, and their dimensional/parameteric variability as given inputs to the error model. For *in-situ* fabrication, links are formed as a consequence of joints inserted into a spatial workspace. Parametric variability, subsequently, is a function of joint-insertion accuracy.

- Conventional (open chain) fabrication always results in tolerance stack-up due to individual parameter/dimensional variations. This is not an issue with *in-situ* fabrication, since joints and end-effectors are placed in the workspace with a known absolute accuracy.

- Gaps and clearances in joints fabricated *in-situ* can be directly controlled in the geometry of the support structure. In conventional fabrication, these features are secondary consequences of the mating/fitting process.

- Conventional error analysis does not explicitly allow for the consideration of variable accuracy within the process workspace. Thus, the configuration (or *pose*) in which a mechanism is fabricated is irrelevant to the analysis.

These differences are accounted for in the general abstract model for *in-situ* fabrication and the associated error analysis techniques presented below.

3.3.1 An Abstract Model for In-Situ Fabrication

The main difference between conventional error analysis, and error analysis for *in-situ* fabrication lies in the form of the inputs into the model. *In-situ* fabrication is a process that proceeds by inserting joints and end-effectors into a workspace, and forming links around these embedded components. Thus, the input to the error model is the *variability of the position and/or orientation of the embedded components, as a function of their location in the build-workspace.* Conventional error-analysis treats parametric variability (i.e. variability in link-lengths etc.) as a given constant input. *In-situ* error analysis estimates parametric variability for each build configuration from the location variability of the joints that make up the linkage. The parametric variability is determined by the sensitivity of each parameter to the joint positions and orientations at a given build pose. An important observation is that the mechanism parameters that result from such fabrication are not independent, but pair-wise correlated. This is because multiple (adjacent) parameters depend upon the same independent inputs (i.e. the joint positions and orientations). Although several parameters can all be adjacent to each other if they share a common joint, their correlation is still taken pair-wise since covariance is defined on random variable pairs. The degree of correlation depends upon the configuration in which the mechanism is fabricated (also called the *build pose*). The output variability, in turn, is determined by the sensitivity of the output function to the mechanism parameters at each operating configuration. Figures 3.9 and 3.10 illustrate the fundamental differences between the two scenarios, for the simple case of a four-bar mechanism.

For linkage error-analysis, *in-situ* fabrication is modeled as a sequence of joint-insertions into a non-homogeneous, non-isotropic, 3-D Cartesian workspace. One can think of this as an abstraction of a robot-arm inserting pre-fabricated joints into a workspace, or alternately, invoking a "joint-subroutine" (which manufactures a high-precision joint) at a given workspace location. Once a joint is inserted, the

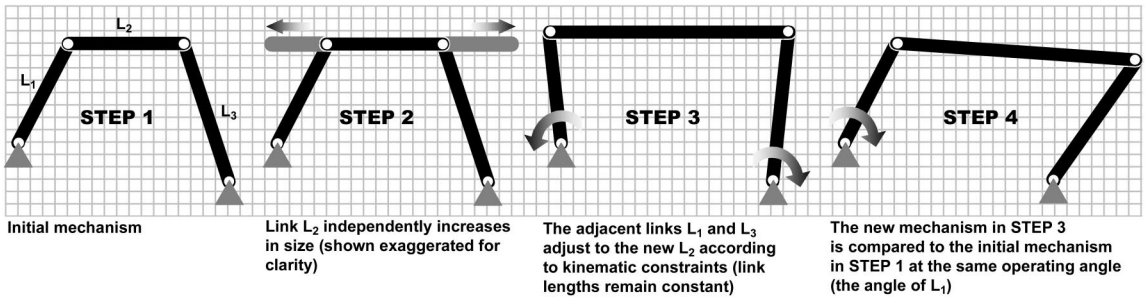

Figure 3.9: Conventional error analysis for link-length variation in a simple 4-bar.

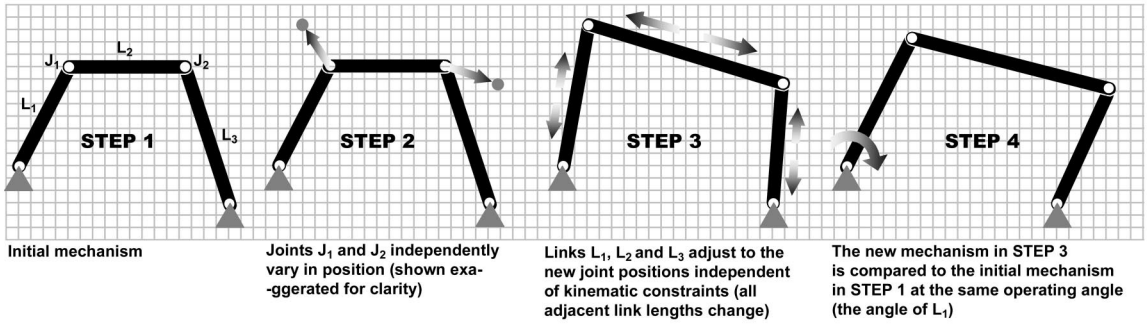

Figure 3.10: *In-situ* error analysis for joint position variation in a simple 4-bar.

adjoining link-bodies are fabricated around the joint without affecting or altering the joint position and orientation.

Frames and Notation

We assign a global workspace datum frame ($OXYZ$) and local datum frames ($o_i x_i y_i z_i$) associated with each feature of interest, typically joints and end-effectors (see Figure 3.11). Without loss of generality, it can be assumed that the z-axis of the global frame is aligned with the process growth direction (e.g. vertical, or spindle-axis). If the feature of interest is a joint, then it is assumed that the local joint z-axis (z_i for the i^{th} joint) is aligned with the joint-freedom axis (i.e. nominal pin/shaft axis for revolute joints, direction of translational motion for prismatic joints etc.). The direction of the x-axis of the i^{th} frame (x_i) is taken as that of the common normal between the i^{th} and (adjacent) $i-1^{th}$ nominal joint axes.

Typically, the position and orientation of each feature frame is specified in the global frame, and the feature geometry (e.g. joint clearance characteristics) is specified in the local frame. The nominal location of the origin in the i^{th} local frame is represented as the position vector $\mathbf{p}_i$ in the global frame (or alternately, as the

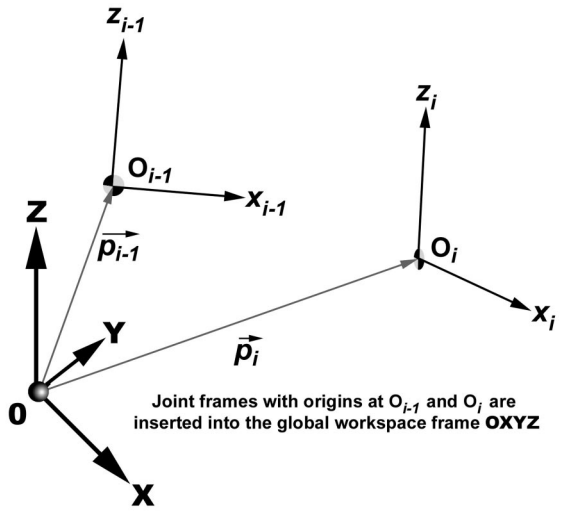

Figure 3.11: Frames and notation for the abstract model of *in-situ* fabrication.

homogeneous coordinates $[x_i, y_i, z_i, 1]$), and the nominal orientation of the i^{th} frame is represented by the direction vector $\mathbf{z}_i$ (with direction numbers $[l_i, m_i, n_i]$). Alternately, the z-axis of the joint frame can be uniquely represented in a global frame in terms of its Plücker (Stolfi, 1991) coordinates $(\mathbf{Q}_i, \mathbf{Q'}_i)$, where:

$$\mathbf{Q}_i \equiv [q_{1i}, q_{2i}, q_{3i}] \tag{3.17}$$

are the direction numbers, and:

$$\mathbf{Q'}_i \equiv \mathbf{p}_i \times \mathbf{Q}_i \equiv [q'_{1i}, q'_{2i}, q'_{3i}] \tag{3.18}$$

is the moment vector of the line. Furthermore, we can let $q_{1i}^2 + q_{2i}^2 + q_{3i}^2 = 1$ without any loss of generality, making these coordinates the same as the (more popular) *direction cosines* of the line.

Thus, using this representation, the nominal configuration ($\mathcal{C}^{nom}$) of a mechanism can be represented in terms of the local frame positions and orientations as:

$$\mathcal{C}^{nom} \equiv \{(\mathbf{p}_i^{nom}, \mathbf{z}_i^{nom})\};\ \ i = 1, 2, \ldots n \tag{3.19}$$

or alternately, in terms of the joint-axis Plücker coordinates as:

$$\mathcal{C}^{nom} \equiv \{(\mathbf{Q}_i, \mathbf{Q'}_i)\};\ \ i = 1, 2, \ldots n \tag{3.20}$$

Fabrication proceeds by embedding (or constructing) non-ideal joints - with position, orientation and clearance errors - at the given nominal locations. By quantifying the extent of these errors, it is possible to predict overall performance errors in mechanisms fabricated *in-situ*. The complete procedure is described in later sections (Sections 3.3.2 and 3.3.3).

Heterogeneous Workspace Modeling

For modeling variable fabrication accuracy within the process workspace, we assume that we have a *precision function* (τ) that returns the variability region $\mathcal{R}$ of a joint in the build space, given the nominal position and orientation, and other process parameters (π). The variability region is simply a worst-case or stochastic characterization of the variation in frame position and orientation, given its nominal location and other process-specific parameters. While this methodology extends to the general spatial scenario, it is illustrated here with a simple planar example.

In the planar case, the orientations of the joint axes (i.e. $\mathbf{z}_i$) are discarded, as all joint axes are assumed parallel. Given a nominal joint location $\mathbf{p}^{nom} \equiv (x^{nom}, y^{nom})$, the precision function returns a region $\mathcal{R}$ as follows:

$$\mathcal{R} = \tau(x^{nom}, y^{nom}, \pi) \tag{3.21}$$

In deterministic worst-case analysis, this function returns the extremal positions of the region in which the actual joint lies, as follows:

$$\mathcal{R} = [worst-case, x^{min}, x^{max}, y^{min}, y^{max}] \tag{3.22}$$

Similarly, in stochastic analysis, the function returns a probability distribution that describes the position of the point as a random variable, as follows:

$$\mathcal{R} = [normal, \mu_x, \sigma_x^2, \mu_y, \sigma_y^2] \tag{3.23}$$

In the most general case, $\mathcal{R}$ is a closed region of arbitrary geometry within which the actual joint position (x, y) lies with a known probability distribution. By applying the precision function τ to all the joint and coupler points (x_i^{nom}, y_i^{nom}) in a planar

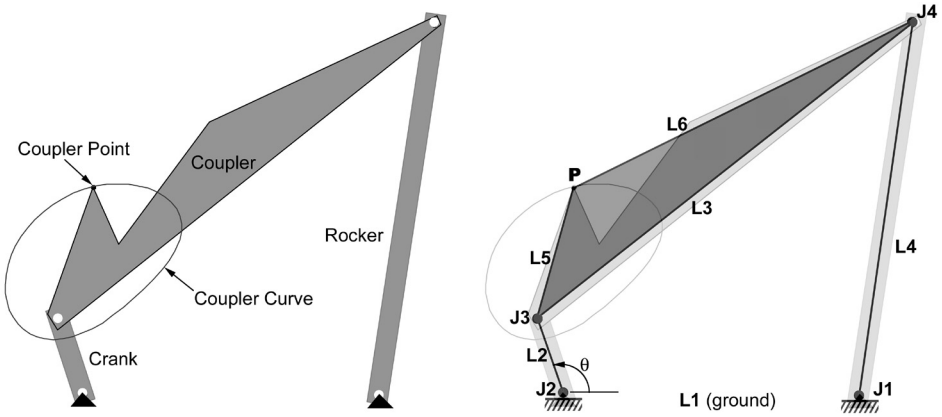

Figure 3.12: Actual and schematic diagrams of the planar 4-bar crank-rocker mechanism used as an example in this thesis. The parameter values are: $L_1 = 15cm, L_2 = 5cm, L_3 = 25cm, L_4 = 20cm, L_5 = 7.5cm, L_6 = 20cm$ (after Mallick and Dhande, 1987).

mechanism, we get joint variability regions $\mathcal{R}_i$ as:

$$\mathcal{R}_i = \tau(x_i^{nom}, y_i^{nom}, \pi) \tag{3.24}$$

In other words, the regions $\mathcal{R}_i$ determine the characteristics of the interval or random values that represent the variable nature of the joint locations. The mechanism parameters ϕ_i are functions (e.g. distance function of the form $\phi_i = \{\sum(x_i - x_j)^2\}^{\frac{1}{2}}$) of the positions and orientations, and the parametric variability is a function of the joint variability regions ($\mathcal{R}_i$), all at the given build configuration ($\mathcal{C}_b$):

$$\Delta_{\phi_i} = \Delta_{\phi_i}(\mathcal{R}_1, \mathcal{R}_2, \ldots \mathcal{R}_n); \;\; i = 1, 2, \ldots n \tag{3.25}$$

Error analysis involves estimating the variability in the link parameters ϕ_i using the above equation, and then applying sensitivity analysis techniques to determine the error in the output function (at various operating configurations) for a mechanism that is fabricated *in-situ*. In the following sections, this process is described, and illustrated using the specific planar 4-bar mechanism shown in Figure 3.12. The mechanism parameter values were chosen to allow checking of results with earlier published work (Mallik and Dhande, 1987). To aid with discussion of the results, the mechanism is also shown in various configurations (i.e. specific values of the driving angle θ) in Figure 3.13. In Section 3.3.4, the analysis has been extended to cover general spatial mechanisms.

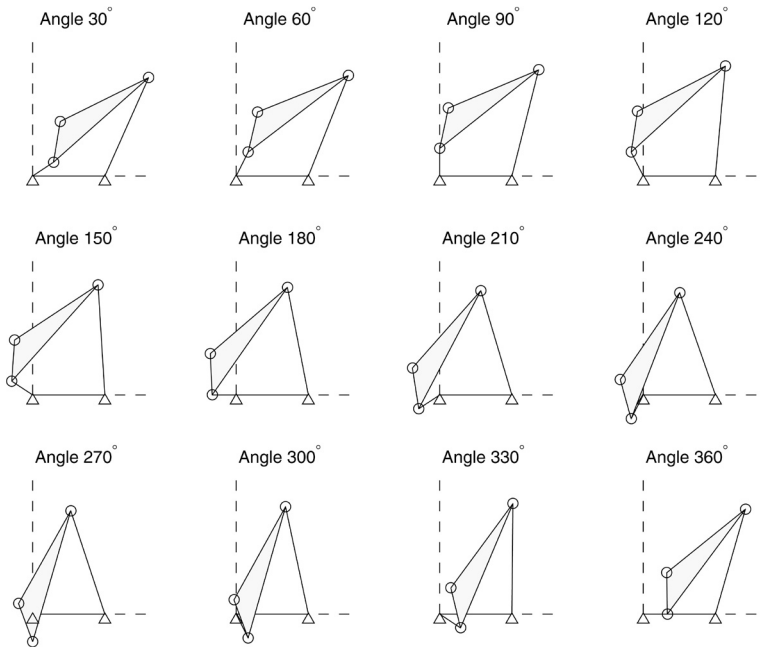

Figure 3.13: Multiple positions of the example 4-bar, 30 deg increments of θ.

3.3.2 Worst-Case, Deterministic Error Estimation

Worst case error estimation for *in-situ* fabrication proceeds in two stages. First, at a candidate build pose $\mathcal{C}_b$, all the worst case parameter values (ϕ_i^{WC}) are evaluated by choosing, in sequence, all possible combinations of the worst-case fabrication input values $\{(\mathbf{p}_i^{WC}, \mathbf{z}_i^{WC})\}$. The precision function (Equation 3.24) returns these extremal values of the position of each joint, given the mechanism nominal build pose. For k fabrication input variables, this process generates 2^k candidate mechanisms at each pose $\mathcal{C}_b$. Figure 3.14 shows the example of a mechanism with square precision regions, and a candidate worst-case build configuration.

In the second stage, the error in the output function ($\mathbf{y}$) is evaluated for each one of the candidate mechanisms produced in the first stage. This calculation is repeated for all operating angles, for every build pose. Overall, if c operating and build positions are considered for a mechanism with m independent degrees of freedom, and k independent fabrication variables, the determination of worst-case error boundaries for the output has computational complexity $O(2^k mc^2)$. Dynamic programming approaches (Fenton *et al*, 1989) can significantly improve upon the computational complexity, but need to be re-stated appropriately for each specific problem.

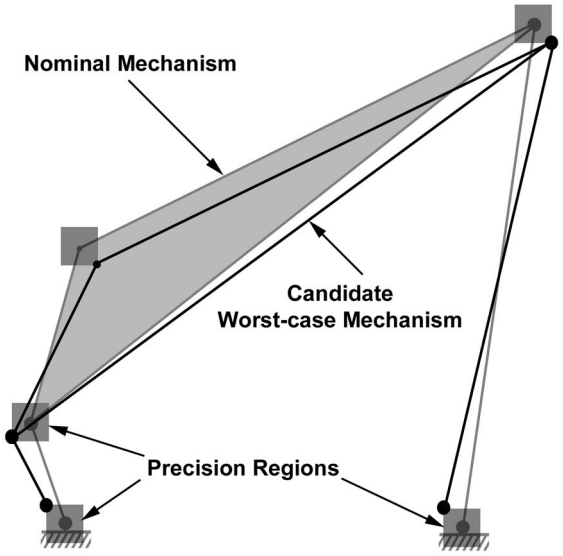

Figure 3.14: Example of worst-case build configuration.

Figure 3.15 illustrates the results of the worst-case error estimation for the example 4-bar mechanism for a few candidate build poses. The coupler-point location is shown as a cloud of points in the vicinity of the nominal coupler-point, with each point corresponding to one combination of worst-case joint locations. Figure 3.16 plots the worst-case variability of the coupler-point location (i.e. half the perimeter of the bounding box for each cloud in Figure 3.15) as a function of the build configuration.

3.3.3 Stochastic Error Estimation

The worst-case method presented in the previous section is both overly conservative, and computationally expensive for most applications. By contrast, a stochastic approach results in superior error estimates in constant-time (as opposed to exponential or linear time for worst-case methods). However, the conventional approach to stochastic error estimation needs modification in order to be applicable to *in-situ* fabrication.

In this analysis, we assume that the joint coordinates (positions and orientations) are independent random variables with known distributions. Given the nominal location of a joint i, the precision function (Equation 3.24) returns the appropriate distribution for its actual location. Mechanism parameters (like link-lengths, joint angles, joint offsets and skew angles) are functions of the independent, random joint

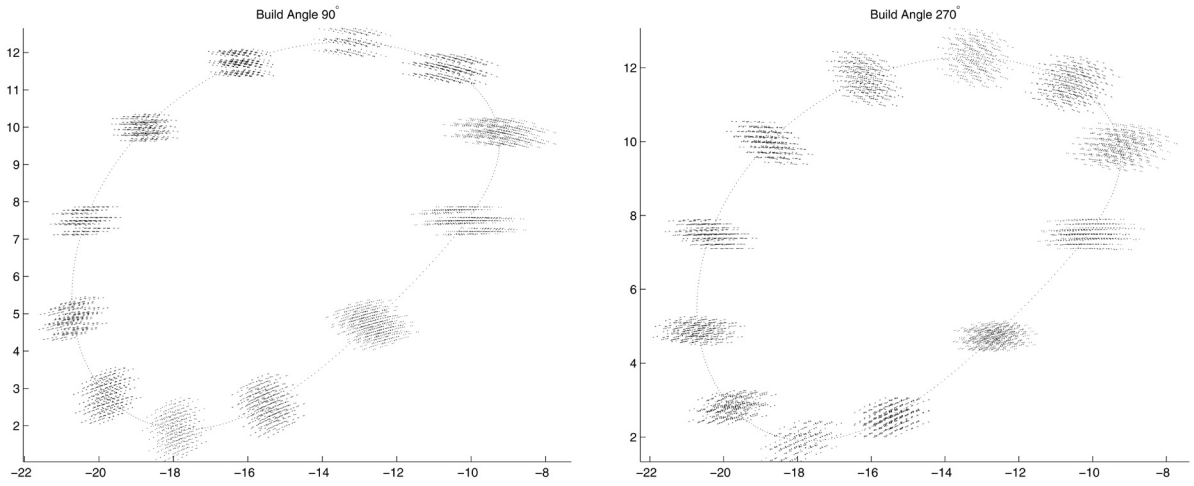

Figure 3.15: Worst case coupler-point positional error, plotted on the coupler path.

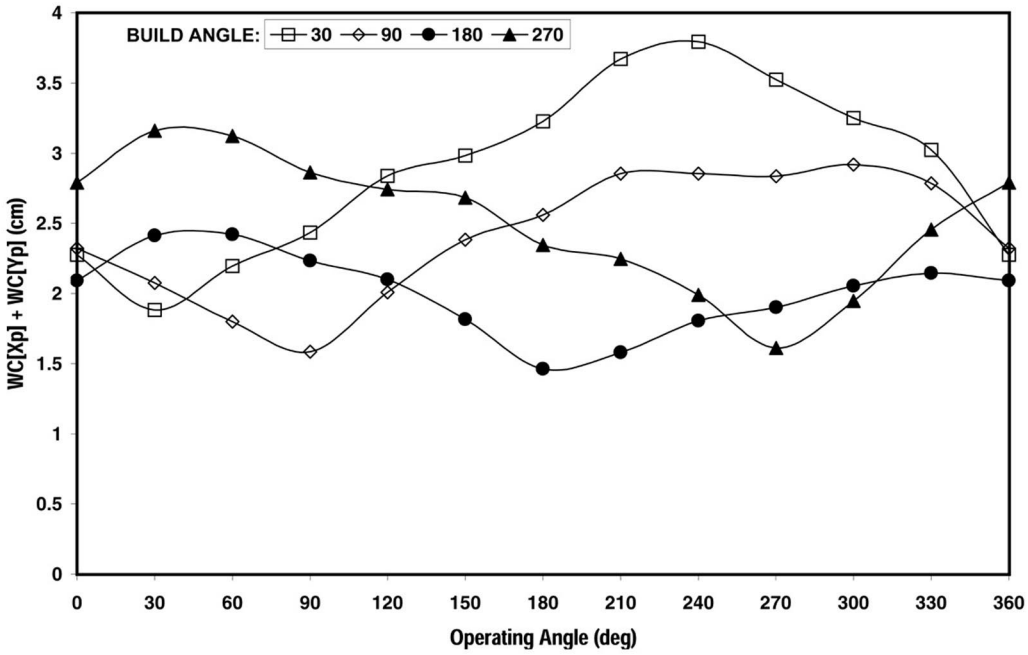

Figure 3.16: Total worst-case coupler-point positional errors, plotted against operating angle. The error values can be compared with 3σ stochastic errors (computed in the next section).

coordinates. This, in turn, makes the parameters themselves random variables which are pairwise correlated (being jointly dependent on the same independent variables). The output, then, is a complex function of correlated random variables.

The probability distribution (i.e. PDF) of a known function of random variables can, in principle, be derived exactly from the given, analytically specified, distributions of the original random variables. However, in practice, the exact derivation is intractable in the absence of certain simplifying assumptions, due to the complexity of the algebra involved. For a weakly non-linear function of independent and uncorrelated random variables, the mean and variance of the function can be approximated directly from the mean and variance of the underlying random variables, as illustrated in Equations 3.15 and 3.16. When the simplifying assumptions (i.e. independent and uncorrelated) do not hold, the function properties need to be determined analytically by integrating the joint-PDF (see Equation 3.28), by modifying the approximation techniques to include the effects of correlation, or by using Monte Carlo simulation techniques. In general, the analytical technique is not tractable for all but the simplest of cases. In the following section, an improved approximation technique for the estimation of the moments of a weakly-nonlinear function of correlated random variables is developed and applied to the problem of stochastic error estimation for mechanisms that are fabricated *in-situ*. The results are compared to those obtained by Monte Carlo simulation.

Estimating the parametric variance

Equation 3.15 can be applied directly to the mechanism parameters (ϕ_i), given the stochastic properties (i.e. mean and variance) of the joint variables (x_k). The parameters are simple functions (i.e. sums, products and differences) of the joint variables, which are assumed independent and uncorrelated. Moreover, the variance in any joint variable can be assumed to be much smaller than its mean (for macro-scale devices), since the precision of fabrication equipment is typically several orders-of-magnitude smaller than the part dimensions. This implies that the variability in the mechanism parameters can be approximated as a linear function (weighted by the sensitivity coefficients) of the variability in the input, as follows:

$$\sigma^2_{\phi_i} \approx \sum_k (\frac{\partial \phi_i}{\partial x_k})^2_\mu \sigma^2_{x_k};\ \ i = 1, 2, \ldots n \tag{3.26}$$

where $\sigma^2_{\phi_i}$ is the variance of the i^{th} mechanism parameter, and x_k represents the k^{th} joint variable, and $\sigma^2_{x_k}$ represents the variance of the k^{th} joint variable. If the joint variables follow Normal distributions (typical for most physical random processes involving many noise factors), then the parameters too will follow a Normal distribution.

The parameters ϕ_i, however, are correlated random variables. The correlation coefficients (ρ_{ij}) of each parameter pair (ϕ_i, ϕ_j) can be approximated using the sensitivity coefficients as follows:

$$\rho_{ij} \approx \frac{\sum_k (\frac{\partial \phi_i}{\partial x_k})_\mu (\frac{\partial \phi_j}{\partial x_k})_\mu \sigma^2_{x_k}}{\sigma_{\phi_i} \sigma_{\phi_j}} \tag{3.27}$$

Figure 3.17 compares the first order estimate of link-length variability against that obtained by Monte Carlo simulation, for four of the links in the example 4-bar in Figure 3.12. Figure 3.18 compares the pairwise correlation coefficients obtained for the approximation in Equation 3.27 against that obtained by Monte Carlo simulation, for the same four links of the example 4-bar. In both cases, the approximation yields results that are very close to the simulation - illustrating the validity of the assumption of independence.

Estimating the output variance

In the previous section, we have established a method for efficiently estimating the variance and correlation coefficients of the parameters of a mechanism that has been fabricated *in-situ*. Our real interest in this treatment, however, is in the behavior of the output function ($\mathbf{y}$) during operation. As indicated earlier, the output is a function of the mechanism parameters which, being dependent functions of the given independent random variables (i.e. the joint variables), are themselves correlated random variables. Thus, the simplifying assumptions which could be made for the estimation of parametric variability are not applicable for the estimation of output variability. No simple analytical technique exists for the determination of the distribution of a general function of correlated random variables. In theory, the cumulative distribution function of the output can be evaluated as follows:

$$P_Y(y) = \int_{-\infty}^{\phi_1} \cdots \int_{-\infty}^{\phi_n} f(\phi_1, \ldots \phi_n).p_{\Phi_1 \ldots \Phi_n}(\phi_1, \ldots \phi_n)\, d\phi_1 \ldots d\phi_n \tag{3.28}$$

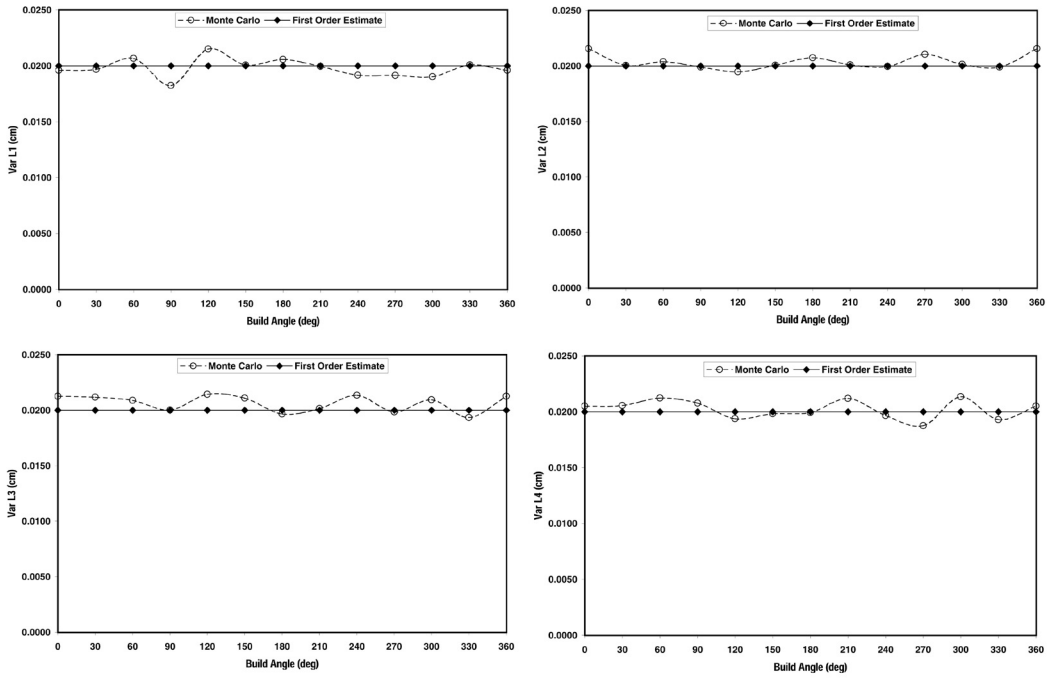

Figure 3.17: First order estimates of the link-length variance compared to the results of a Monte Carlo simulation.

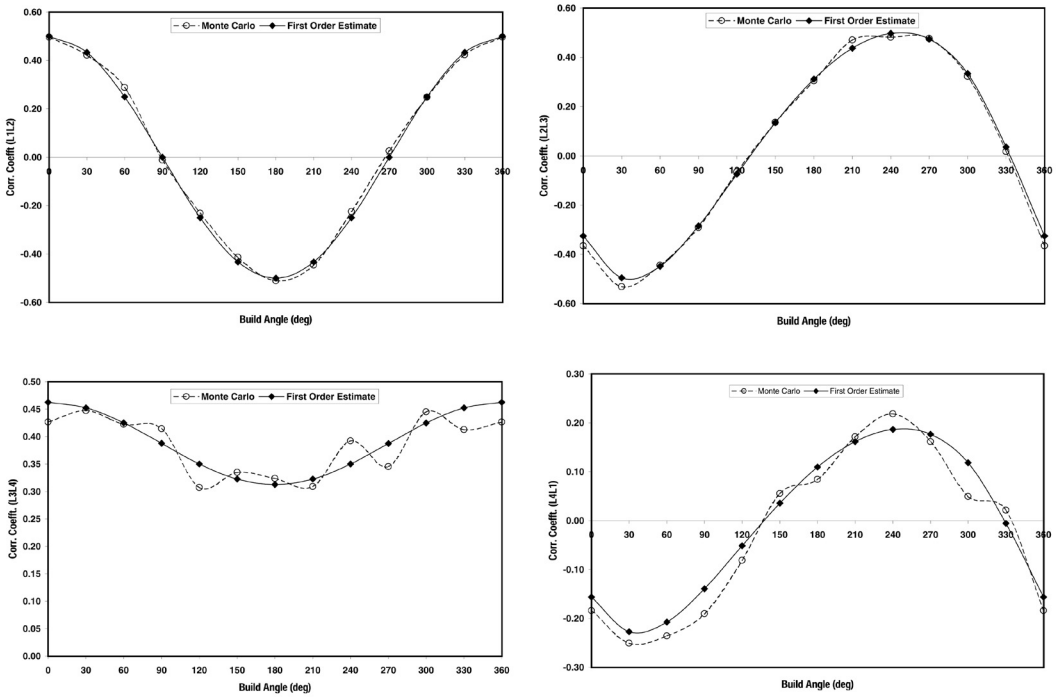

Figure 3.18: Pairwise correlation coefficients of the link lengths - first-order results compared to the Monte Carlo simulation.

However, the joint distribution function $p_{\Phi_1 \ldots \Phi_n}(\phi_1, \ldots \phi_n)$ is not easy to determine when the random variables ϕ_i are correlated. Furthermore, the upper limits of the multiple integral need to be expressed in terms of the output variables, which is not analytically feasible except for the simplest of cases.

The assumption that makes this problem tractable, once again, is that of weak-nonlinearity in the output function. In other words, if we can assume that the second and higher-order terms in the Taylor Series expansion of the output function can be discarded, then it is possible to derive an expression that directly produces an approximate estimate for the output variance, given the variance ($\sigma^2_{\phi_i}$) and correlation coefficients (ρ_{ij}) of the mechanism parameters. Furthermore, if the total number of parameters are large (i.e. $n > 5$), then, according to the Central Limit Theorem, the output function will follow an approximately Normal distribution, regardless of the individual parameter distributions (Feller, 1957). Thus, by making the linear approximation, we completely side-step the evaluation of the extremely problematic multiple integral in Equation 3.28. The derivation of the approximation equation is given in Appendix A, and the final result is summarized below:

$$\sigma^2_{\mathbf{y}} \approx \sum_{i=1}^{n} (\frac{\partial f}{\partial \phi_i})^2_{\mu} \sigma^2_{\phi_i} + 2 \sum_i \sum_j \frac{\partial f}{\partial \phi_i}]_{\mu} \frac{\partial f}{\partial \phi_j}]_{\mu} \rho_{ij} \sigma_{\phi_i} \sigma_{\phi_j} \tag{3.29}$$

where $i = 1, 2, \ldots n$ and $j \neq i$. In the special case where only *adjacent* parameters share a joint variable, $\rho_{ij} = 0$ for non-adjacent parameters, and the above equation needs to be evaluated only for the cases where $j = i - 1$. Note that all the sensitivity coefficients in the above equation are evaluated at the nominal operating configuration (μ) of the mechanism. Comparison of Equation 3.29 and Equation 3.15 reveals that they differ only in the second term on the RHS. This term, then, is the adjustment term that accounts for the correlation effect that results from the co-dependence of the mechanism parameters on the same joint coordinates.

Summarizing, the first order approximations are the only tractable, general purpose estimates of the output function variability. Equation 3.29 indicates that the output error depends upon the output function sensitivity coefficients (evaluated at the nominal operating configuration), the parametric variances, and the pairwise correlation coefficients of the parameters. The parametric variances and the correlation coefficients are functions of the mechanism build pose, during *in-situ* fabrication. Equation 3.29 succinctly relates the fabrication workspace to the operational

workspace, thereby presenting us with a method for evaluating the optimal build pose, given an operational tolerance specification. This issue is explored in more detail in Chapter 4.

Figure 3.19 compares the first order estimated coupler-point error for the example 4-bar fabricated *in-situ* against the Monte Carlo simulations of the same quantity. Also included are the estimates using the conventional approach, which does not include the consideration of correlation effects. Comparisons can also be made between these results, and those of the worst case error estimate presented earlier (see Figure 3.16). The worst-case and stochastic estimates for a specific build angle are compared in Figure 3.20. It is clear from the comparison that the worst-case method is significantly more conservative in its estimation of output error.

Figure 3.21 plots the simulated coupler-point variance against the number of random trials. This helps with the estimation of the minimum number of trials needed in order for the random estimates to converge to a steady value (between 4000 and 10,000 in this case).

3.3.4 Extension to Spatial Parameters

The extension of the error analysis techniques presented above to spatial systems is straightforward, once the essential concepts have been established. Spatial systems are traditionally described in terms of the Denavit-Hartenberg parameters (see Section 3.2.1), or modifications thereof. Spatial error analysis is the process of relating variability in the spatial parameters to errors in the output function.

For *in-situ* fabrication, parametric variability is not directly available, but is a function of the position and orientation variability in joint placement. Earlier sections in this chapter have dealt with the issue of estimating the output variance, given the stochastic characteristics of the joint variables. The approach has been illustrated using a planar example, and the technique is extended here to cover general spatial mechanisms. The basic issue that remains to be addressed for the spatial case is that of explicitly expressing the spatial parameters illustrated in Figure 3.4 in terms of the joint-frame positions illustrated in 3.11. This is a fairly simple problem in the analytical geometry of three dimensions (Sommerville, 1959).

Given the origin coordinates $(\mathbf{p}_i, \mathbf{p}_j, \mathbf{p}_k)$ and the direction numbers $(\mathbf{z}_i, \mathbf{z}_j, \mathbf{z}_k)$ of the axes of three *adjacent* spatially located joints, the modified Denavit-Hartenberg parameters of the j^{th} joint can be expressed in terms of the joint Plücker coordinates

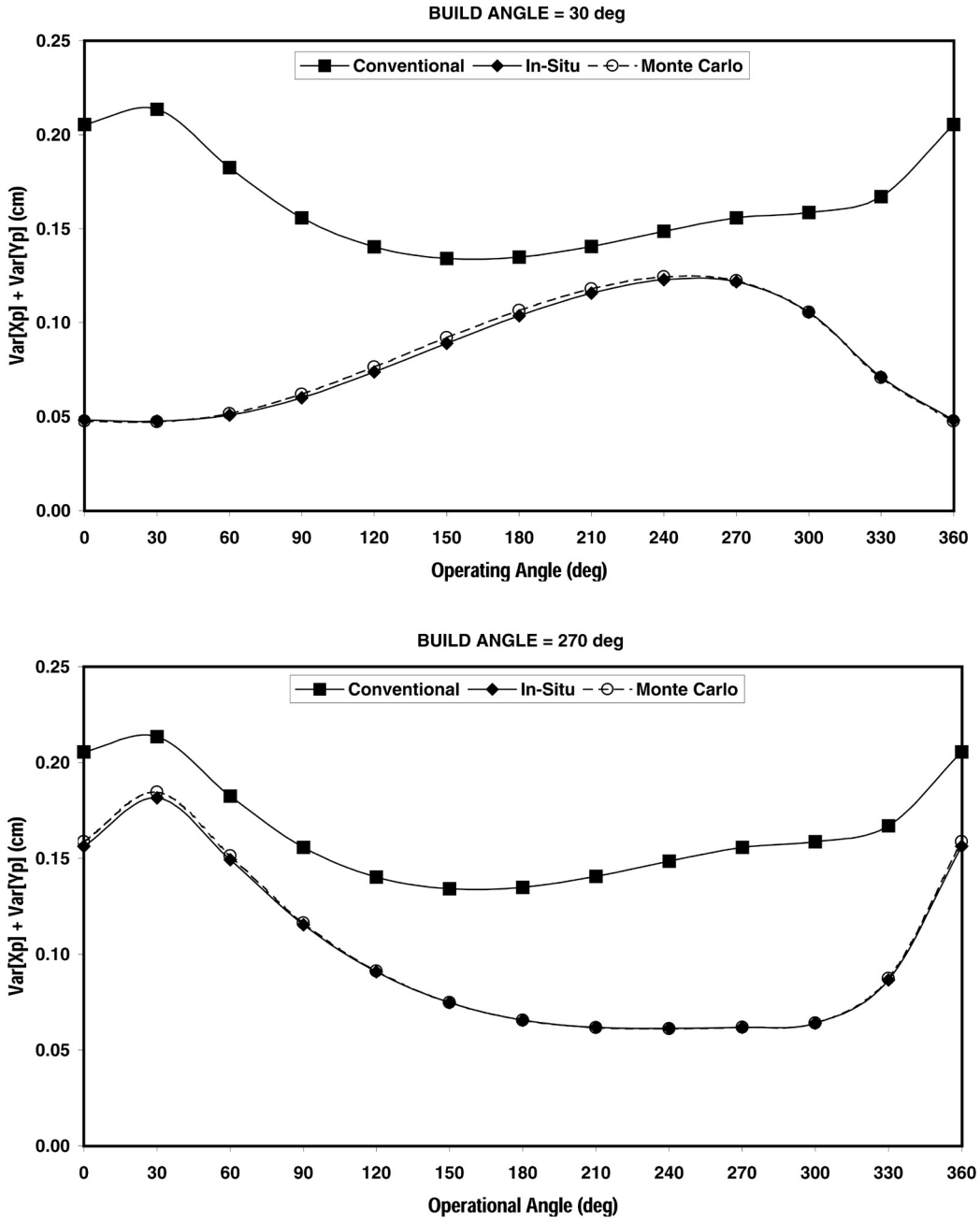

Figure 3.19: First order estimates of coupler-point variance for the planar crank-rocker (Figure 3.12), conventional and *in-situ*, compared to simulated results. Results for additional build angles are presented in Appendix C.

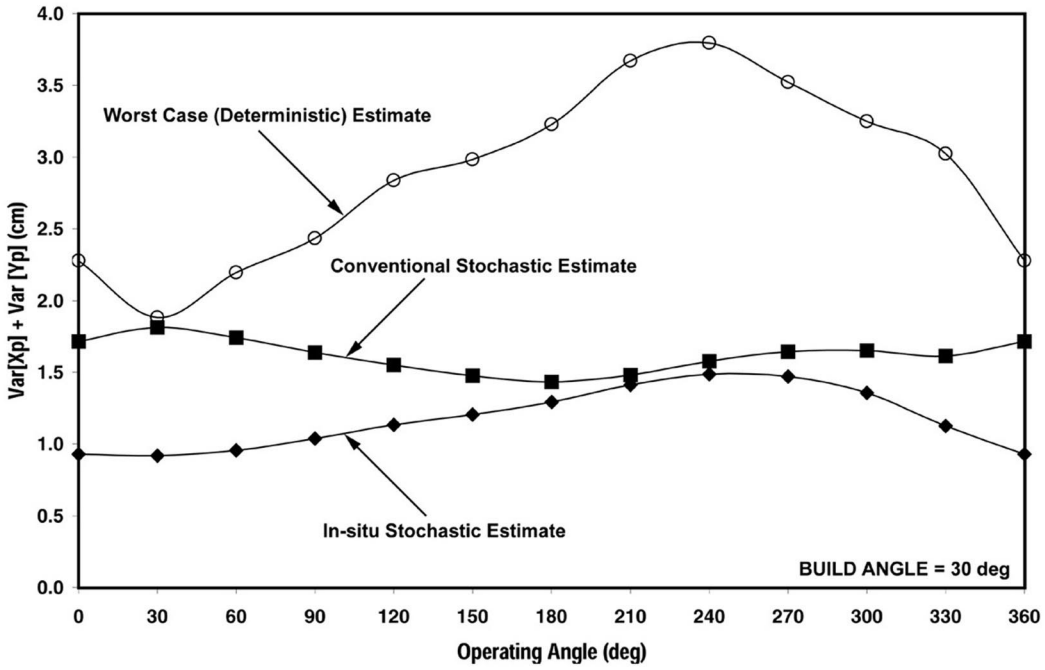

Figure 3.20: Comparison of 3σ stochastic and worst-case (deterministic) error estimates.

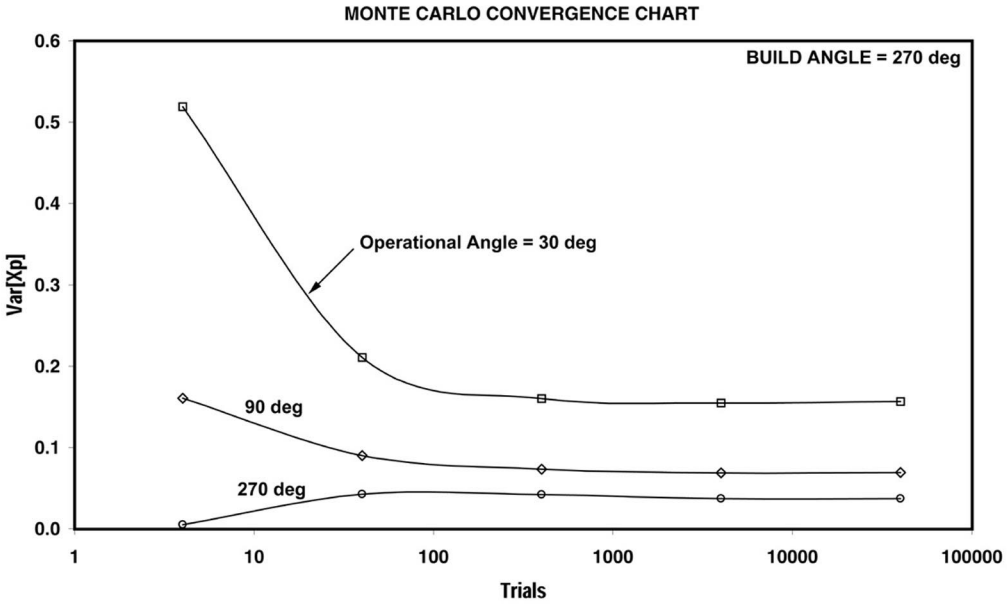

Figure 3.21: Convergence rate of the Monte Carlo simulation.

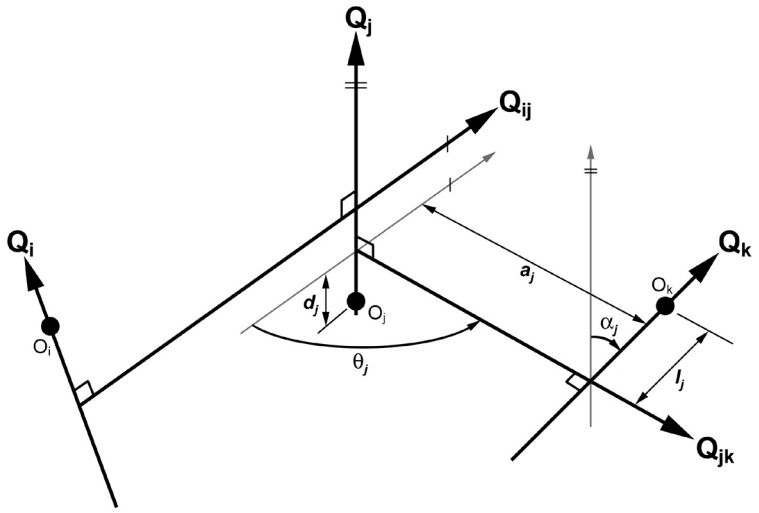

Figure 3.22: Notation for the derivation of modified Denavit-Hartenberg parameters from joint Plücker coordinates.

(see Section 3.3.1) of the three joint axes $(\mathbf{Q}_i, \mathbf{Q'}_i)$, $(\mathbf{Q}_j, \mathbf{Q'}_j)$ and $(\mathbf{Q}_k, \mathbf{Q'}_k)$, and those of the two common normals $(\mathbf{Q}_{ij}, \mathbf{Q'}_{ij})$ and $(\mathbf{Q}_{jk}, \mathbf{Q'}_{jk})$. This notation is illustrated in Figure 3.22. The direction coordinates of the common normal are given as:

$$\begin{aligned} \mathbf{Q}_{ij} &\equiv [q_{1ij}, q_{2ij}, q_{3ij}] \ \ where \\ q_{1ij} &= q_{2i}q_{3j} - q_{3i}q_{2j} \\ q_{2ij} &= q_{3i}q_{1j} - q_{1i}q_{3j} \\ q_{3ij} &= q_{2i}q_{3j} - q_{3i}q_{2j} \end{aligned} \tag{3.30}$$

and the moments of the common normal between axes i and j are given as follows (this can be extended to j and k by symmetry):

$$\begin{aligned} \mathbf{Q'}_{ij} &\equiv [q'_{1ij}, q'_{2ij}, q'_{3ij}] \ \ where \\ q'_{1ij} &= \frac{\mathbf{Q}_{ij} \cdot [(q_{2ij}q_{3j} - q_{3ij}q_{2j})\mathbf{Q'}_i - (q_{2ij}q_{3i} - q_{3ij}q_{2i})\mathbf{Q'}_j]}{\|\mathbf{Q}_{ij}\|^2} \\ q'_{2ij} &= \frac{\mathbf{Q}_{ij} \cdot [(q_{3ij}q_{1j} - q_{1ij}q_{3j})\mathbf{Q'}_i - (q_{3ij}q_{1i} - q_{1ij}q_{3i})\mathbf{Q'}_j]}{\|\mathbf{Q}_{ij}\|^2} \\ q'_{3ij} &= \frac{\mathbf{Q}_{ij} \cdot [(q_{1ij}q_{2j} - q_{2ij}q_{1j})\mathbf{Q'}_i - (q_{1ij}q_{2i} - q_{2ij}q_{1i})\mathbf{Q'}_j]}{\|\mathbf{Q}_{ij}\|^2} \end{aligned} \tag{3.31}$$

The modified Denavit-Hartenberg parameters for link j can now be written as:

$$\begin{aligned}
\alpha_j &= \arcsin(\|\mathbf{Q}_{jk}\|) \\
a_j &= \frac{\mathbf{Q}_j \cdot \mathbf{Q'}_k + \mathbf{Q}_k \cdot \mathbf{Q'}_j}{\sin(\alpha_i)} \\
d_j &= (\mathbf{p}_k - \mathbf{p}_j) \cdot \frac{(\mathbf{Q}_{jk} \times \mathbf{Q}_j)}{\|\mathbf{Q}_{jk}\|^2} \\
l_j &= (\mathbf{p}_j - \mathbf{p}_k) \cdot \frac{(\mathbf{Q}_{jk} \times \mathbf{Q}_j)}{\|\mathbf{Q}_{jk}\|^2} \\
\theta_j &= \arcsin(\|\mathbf{Q}_{jk} \times \mathbf{Q}_{ij}\|)
\end{aligned} \tag{3.32}$$

Since the mechanism parameters are now known in terms of the joint positions and orientations, it is possible to estimate the error in output function given the variability in joint location using techniques similar to those outlined for the planar case earlier. The process proceeds by writing the product of homogeneous transformation matrices (three translations and two rotations), that transform one local coordinate frame to the adjacent frame (the j^{th} frame to the k^{th} frame in this case), as follows:

$$\mathbf{A}_k^j = \mathcal{T}(0,0,d_j) \times \mathcal{R}(\mathbf{z}_j,\theta_j) \times \mathcal{T}(a_j,0,0) \times \mathcal{R}(\mathbf{x}_j,\alpha_j) \times \mathcal{T}(0,0,l_j) \tag{3.33}$$

Next, the first-order Taylor Series approximation of the transformation matrix is written as follows:

$$\Delta_{\mathbf{A}_k} = \frac{\partial \mathbf{A}_k^j}{\partial d_j}\Delta_{d_j} + \frac{\partial \mathbf{A}_k^j}{\partial \theta_j}\Delta_{\theta_j} + \frac{\partial \mathbf{A}_k^j}{\partial a_j}\Delta_{a_j} + \frac{\partial \mathbf{A}_k^j}{\partial \alpha_j}\Delta_{\alpha_j} + \frac{\partial \mathbf{A}_k^j}{\partial l_j}\Delta_{l_j} \tag{3.34}$$

Each of the parameter variabilities (i.e. $\Delta_{d_j}, \Delta_{\theta_j}, \Delta_{a_j}, \Delta_{\alpha_j}$ and Δ_{l_j}) are now either interval (for worst-case analysis) or random (for stochastic analysis) parameters, the variances and correlation coefficients of which can be obtained using the relationships derived in Equation 3.32.

3.3.5 Clearance Errors for In-Situ Mechanisms

Clearances in "embedded" joints influence output errors in *in-situ* mechanisms in exactly the same manner as in mechanisms fabricated using conventional techniques. This is because clearance is largely a local joint phenomenon, that is not dependent on the fabrication position of the mechanism. However, clearances in joints that

are fabricated directly by freeform fabrication (as opposed to embedded joints) do present some new issues, which are discussed in this section.

Existing research has rarely, if at all, dealt with the issue of correlated clearance errors when two adjacent pins share the same link (see Section 3.1.2, and Figure 3.2). Most treatments incorrectly assume that clearance errors are always independent random parameters, regardless of mechanism construction. We do not delve here into prediction of clearance errors due to embedded joints, correlated or otherwise, since the issue is not unique to *in-situ* fabrication. It is likely that this problem can be solved by appropriately applying the method for including correlation effects in error analysis, presented in Section 3.3.3 and Equation 3.29. We do, however, explore the case of worst-case error analysis of joints that are fabricated in a free-form manner in the following treatment. The primary observations made in this section are:

- Output link position is typically more sensitive to the geometry of the joint clearance, as opposed to the individual geometries of the the features (e.g. hole and shaft) that create the clearance.
- Clearances are directly manifest in the support structure geometry for *in-situ* fabrication, rather than as a residue of the assembly of mating features.
- Clearance geometry can be controlled more accurately by *in-situ* fabrication than by sequential shape-and-assemble techniques.

Clearance Issues in Freeform Joints

Freeform joints are those that are fabricated *in-situ* along with the rest of the mechanism. Designers of such joints have the option of directly specifying tolerance limits on the geometry of gaps and clearances. This is due to the fact that in processes like Shape Deposition Manufacturing (SDM), clearance features are directly manifest in the geometry of the support structure. In many cases, it is these "shadow" features that most directly and substantially govern the behavior of the artifact being built. Clearly, there are no assemblability issues involved in the use of freeform joints, since the joints are simultaneously manufactured and assembled *in-situ*. Relaxation of the assemblability constraints result in looser manufacturing tolerances and better control over gap geometry. In this section, we illustrate this concept with the example of a simple, isolated pin-joint (or journal bearing). The kinematic behavior of a pin-joint is typically most sensitive to errors in the designed geometry of the

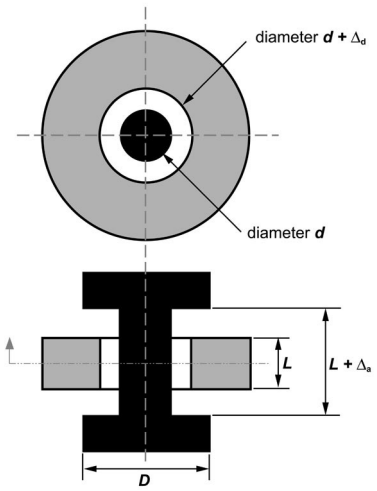

Figure 3.23: A simple, isolated pin-joint with axial and diametral clearances.

gap (i.e. the differential geometry between the hole and shaft), and not the specific geometry of the hole or shaft (Rajagopalan and Cutkosky, 1998)(also see Table 3.2 and Figure 3.25). Here, we explore the link between variability in the gap geometry and predicted behavior, using a simple kinematic fragment. Figure 3.23 shows the typical geometric parameters associated with an isolated pin-joint. The parameters d, D, and L are regular feature sizes, while Δ_a and Δ_d are gap/clearance size parameters. An ideal pin-joint would completely restrict all motion except rotational motion in the plane orthogonal to the joint axis. In a real pin-joint, however, the behavior of the joint depends upon the axial and diametrical clearances that result upon its manufacture. These gaps are not merely manufacturing aberrations, but typically are designed into the joint to facilitate assembly and smooth (low-friction) operation.

Researchers in applied kinematics (Lakshminarayana and Ramaiyan, 1976) (Wang and Roth, 1989) have addressed the problem of determining the maximum positional errors in mechanisms with non-ideal joints. Using their results, it is possible to compute the maximum allowable axial and diametrical clearances given some desired task tolerances and a contact configuration. Figure 3.24 shows one possible configuration, Mode 1-1 in (Wang and Roth, 1989), of an isolated pin-joint with a given allowable tolerance (δ_{max}) at the task location **A**.

Wang and Roth's results can be re-written for the specific cases where the axis of constrained rotation (not the primary rotational axis of the pin) is taken orthogonal to the plane of the paper for all contact modes - with no loss of generality in our

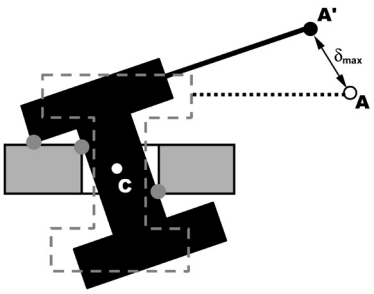

Figure 3.24: A possible contact configuration for the isolated pin-joint.

forthcoming analysis. This provides a simplified view of the maximum positional error (i.e. worst-case error) at the task location based upon the pin geometry.

These results have been summarized for all possible contact modes in Figure 3.1, where **A** is the task location (a point in 3-D Cartesian space), **C** is the geometric center of the shaft, l_{CA} is the Cartesian distance from point **A** to **C**, and δ_{max} is the upper bound on the positional error of the task location. Recall that Δ_a and Δ_d are the axial and diametral clearance parameters as defined in Figure 3.23. At zero positional error, the point **C** on the shaft is lined up with the center of the hole and the hole and shaft axes are collinear. The zero error locations of points **A** and **C** are denoted by **A'** and **C'** respectively. The contact constraint for each mode needs to hold in order to maintain the illustrated contact configuration. The equations in Table 3.1 provide a basis for constraining the geometry of the pin-joint in order to assure that a certain task tolerance (δ_{max}) is achieved. Alternately, given the task tolerance (which depends upon the precision required for the task being performed), one can determine allowable values for axial and diametrical clearances based upon the geometry of the mechanism.

Table 3.2 examines the sensitivity of the positional error to variations in the pin geometry, both for feature parameters (i.e. D, d and L) and gap parameters (Δ_d and Δ_a). Two trends are identifiable from this table. First, based upon the signs of the sensitivity terms, an increase in feature size results in a decrease in maximum positional error while an increase in gap size results in an increase in positional error. Second, given that gap sizes are typically much smaller than feature sizes (i.e. $\Delta_a, \Delta_d \ll D, d, L$), the value of the maximum positional error is much more sensitive to variations in gap sizes than to variations in feature sizes. In short, this preceding analysis establishes the following for the case of the positional accuracy of a simple, isolated pin joint:

MODE	CONTACT CONFIGURATION	CONSTRAINT	MAX. POSITIONAL ERROR
1	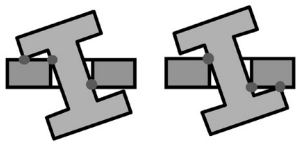	$\frac{\Delta_a}{\Delta_d} > \frac{D}{L}$	$\delta_{\max} = \frac{\Delta_a}{2} + \left(\frac{2l_{CA} - d}{2L}\right)\Delta_d$
2	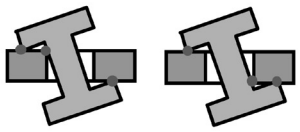	$\frac{\Delta_a}{\Delta_d} < \frac{D}{L}$	$\delta_{\max} = \left(\frac{2l_{CA} - L}{2D}\right)\Delta_a + \frac{\Delta_d}{2}$
3	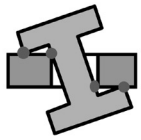	$\frac{\Delta_a}{\Delta_d} = \frac{D}{L}$	$\delta_{\max} = \frac{l_{CA}}{D}\Delta_a$
4	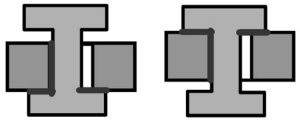	—	$\delta_{\max} = \frac{1}{2}\sqrt{\Delta_a^2 + \Delta_d^2}$

Table 3.1: Maximium positional error at the task location for each contact condition (see Figure 3.24)

- Larger pins with smaller clearances are more accurate (this is a well known rule-of-thumb in mechanical design).
- In manufacturing accurate pin-joints, it is more important to control gap sizes than to control individual feature sizes.

Figure 3.25 graphically illustrates how the task tolerance varies with pin geometry for a specific pin-joint with $D = 0.723in, d = 0.623in, L = 0.625in, l_{CA} = 4in, \Delta_a = 0.004in, \Delta_d = 0.004in$. The aspect ratios used in this example are typical for most applications. The particular values used have been selected from a standard test specimen used to evaluate the fatigue life of a lubricated air-frame bearing as specified in the Thomas Register. In each of the graphs in Figure 3.25, one of the five design parameters is varied, with the others held constant at the design point until the contact condition is lost. Additional geometric and non-negativity constraints also apply (i.e. $D > d$ and $D, d, L, \Delta_a, \Delta_d > 0$).

The example in this section has demonstrated that for the isolated pin-joint, the kinematic behavior of the joint is more sensitive to errors in the designed geometry of the gaps than to errors in the size of the hole and shaft features. It can also be

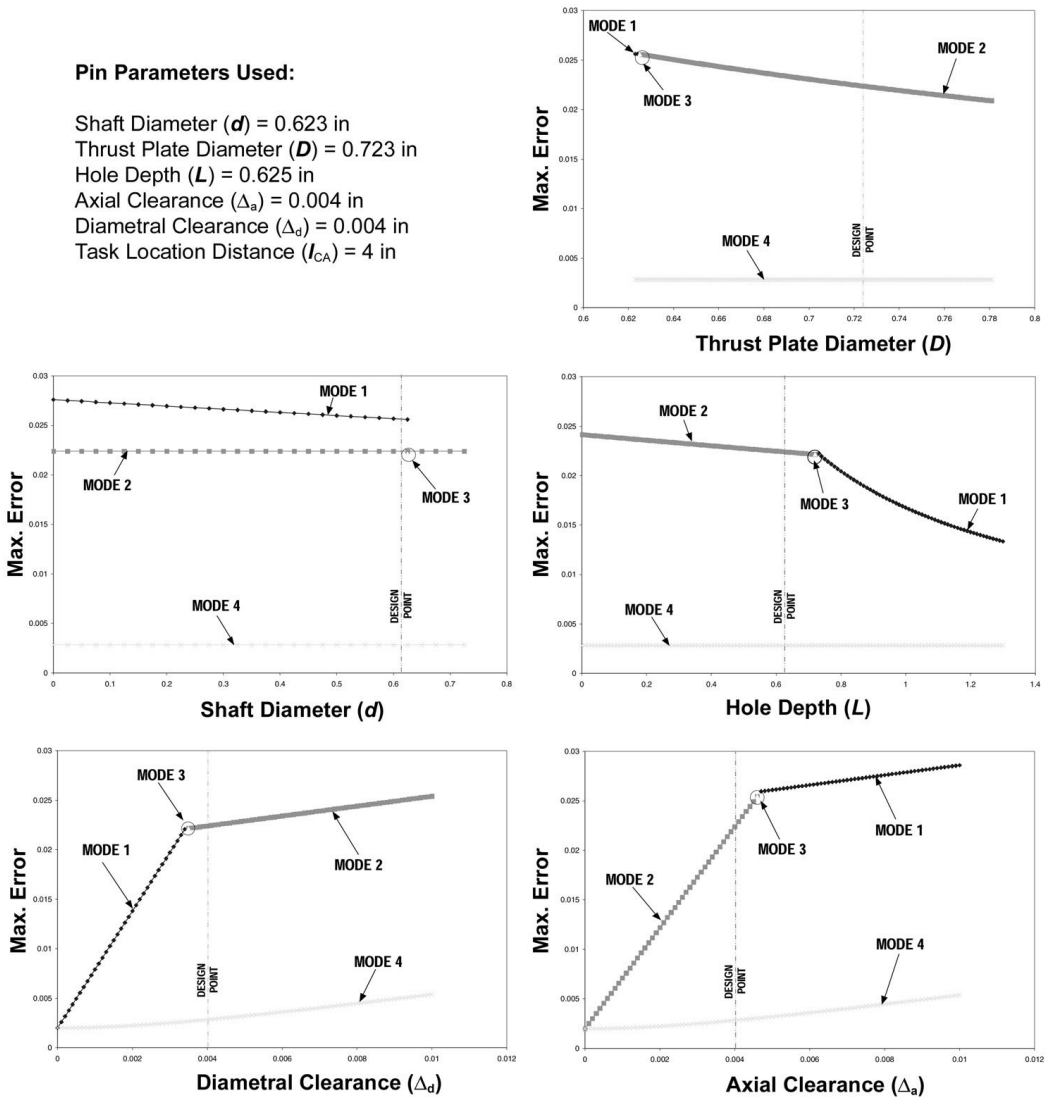

Figure 3.25: Sensitivity of the maximum positional error of the task location to the joint parameters. The modes refer to the contact conditions illustrated in Table 3.1.

MODE	Sensitivity of Task Error to Errors in Geometry				
	$\frac{\partial \delta_{\max}}{\partial D}$	$\frac{\partial \delta_{\max}}{\partial d}$	$\frac{\partial \delta_{\max}}{\partial L}$	$\frac{\partial \delta_{\max}}{\partial \Delta_a}$	$\frac{\partial \delta_{\max}}{\partial \Delta_d}$
1	0	$-\frac{\Delta_d}{2L}$	$-\frac{l_{CA}}{L^2}\Delta_d$	$\frac{1}{2}$	$\frac{2l_{CA}-d}{2L}$
2	$\frac{L-2l_{CA}}{2D^2}\Delta_a$	0	$-\frac{\Delta_a}{2D}$	$\frac{2l_{CA}-L}{2D}$	$\frac{1}{2}$
3	$-\frac{l_{CA}}{D^2}\Delta_a$	0	0	$\frac{l_{CA}}{D}$	0
4	0	0	0	$\frac{\Delta_a}{2\sqrt{\Delta_a^2+\Delta_d^2}}$	$\frac{\Delta_d}{2\sqrt{\Delta_a^2+\Delta_d^2}}$

Table 3.2: Sensitivity of task location error to the joint parameters

established that *in-situ* processes are able to control gap geometry more easily and accurately than conventional processes with sequential shape and assembly. This is largely due to the fact that *in-situ* methods have direct access to the geometry of the gap in the form of support-structure geometry, and that no assembly constraints are present. A detailed example of how this access results in superior gap-size control is shown in Appendix B. The basic idea can be illustrated by visualizing a thin isolated "gap" that is pre-fabricated out of sacrificial support structure material, using a precise process such as centerless grinding. This "gap" is then embedded into the part during *in-situ* fabrication, and then removed along with all other support material after the entire part is fabricated. This would result in a more accurate gap than one that is subject to the stack-up effects inherent in the independent fabrication of the hole and shaft pair which result in a gap in conventional methods. Figure 3.26 illustrates this concept.

Summarizing, it has been demonstrated that conventional tolerancing of mechanisms with mating and fitting surfaces is typically complicated by constraints that ensure interference-free assemblability. *In-situ* fabrication makes it possible to simultaneously shape and assemble parts, whereby the tolerances required to ensure desired behavior are looser, the location tolerances on complementary surfaces (e.g. the hole and shaft) are de-coupled from each other and better control is achieved over the behavior of the joint.

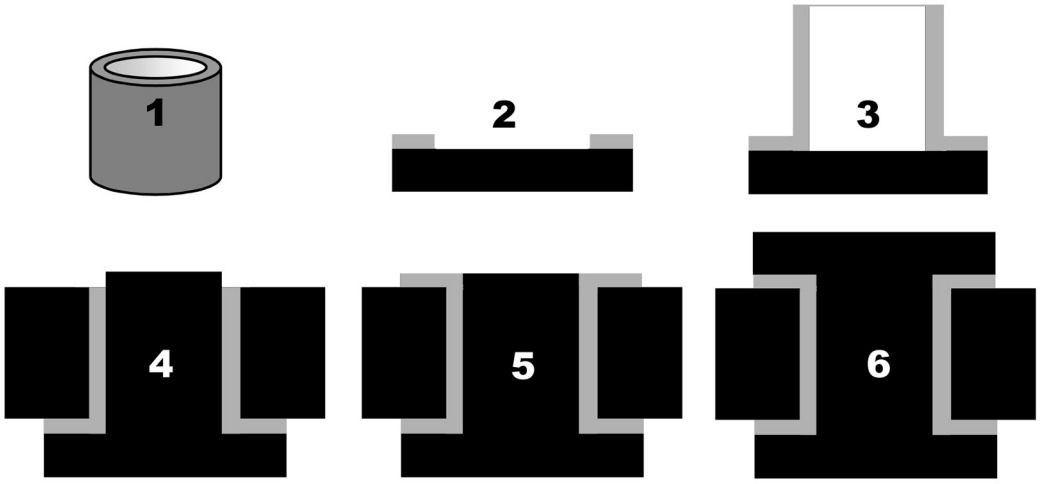

Figure 3.26: Precise control of *in-situ* gap geometry could proceed as shown: (1) An annulus of sacrificial support structure material is fabricated using a precise process such as centerless grinding (2) A locating ring that also serves as the axial gap is fabricated on the lower flange (3) The annulus is inserted into the workpiece, constituting the diametral gap (4) The joint hole and shaft are deposited around the annulus and machined to shape (5) Sacrificial material is deposited to make up the axial gap (6) The upper flange is deposited and machined. On removal of the sacrificial support material (grey), a pin-joint is obtained.

Chapter 4

Optimal Pose Selection

The previous chapter dealt with the estimation of error in the kinematic function of a mechanism, given the variability in joint placement (position and orientation) during fabrication. *In-situ* mechanisms experience two distinct workspaces in their life-cycle - the fabrication workspace, and then the operational workspace. In the fabrication workspace, joints are inserted and the mechanism body is constructed *in-situ*. Once fabrication is complete, the mechanism is freed from its encapsulating support structure, and installed into the operational workspace, where it performs its designed task. Errors created within the mechanism embodiment during its tenure in the fabrication workspace manifest themselves as task performance errors in the operational workspace. The natural question that arises in this regard is - *given a performance specification in the operational workspace, is it possible to determine the most appropriate configuration, or pose, in which the mechanism should be fabricated, in order to minimize performance errors?* Note that this question is quite moot for most conventional fabrication techniques, since fixed dimensional errors have already been introduced into each individual mechanism component by the time they are actually assembled into an entity that can be called a "mechanism."

In a non-homogeneous, anisotropic workspace (i.e. when the achievable joint positioning and orientation accuracy varies arbitrarily within the process workspace), the fabrication pose will clearly affect the parameters and performance of a mechanism. We establish that this holds true even for homogeneous workspaces. This is due to fact that the sensitivity of each mechanism parameter to joint placement error, and the correlation coefficients of "adjacent" parameters, both vary with pose -

regardless of workspace homogeneity. The following sections detail a couple of methods (analytical and computational) that can be used in order to solve the problem of optimal pose selection in the *in-situ* fabrication of mechanisms.

4.1 Analytical Approach to Optimal Pose Selection

Equation 3.29 in the previous chapter gives us a very elegant way of linking output performance in the operational workspace to the manufacturing variability in the fabrication workspace. Here we examine it in more detail. Restating it:

$$\sigma_{\mathbf{y}}^2 \approx \sum_{i=1}^{n} (\frac{\partial f}{\partial \phi_i})_{\mu}^2 \sigma_{\phi_i}^2 + 2 \sum_i \sum_j (\frac{\partial f}{\partial \phi_i})_{\mu} (\frac{\partial f}{\partial \phi_j})_{\mu} \rho_{ij} \sigma_{\phi_i} \sigma_{\phi_j} \tag{4.1}$$

Equation 4.1 indicates that the variance of the output function ($\sigma_{\mathbf{y}}^2$) is the sum of two terms. The first term is the sensitivity-weighted sum of the individual parameter variances (i.e. $\sigma_{\phi_i}^2$). Note that this term is identical with the entire RHS term for the error equation for un-correlated and independent parameters (see Equation 3.15). The second term is a summation of the pair-wise products of output sensitivities, correlation coefficient, and standard deviations of the mechanism parameters. This is the term that is correcting for the correlative effect of manufacturing variability during *in-situ* fabrication.

For ease of discussion, we rewrite Equation 4.1 as follows:

$$\sigma_{\mathbf{y}}^2 \approx \sum_{i=1}^{n} a_i^2 \sigma_{\phi_i}^2 + \sum_i \sum_j b_{ij} \rho_{ij} \sigma_{\phi_i} \sigma_{\phi_j} \tag{4.2}$$

where $a_i \equiv (\frac{\partial f}{\partial \phi_i})_{\mu}$ and $b_{ij} \equiv 2(\frac{\partial f}{\partial \phi_i})_{\mu} (\frac{\partial f}{\partial \phi_j})_{\mu}$. Note that the terms under the first RHS summation of Equation 4.2 are always positive and additive to the total variance. The terms under the second (double) summation can either be positive or negative, depending upon the signs of b_{ij} and ρ_{ij}. Thus the second RHS summation can either add-to or subtract-from the first summation.

We can examine the output variance equation more closely, and try to intuitively reason about the optimal build pose. This reasoning is presented in the next section.

4.1.1 Intuitive Assessment of the Optimal Pose Problem

We note that the quantities a_i and b_{ij} depend upon the sensitivity of the output equation to the mechanism parameters at the operational configuration. Thus, for a given nominal operational configuration $\mathcal{C}^{nom}$, these quantities are fixed. The quantities ρ_{ij} and $\sigma^2_{\phi_i}$ depend upon the build pose ($\mathcal{C}_b$), and vary with each candidate build pose in the optimization problem. In addition, $\sigma_{\phi_i} \geq 0$, and $(-1 \leq \rho_{ij} \leq 1)$.

If the goal of the optimization problem is to minimize the total output variance $\sigma^2_{\mathbf{y}}$ for a given operational configuration $\mathcal{C}^{nom}$, then it is clear just from observing the structure of Equation 4.2 that:

- It is, in general, preferable to choose a build pose where the highly influential parameters (i.e. large a_i) have the least variance ($\sigma^2_{\phi_i}$).
- It is always preferable to have the product $b_{ij} \times \rho_{ij}$ for each term in the second summation be subtractive (i.e. the two terms b_{ij} and ρ_{ij} should always have opposite signs).

Simply put, the second point above recommends that when two "adjacent" parameters (i.e. parameters that do not have zero correlation) influence the output in the same direction , then a build pose in which the two parameters are negatively correlated should be chosen to reduce the output variation. On the other hand, when the two adjacent parameters each influence the output in different directions, then a build pose where the two parameters are positively correlated should be chosen. This recommendation can be explicitly stated for a given operational configuration $\mathcal{C}^{nom}$ as follows:

$$
\begin{aligned}
&if\ (\frac{\partial f}{\partial \phi_i})_\mu > 0\ and\ (\frac{\partial f}{\partial \phi_j})_\mu > 0, \quad choose\ \mathcal{C}_b\ such\ that\ \ \rho_{ij} < 0 \\
&if\ (\frac{\partial f}{\partial \phi_i})_\mu < 0\ and\ (\frac{\partial f}{\partial \phi_j})_\mu < 0, \quad choose\ \mathcal{C}_b\ such\ that\ \ \rho_{ij} < 0 \\
&if\ (\frac{\partial f}{\partial \phi_i})_\mu > 0\ and\ (\frac{\partial f}{\partial \phi_j})_\mu < 0, \quad choose\ \mathcal{C}_b\ such\ that\ \ \rho_{ij} > 0 \\
&if\ (\frac{\partial f}{\partial \phi_i})_\mu < 0\ and\ (\frac{\partial f}{\partial \phi_j})_\mu > 0, \quad choose\ \mathcal{C}_b\ such\ that\ \ \rho_{ij} > 0
\end{aligned}
$$

Table 4.1 summarizes these guidelines. This reasoning, then, makes intuitive

$$\sigma_{\mathbf{y}}^2 \approx \sum_{i=1}^{n} (\frac{\partial f}{\partial \phi_i})_{\mu}^2 \sigma_{\phi_i}^2 + 2 \sum_i \sum_j \frac{\partial f}{\partial \phi_i}]_{\mu} \frac{\partial f}{\partial \phi_j}]_{\mu} \rho_{ij} \sigma_{\phi_i} \sigma_{\phi_j}$$

$\frac{\partial f}{\partial \phi_i}]_{\mu}$	$\frac{\partial f}{\partial \phi_j}]_{\mu}$	ρ_{ij}
+	+	-
+	-	+
-	+	+
-	-	-

Table 4.1: An intuitive assessment of the optimal pose selection problem. This table shows the preferred combination of the signs for the output influence coefficients and correlation coefficients for adjacent parameters.

sense. The correlative effect of *in-situ* fabrication can be used to minimize the output variance in a given operational configuration by choosing the build pose that tends to cancel the pair-wise contribution of mechanism parameters to output error. Of course, no single build pose ($\mathcal{C}_b$) is likely to simultaneously result in the appropriate sign for every parameter-pair (i.e. these items cannot all be selected independently). Thus, we need to construct a cost function, and explicitly state the dependency constraints so that the best possible solution can be found for the build-pose optimization problem. This is the basis for the formalization presented in the next section (Section 4.1.2).

4.1.2 Constrained Optimization Formal Statement

The constrained optimization problem (for minimizing the performance error at a single given operational configuration $\mathcal{C}^{nom}$) can be formally stated as follows:

$$minimize \;\; \sigma_{\mathbf{y}}^2 = \sum_{i=1}^{n} a_i^2 \sigma_{\phi_i}^2(\Theta_b) + \sum_i \sum_j b_{ij} \rho_{ij}(\Theta_b) \sigma_{\phi_i}(\Theta_b) \sigma_{\phi_j}(\Theta_b) \qquad (4.3)$$

subject to:

$$\lambda_k^b(\Phi, \Theta_b) = 0; \;\; k = 1, 2, \ldots, K \tag{4.4}$$

where σ_{ϕ_i} and ρ_{ij} are given as in Equations 3.26 and 3.27, respectively. $\lambda_k^b(.)$ represents the k^{th} kinematic loop equation in a K loop mechanism, stated at the candidate build pose $\mathcal{C}_b$. The vector Θ_b denotes the independent driving parameters at the candidate build pose - which ultimately are the variables in this optimization problem. The vector of driving variables which solves the above optimization problem is denoted as $\Theta_b^\star$.

To extend this problem to the minimization of the total error for R design points on the output function, the cost function can be rewritten as follows:

$$minimize \;\; \mathcal{E} = \sum_{r=1}^{R}\{\sum_{i=1}^{I} a_i^r \sigma_{\phi_i}^2(\Theta_b) + \sum_i \sum_j b_{ij}^r \rho_{ij}(\Theta_b)\sigma_{\phi_i}(\Theta_b)\sigma_{\phi_j}(\Theta_b)\} \tag{4.5}$$

subject to:

$$\lambda_k^b(\Phi, \Theta_b) = 0; \;\; k = 1, 2, \ldots, K \tag{4.6}$$

There are many techniques for solving constrained optimization problems such as the one detailed above. At each candidate build pose, the equations that estimate the values of the variance and correlation coefficients (i.e. Equations 3.26 and 3.27), are first-order approximations. Thus the simplest method for solving the problem is to apply an iterative numerical technique, where the quantities σ_{ϕ_i} and ρ_{ij} are tabulated at discrete intervals of the driving variables Θ_b. Next, the cost function (Equation 4.3 or 4.5) is evaluated at each interval to determine an approximation of the minima. This process is repeated for smaller and smaller intervals in the vicinity of the solution to iteratively determine the solution $\Theta_b^\star$.

Figures 4.1 and 4.2 illustrate this technique applied to the simple four-bar mechanism introduced as an example in the previous chapter.

4.2 Computational Approach to Optimal Pose Selection

This section details an alternate approach for solving the problem of optimal pose selection. If the optimization task can be described as one of minimizing or maximizing a *distance metric* (i.e. a distance function, or a sum of distances etc.), then

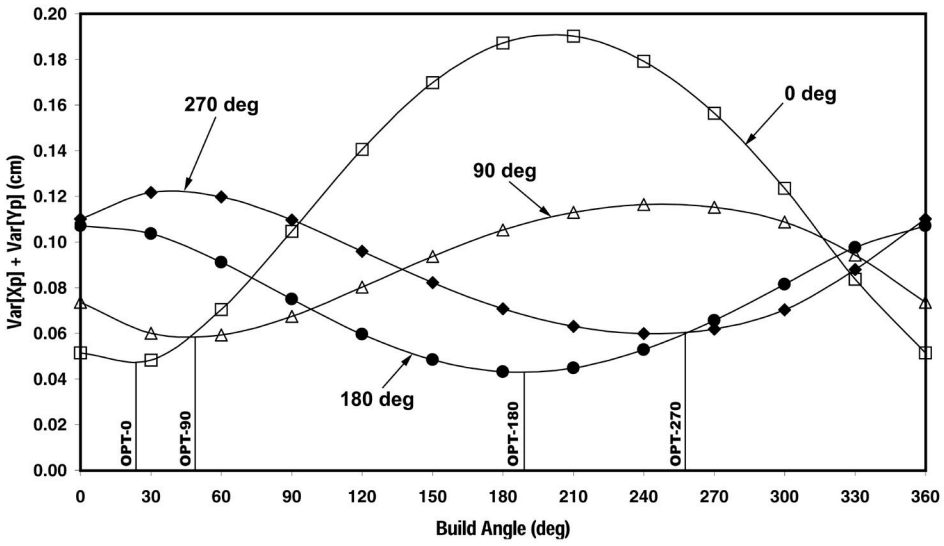

Figure 4.1: Optimal pose selection for the example crank-rocker mechanism in Figure 3.12 - each curve represents the total coupler-point variance for a given operational angle. The optimal pose corresponds to the minima point on each curve

then it is possible to cast it as a problem in computational geometry. Application of computational geometry techniques to the mechanical tolerance analysis arena is not new, but has been introduced under the name *kinematic tolerance analysis* by (Joskowicz *et al*, 1997). Here, we do not employ configuration space analysis to clearance and multiple-contact kinematics as in the earlier work, but the underlying technique is comparable.

The technique is illustrated for a simple planar mechanism, but it is not explored extensively due to the inherent limitations (e.g. restriction to worst-case estimation, difficulty in expressing alternate performance criteria like output angles, etc.). However, it should be possible to extend the geometric concepts presented here (i.e. distances between points and orthogonal distances from points to lines and planes) to spatial problems in a straightforward manner. The computational approach proceeds by formulating the optimization task in geometric terms (e.g. minimizing a distance metric), and then using theorems in computational geometry in order to make the search for the optimal configuration more efficient.

For this treatment, we make the simplifying assumption that the task requirements can be best satisfied by minimizing variability of link-lengths. We cast the problem of minimizing variability in link length as that of determining the relative position of two joint location precision regions for which the difference between their

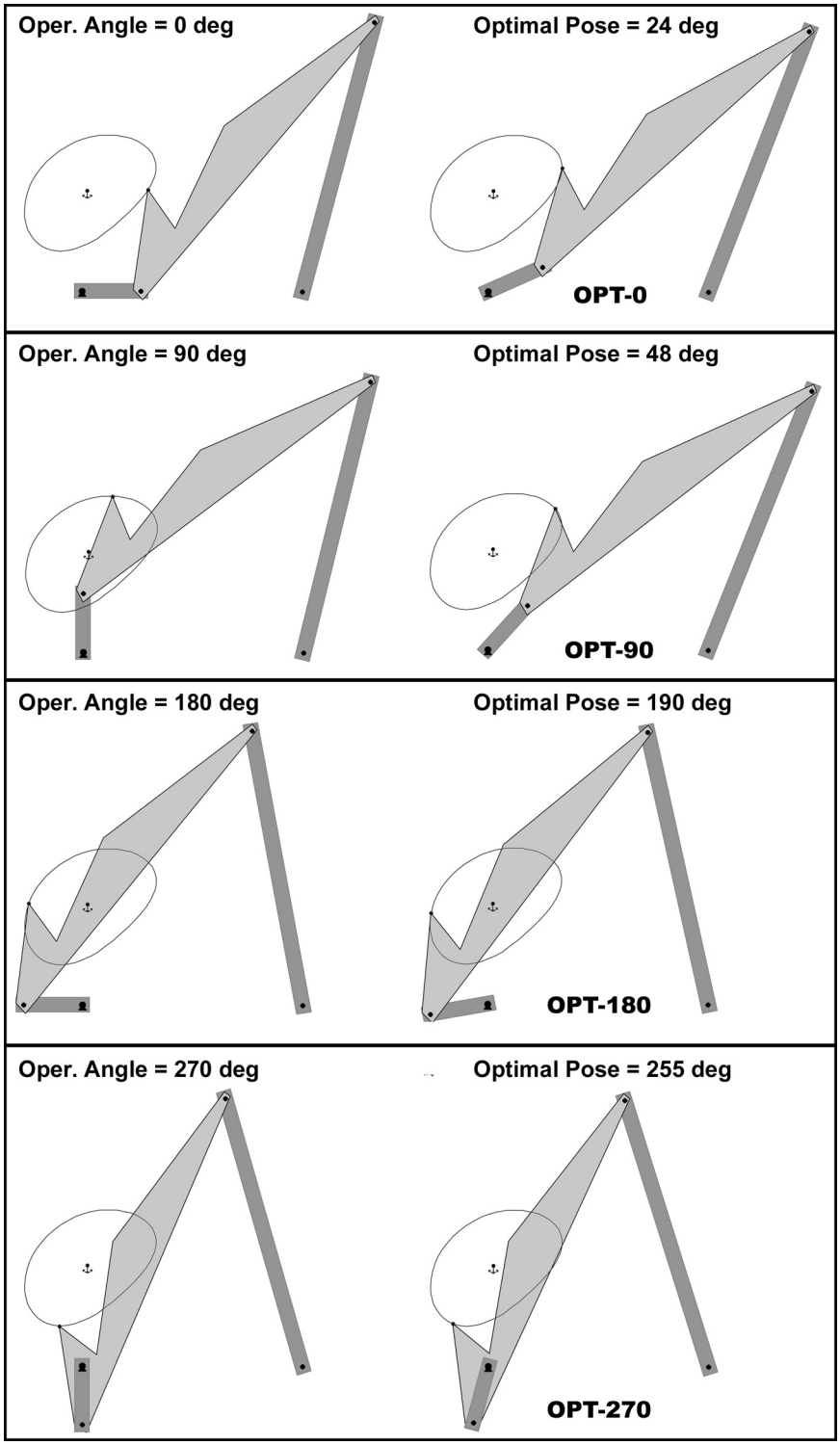

Figure 4.2: The 4-bar mechanism at its operational angles (left-side images), and the corresponding optimal build pose for each angle (right-side images).

extremal distances is at a minimum (i.e., as they undergo constrained relative motion in the Euclidean plane). Algorithms for determining the extremal distances between point-sets, and the associated complexity analysis, have been developed in the computational geometry community with regards to pattern matching (Huttenlocher *et al*, 1994) (Toussaint, 1984) (Bhattacharya *et al*, 1983) and robot motion planning (Latombe, 1991). The approach used here is similar, with some important differences which are discussed in subsequent sections (see Section 4.2.1).

The task at hand is seen as one of examining pairs of regions (or alternately, discrete point-sets) moving in a Euclidean plane. Achievable positional accuracy at build time is modeled as a pre-specified *precision region* of arbitrary geometry, in the neighborhood of the nominal position. In the most general case, this region can have arbitrary geometry (anisotropic and non-homogeneous) depending upon the characteristics of the process workspace. This is similar to the precision region concept introduced earlier, in Section 3.3.1. The worst-case (minimum and maximum) link lengths are represented by the extremal distances between the precision regions of each joint. Behavioral requirements are expressed as restrictions on the allowable variability of either links or link-chains. In this thesis, we consider the simple case of maintaining the individual link lengths as close as possible to their designed length. The problem is then reduced to finding the configuration for which the difference in the extremal distances between the precision regions of adjacent joints is minimized, as the nominal joint positions (and hence their associated precision regions) undergo constrained motion in the Euclidean plane. Clearly, similar analysis would also apply to determining the best build pose for parts that have multiple critical dimensions among features (such as holes in a bolt circle).

4.2.1 Computational Geometry: Definitions and Assumptions

In this section, we define some of the entities and concepts that are important in the later treatment of the problem.

Compact and Simply-Connected: We make the assumption that the regions under consideration are compact (i.e. closed and bounded) and simply connected. This assumption is realistic for most engineering applications, and will eliminate many

special cases in our analysis. From this point on, any reference to a set/space/region will imply compactness and simply-connectedness, unless otherwise specified.

Distances: Mathematicians have developed a generalized notion of *distance* (Blumenthal, 1953). Closely related to distance are *position* and *size*, both of which are concepts central to our discussion. The most common understanding of distance is in the Euclidean sense, where one is concerned with the shortest path between two geometric entities (e.g. points) in a Euclidean n-space. A function δ defined on two elements a and b of a metric space $\mathcal{M}$ is called a *distance* iff $\delta(a, b)$ is *positive, symmetric,* and obeys the *triangle inequality*. In this treatment we are concerned with the Euclidean distance metric, which is given by the Pythagorean Theorem.

There are two approaches to determining the distance between geometric entities like points, curves and regions (surfaces and volumes) – analytical and computational. Given an analytic description of the entities, it may be possible to compute the extremal distances between the entities in closed form. However, the problem of computing raw distances between these entities is analytically tractable only for the simplest of cases (e.g. points, straight lines, simple conics) due to the highly non-linear algebraic equations generated (for example, computing the minimum distance between two non-intersecting spatial cubics is a non-trivial problem analytically). An alternative approach is to discretize the entities (into finite point-sets) within some region of interest, and to arrive at the solution by executing an efficient search algorithm. This approach works for most practical applications, and is especially appropriate when the geometry has special properties like being convex, disjoint and polygonal. This has been the preferred approach in robotics and in pattern recognition, and computational geometers have mostly concentrated on developing algorithms for determining distances between discrete point sets and polygonal regions. As noted earlier, there has been extensive research in the area of algorithms for computing distance properties, along with complexity and performance evaluation for various algorithms (Huttenlocher *et al*, 1994) (Toussaint, 1984) (Bhattacharya *et al*, 1983). The main difference between the approaches in these areas and that presented here is that they are concerned with intersections and Minkowski Sums of regions (for collision detection and navigation in robot motion planning), and Hausdorff distances between point-sets (for pattern matching). We are interested in extremal distances between disjoint precision regions, which have their relative

motion restricted by kinematic constraints.

To keep the applicability of the approach as general as possible, we pose the problem assuming analytical descriptions of precision regions about the nominal joint positions. However, for tractability, we discretize the problem (or assume simple geometries), and look at efficient computational methods to solve it.

Extremal Distances Between Regions: The extremal distances (see Figure 4.3) between any two regions in space are the minimum and maximum Euclidean distances (denoted by D_{max} and D_{min}) between any two points in the spaces. i.e., if $\mathcal{R}_1$ and $\mathcal{R}_2$ represent two regions in Euclidean space, and p_i is a point in $\mathcal{R}_1$, q_j is a point in $\mathcal{R}_2$, then:

$$\begin{aligned} D_{max}(\mathcal{R}_1, \mathcal{R}_2) &= \max[\delta(p_i, q_j)] \\ D_{min}(\mathcal{R}_1, \mathcal{R}_2) &= \min[\delta(p_i, q_j)] \\ & \quad \forall p_i \in \mathcal{R}_1, q_j \in \mathcal{R}_2 \end{aligned} \tag{4.7}$$

Researchers in pattern matching have mostly been concerned with determining efficient algorithms for optimizing a distance metric (typically minimizing the Hausdorff distance (Huttenlocher *et al*, 1994)) between point-sets with a finite number of points. Efficient algorithms for determining the minimum and maximum Euclidean distances between point-sets have also been developed, along with the associated complexity analysis.

Minimum Distance between Point-Sets: If $\mathcal{S}_1 = \{p_1, p_2, \cdots, p_n\}$ and $\mathcal{S}_2 = \{q_1, q_2, \cdots, q_n\}$ represent two sets of points on a plane, then the minimum distance between the two sets is given as:

$$D_{min}(\mathcal{S}_1, \mathcal{S}_2) = \min_{i,j} [\delta(p_i, q_j)]; i, j = 1, 2, \cdots, n \tag{4.8}$$

The naive strategy of examining the distance between every point-pair (p_i, q_j) results in $O(n^2)$ complexity. Algorithms that run at $O(n \log n)$ worst case complexity have been demonstrated (Toussaint, 1984). It has been shown that the lower-bound on the complexity of this problem is $\Omega(n \log n)$. The optimal algorithms work by computing the Minimum Spanning Tree (MST) of the union of the two given sets

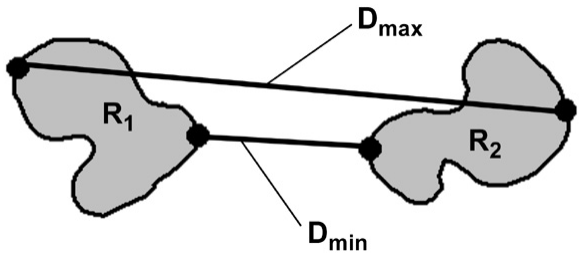

Figure 4.3: Extremal distances between two planar precision regions.

(i.e. $\mathcal{S}_1 \cup \mathcal{S}_2$). The minimum distance is an edge of the MST.

Maximum Distance between Point-Sets: If $\mathcal{S}_1 = \{p_1, p_2, \cdots, p_n\}$ and $\mathcal{S}_2 = \{q_1, q_2, \cdots, q_n\}$ represent two sets of points on a plane, then the maximum distance between the two sets is given as:

$$D_{max}(\mathcal{S}_1, \mathcal{S}_2) = \max_{i,j} [\delta(p_i, q_j)]; i, j = 1, 2, \cdots, n \tag{4.9}$$

Once again, the naive strategy of comparing the distance between every point pair results in $O(n^2)$ complexity. Optimal algorithms that run in $O(n \log n)$ worst case complexity, which are within a constant factor of the theoretical lower bound of complexity, have been demonstrated (Bhattacharya *et al*, 1983). The algorithms work by proving that the maximum distance is supported by points on the convex-hulls of the two regions.

Boundary of a Planar Region: The *boundary* $B(\mathcal{R})$ of a set (or region in space) $\mathcal{R}$ is the set of all points that belong to the closure of the set $\mathcal{R}$ as well as the closure of the complementary set $\bar{\mathcal{R}}$ (Figure 4.4). The boundary is also sometimes called the *frontier* of the region. The boundary of a compact and simply-connected planar region is a non-self-intersecting closed planar curve. The *sense* or *orientation* of the curve is defined such that traversal of the curve along its positive sense puts the interior of the region on the RHS. When defining precision regions, the interior of the region contains the nominal position of the feature.

Boundary Points and Internal Points: A *boundary point* is a point on the boundary of a set or region. It has the property that its neighborhood has at least one point within the set, and at least one outside of it. An *internal point* is any

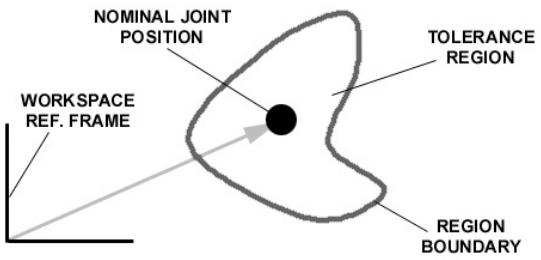

Figure 4.4: Boundary of a planar region of arbitrary geometry.

point in the set that is not a boundary point. All points in the neighborhood of an internal point lie within the set.

4.2.2 Computational Geometry: Theorems

Here, we state some relevant theorems without the associated proofs. Proofs of these theorems are either covered by texts and research papers in computational geometry (Preparata, 1985), pattern matching and robot motion planning (Latombe, 1991), or are simple extensions of the known concepts.

Theorem 1: The extremal distances between two compact and simply-connected regions in Euclidean space are supported by points on the boundary of the regions.

Lemma 1.1: The minimum distance between two convex, disjoint, and polygonal regions is either supported by vertices of the polygons, is an orthogonal distance between a vertex and an edge of the polygons, or is an orthogonal distance between two edges of the polygons.

Lemma 1.2: The maximum distance between two convex, disjoint and polygonal regions is supported by vertices of the two polygons.

Theorem 2: Given two finite point sets, the minimum distance between them is supported by an edge of the *minimum spanning tree* of the union of the two sets.

Theorem 3: Given two finite point-sets, the maximum distance between them is supported by points on the *convex hulls* of the two sets.

These theorems imply that, in general, it is adequate to examine the boundaries of regions to determine extremal distances between them. Furthermore, for some special regions (like convex polygonal regions and discrete point-sets) it is adequate to examine just a subset of the boundary itself.

4.2.3 Problem Formulation

As mentioned earlier, our approach is to cast the problem of finding the optimal build pose as that of locating the configuration of the mechanism for which the worst-case variation of the link sizes is at a minimum. We are given regions of arbitrary geometry in the neighborhood of the *nominal* joint positions, inside which the actual joint is assumed to lie. These regions are assumed to be dense, compact (i.e. closed and bounded) and simply-connected. Each point within the region is assumed equiprobably to be a candidate for the actual joint position. The shape of the precision region around each nominal joint position is a function of the workspace within which the mechanism is being built. In the most general case, the workspace is both non-homogeneous and anisotropic (i.e. the precision region varies both as a function of absolute position and of direction).

The Single Link

We now look at the problem of finding the optimal build position for a single isolated link. If the desired objective is to maintain the resultant link-length as close as possible to the nominal link length, the problem is identical to finding the orientation (relative to a workspace datum frame) for which the difference between the two extremal distances (i.e. max and min distances) is a minimum (see Figure 4.5). The problem can be solved by examining the extremal distances under constrained relative motion of the nominal joint positions (and consequently, the relative motion of the precision regions for the nominal positions).

As defined in Section 4.2.1, we denote the maximum and minimum distances between two precision regions $\mathcal{R}_1$ and $\mathcal{R}_2$ by $D_{max}(\mathcal{R}_1, \mathcal{R}_2)$ and $D_{min}(\mathcal{R}_1, \mathcal{R}_2)$ respectively. These distances can either be determined by discretizing the boundary of the regions, or by examining the vertices and edges (for convex, polygonal regions), as appropriate.

Any relative Euclidean motion in the plane for the two regions can be thought

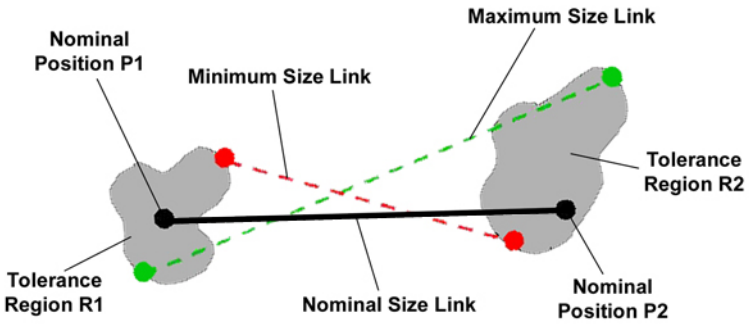

Figure 4.5: Precision regions representing link-length variability for a single link.

of as a combination of a rotation and a translation. Thus, without any loss of generality, we can attain all relative positions by allowing region $\mathcal{R}_1$ to purely rotate, and region $\mathcal{R}_2$ to purely translate with respect to a local reference frame. In the case of a revolute joint, however, the nominal positions of the two regions stay at a fixed distance with respect to each other. Thus, it is adequate (Figure 4.6) to let one region purely rotate about the origin, while the other remains stationary with respect to the local frame. The origin of the local frame can itself translate anywhere in the fixed reference frame, and the regions can, in general, transform shape as they navigate the workspace (this could happen, for example, in a compliant robotic manipulator that inserts joints with different locational accuracy at various points in its work envelope). The nature of these transforms will depend upon the workspace characteristics, but they cannot affect the nominal position of the joints. The optimization problem can now be formulated as follows:

Find the orientation $\{\theta^\star, x^\star\}$ for the link such that the minimum variability, defined as:

$$\Delta_{min}(\mathcal{R}_1, \mathcal{R}_2) = \min_{\theta, x} \{D_{max}[s_{\theta x}(\mathcal{R}_1), g_{\theta x}(\mathcal{R}_2)] - D_{min}[s_{\theta x}(\mathcal{R}_1), g_{\theta x}(\mathcal{R}_2)]\} \qquad (4.10)$$

is achieved, where θ and x are parameters that denote the orientation of the link in the local frame, and the absolute position of the local frame, and $s_{\theta x}$ and $g_{\theta x}$ are general transformations that operate on precision regions. Examples of possible transforms are linear, affine transforms (scale, rotate etc.), or non-linear mappings that characterize the workspace of a compliant robot. For the special case where the shape of the precision region attached to a joint location is independent of its

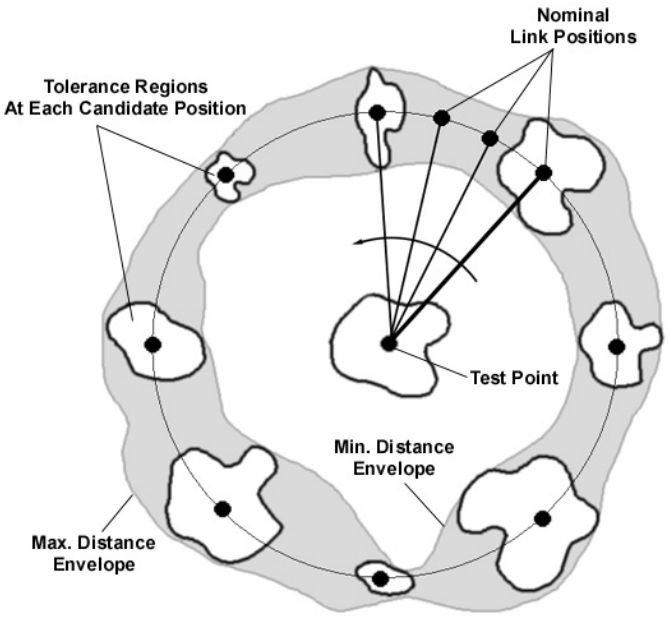

Figure 4.6: Precision region undergoing constrained motion in the Euclidean plane.

absolute position in the workspace, Equation 4.10 becomes:

$$\Delta_{min}(\mathcal{R}_1, \mathcal{R}_2) = \min_{\theta} \{D_{max}[S_\theta \cdot \mathcal{R}_1, \mathcal{R}_2] - D_{min}[S_\theta \cdot \mathcal{R}_1, \mathcal{R}_2]\} \tag{4.11}$$

where $S_\theta \cdot \mathcal{R}_1 = \{S_\theta r_i \mid r_i \in \mathcal{R}_1\}$ is a rigid body rotation matrix applied to $\mathcal{R}_1$.

Since $\Delta_{min} = D_{min} - D_{max}$ can be calculated at each position in $O(n \log n)$ time, the complexity of the optimization problem is $O(C^3 n \log n)$, where C depends upon the resolution with which θ and x are discretized. The cubic term in the complexity is on account of the three degrees of freedom of the link - position and orientation on a plane.

The Multi-Link Mechanism

The multi-link problem is a simple extension of the single link problem, if the objective is still to keep the resultant error in link-lengths as small as possible. In this case, the single link problem is successively encountered at each nominal joint position, with regards to the next adjacent link in the mechanism. If there are m links and k degrees of freedom for the mechanism, we want to determine the mechanism configuration $\{\theta_1^\star, \theta_2^\star, \theta_3^\star, \ldots, \theta_{k-2}^\star, x^\star\}$, such that the minimum cumulative variability,

defined as:

$$\Delta^{T}_{min} = \theta_1, \theta_2, \min_{\theta_3, \ldots, \theta_{k-2}, x} \{ \sum_{i=1}^{m-1} \Delta_{min}(\mathcal{R}_i, \mathcal{R}_{i+1}) \} \tag{4.12}$$

is attained, where Δ_{min} is obtained as in the previous section.

Note that this is the configuration for which the global minimum of the cumulative variability of all links is attained. We call this the *optimal pose*. The complexity of the search is $O(mC^k n \log n)$.

4.2.4 Examples

Here, we present some simple examples that serve to illustrate the concepts presented in the earlier sections. These examples were solved using spreadsheet simulation.

Single Link

For convex, polygonal precision regions, the analysis is greatly simplified. The problem can be solved by writing pairwise loop-closure equations on boundary points on the two precision regions. For computing the minimum link length, vertices and points on the polygon edges need to be tested. However, for maximum link length, it is adequate to test the vertices of the polygons. The loop-closure procedure is illustrated in Figure 4.7. It yields a vector equation of the form:

$$Z_{O_A A_i} + Z_{A_i B_j} + Z_{B_j O_B} = Z_{O_A O_B} \tag{4.13}$$

which can be algebraically solved for the unknown scalar length $\|Z_{A_i B_j}\|$. The simulation proceeds by solving for the maximum and minimum link lengths at each step in the link orientation.

To illustrate this method, we have used the case of rectangular precision regions around the nominal position of the joints. Figure 4.8 shows a diagram of this type of region. This would correspond to the case where the worst-case positional accuracy of the process is expressed in the plus/minus sense for the two axes on the working plane. In this example, we have assumed that the precision regions for the two joint positions are different (this could happen, for example, when the position of the first-built joint is known to a higher accuracy than that of the second-built joint due to some in-process measurements), and that they are indifferent to the absolute position of the link in the workspace.

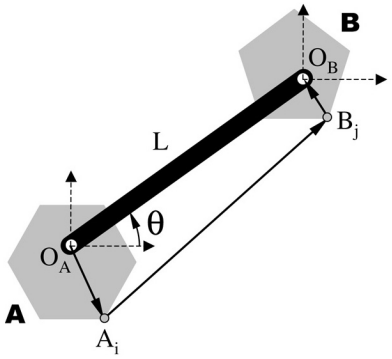

Figure 4.7: Vector loop equations for a single link with convex, polygonal precision regions.

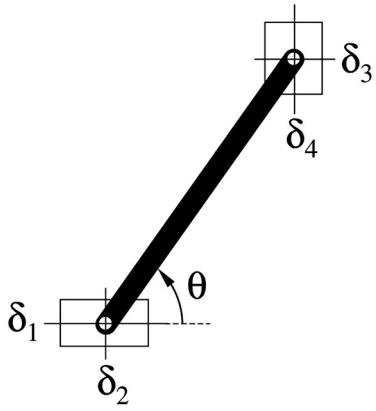

Figure 4.8: A single link with rectangular precision regions.

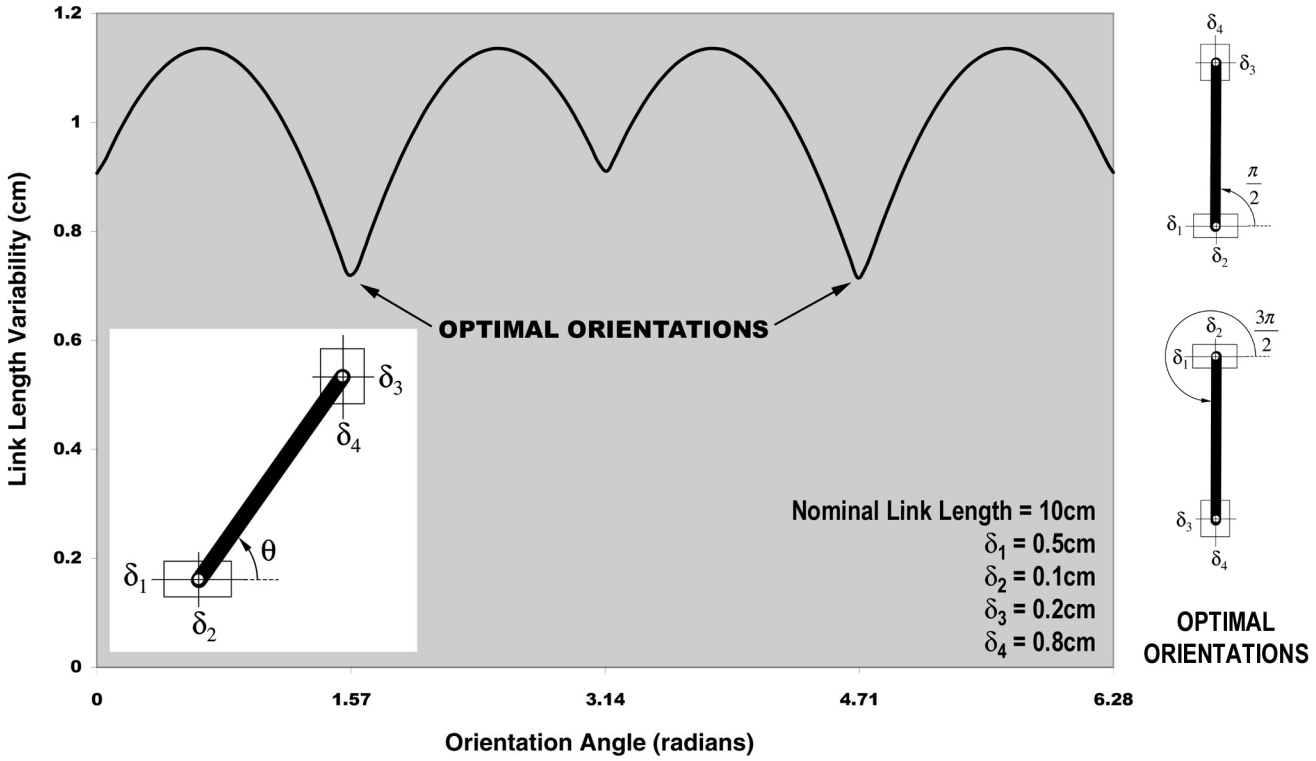

Figure 4.9: Optimal orientations for a single link with rectangular precision regions.

Figure 4.9 shows a plot of the variability in the link length as a function of the orientation of the link in the workspace. The "link length variability" plotted on the Y-axis is simply the difference between the maximum and minimum possible link lengths at each candidate orientation angle (θ). The optimal orientations (indicated) are those for which the link-length variability is at a minimum.

Multi-link Mechanism

Here, we consider the example of a four-bar mechanism. The figure (Figure 4.10) shows the mechanism with the rectangular precision regions associated with each joint. Also shown is the resultant optimal orientation, after some practical constraints (see Section 4.3) have been taken into account. We again assume that the shapes of the precision regions are independent of the absolute position within the workspace, hence there are two degrees of freedom (i.e. two orientations) associated with this mechanism. Given the shape of the precision regions (elongated along the X-axis), one would intuitively expect the optimal pose to be fully folded along the Y-direction. However, the physical constraints (e.g. link overlap) would not allow that

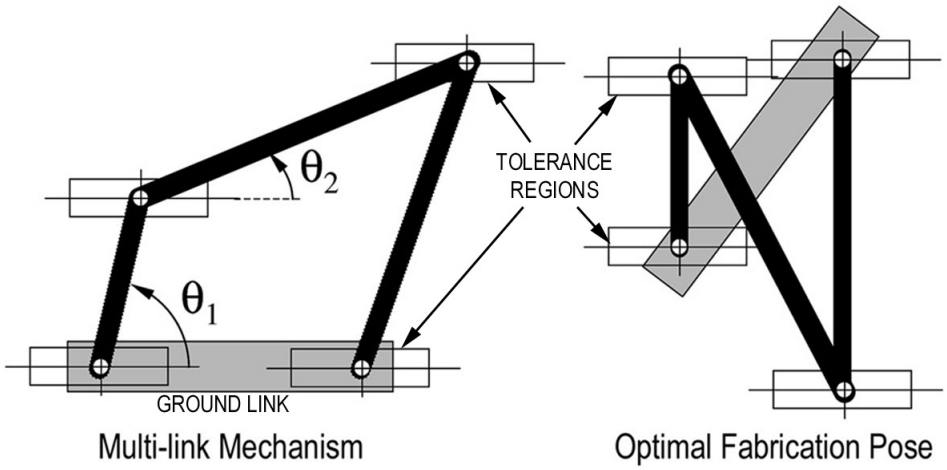

Figure 4.10: Optimal orientation for a 4-bar mechanism with rectangular precision regions.

configuration, and the illustrated pose implements a minimum link angle constraint between adjacent links.

4.3 Practical Considerations

The techniques for finding the optimal pose outlined above have no awareness of the many practical constraints that may limit the domain of available choices for mechanism poses. An obvious example of such a limitation is that joints in the same plane cannot overlap, and links in the same plane cannot cross each other. Another possible constraint is that mechanisms cannot stretch outside the available machine workspace (in general, smaller mechanism footprints are preferable). In addition to these workspace constraints, the program has no kinematic knowledge (e.g. branching). For example, a closed-link mechanism built in the optimal pose may not be able to return to every working configuration without dis-assembly of the joints.

It is necessary for the optimizing algorithm to take such constraints and preferences into account in order to produce a viable set of optimal mechanism poses. Non-overlap and non-crossing constraints are easily encoded in the solver as restrictions on the relative orientations of links (either adjacent links or all links), for example:

$$\theta_{min} \leq \|\theta_i - \theta_j\| \leq \theta_{max} \tag{4.14}$$

Other constraints (e.g. kinematic constraints) are more complicated to encode mathematically - but can be eliminated by inspection after the fact.

Chapter 5

Conclusions

5.1 Thesis Summary

A framework has been presented for reasoning about errors in the performance of mechanisms that are slated to be built using the increasingly popular "freeform" fabrication techniques. This is achieved by formulating an abstract model for the *in-situ* fabrication of mechanisms, and solving the problem of analytical estimation of the variance of the kinematic function, in the presence of correlated random parameters. The fundamental assumptions in this treatment of error analysis are:

- The desired performance of the mechanism is specified in terms of a kinematic output function, which is a continuous and differentiable mapping from a parameter space to the operational workspace (usually a Cartesian space). This assumption limits the application of the methods presented to linkages with lower pairs and "well-behaved" higher pairs only.
- The output is a weakly non-linear function of the inputs. This enables a first-order Taylor Series approximation of the error at the points of interest.
- *In-situ* fabrication is abstracted as a process of independent insertions of joints (which could have internal clearances) into a fabrication workspace, with a known accuracy. The inaccuracy is specified as worst-case limits on position and orientation (for deterministic error analysis) or variances with known distributions (for stochastic error analysis).

Note that no assumptions of planarity or of homogeneity in workspace characteristics are made anywhere in the methodology. Analysis of parametric errors in spatial

mechanisms has also been covered in the theoretical formulation. However, the examples presented in the thesis are planar systems in homogeneous fabrication spaces.

Errors due to joint clearances in *in-situ* fabricated joints have also been analyzed, inasmuch as the issues are unique to this manner of fabrication. The additional issue of determining the best *pose* for the fabrication of the mechanism in order to minimize the kinematic performance errors (from a stochastic perspective), has also been addressed. The techniques have been illustrated using the example of a planar 4-bar crank-rocker mechanism, and validated using Monte Carlo simulation.

To the best knowledge of the author, this work is unique amongst all contemporary treatments on mechanism error analysis, due to its focus on *in-situ* fabrication techniques. Specifically, it is unique in its consideration of correlation effects in error analysis, as these are intrinsic to this manner of fabrication.

5.2 Statement of Impact on the Community

The material presented in this thesis is expected to be found useful by the following members of the industry and academic communities:

- **Mechanism Designers:** One of the primary motivations for this work is to feed back information about manufacturability and manufacturing errors to the mechanism designer (especially designers of SFF and MEMS devices). While there is a fair body of work - academic research, design handbooks and industry standards - that strive to assist with the design of mechanisms slated for conventional fabrication, there is very little similar material in the area of *in-situ* fabrication. While this work is possibly not as immediately as useful to a designer as a design handbook, primer or software, it is hoped that it will be successful in informing the advanced designer of mechanisms about the issues that need to be examined during the design and rapid fabrication of precise mechanism prototypes. Guidelines for improving the accuracy of *in-situ* mechanisms can also be derived from the results presented (see Section 4.1.1).

- **Manufacturing Service Providers:** The providers of manufacturing services, whether internal to a firm or a third-party, are always challenged by the

task of providing the customer with a reasonable evaluation of the capabilities of their service. The challenge is in effectively highlighting the unique or attractive features of the service, while simultaneously presenting an accurate picture of its shortcomings. Providers of "freeform" fabrication services have traditionally resisted publication of detailed process capability information, largely due to the evolutionary nature of the processes, and due to the lack of a reliable framework on which to base such publications. The work presented in this thesis can serve as such a framework, enabling effective communication of process capability between designers and manufacturers of mechanism prototypes.

- **CAD System Developers:** The widespread adoption of any theoretical analysis technique is unlikely unless it is seamlessly incorporated into one of the ubiquitous CAD platforms used by industry designers. CAD system developers are also increasingly under pressure to differentiate their products by providing more sophisticated analysis and reasoning engines - either integrated with the base platform, or as "add-ins" and "plug-ins". Recently, plug-ins have been made available on all the major CAD platforms that let designers of 3-D objects automatically convert their models into formats compatible with rapid prototyping (RP) equipment. The natural next step is to include modules that assist designers with manufacturability reasoning, error analysis and design-optimization. The work presented here can serve as the analysis engine for the specific area of mechanism design, and can eventually be expanded to cover all aspects of error-analysis and design-optimization of rapidly fabricated mechanical and electro-mechanical devices.

- **Researchers:** The area of *in-situ* fabrication - whether macro, meso or micro-scale systems - is still relatively in its infancy. The design space is yet to be fully explored, with constant innovations in processing, material science and system integration. The primary focus of the academic community till date, undoubtedly, has been in demonstrating "one-of" prototypes, built with new materials, with multiple materials, with more complex geometry, at a smaller scale, or with better integration of transducers and electronics. Only recently has the attention of the community turned to making the fabrication processes more robust - either by characterizing its capability, by building an automated interface to the process for designers, or by productizing the process. In this

regard, the current work is a first step. It is hoped that it will serve as a stepping stone for researchers who want to develop a more comprehensive framework for understanding the capability new fabrication techniques. Some ideas for extending the research initiated in this thesis are discussed in the next section. In addition, researchers interested in the area of general error analysis could benefit from the review of the topic that is undertaken in this thesis.

5.3 Recommendations for Future Work

The author suggests the following avenues for extension of the work presented in this thesis. Depending upon the scope of the work, these could be appropriate for either Masters or Doctoral level research projects, or alternately, as industry projects.

- **Extension of the error-analysis technique to include other performance metrics:** The current work is focused on performance of a mechanism in the kinematic sense - and further, only on position or displacement errors. It is natural that this scope is very restrictive for many real applications - where non-kinematic (e.g. strength, force transmission etc.) and dynamic (i.e. velocity, acceleration etc.) performance are also extremely critical. A comprehensive error analysis treatment for *in-situ* fabrication of mechanisms, which includes all performance metrics needed in real applications, would be an extremely valuable extension of this work.

- **Inclusion of other factors in the error-analysis:** Many error-inducing factors prevalent in *in-situ* fabrication environments were not included in this work (see Section 3.1). To a large extent, these factors were excluded only in order to make the scope of this thesis realistic, given the allocated timeframe for completion of the thesis. Some of these factors, especially issues like deflection, shrinkage or warpage of links, are likely to be large contributors to the total performance errors in *in-situ* mechanisms. However, some of the results obtained in this thesis are likely to be directly compatible with the inclusion of these additional factors. For example, isotropic shrinkage clearly influences the parameters of a mechanism in a random, but correlated fashion. Future work could address *in-situ* mechanism error analysis in the presence of comprehensive error factors.

- **Extension to general assembly analysis:** This thesis is restricted to the error analysis of mechanisms built *in-situ*. However, there are many similarities between mechanisms and general static assemblies, when it comes to their kinematic performance. Instead of being concerned about the locus of a coupler point or the angle of an output link, error analysis of static assemblies is concerned with the value of a *key-characteristic*, which is usually a gap feature. Every geometric feature introduced into an *in-situ* fabricated object clearly influences all the components that share the feature. Furthermore, gaps and clerances in general assemblies can be controlled directly using the geometry of the sacrificial support material - exactly as detailed in Section 3.3.5. These similarities make the extension of the work of this thesis to general assembly analysis a natural one.

- **Focus on micro-fabrication techniques:** To the extent that micro-fabrication techniques resemble the macro-scale processes that are the focus of this thesis, the results of the thesis are directly applicable. However, there are many issues with micro-fabrication that are unique to the scale, for example - mask alignment accuracy for the photo-lithography, optical errors, particle contamination, adhesion etc. Furthermore, many geometric parameters scale unfavorably with regard to the kinematic precision of mechanisms built using this technique, making the analysis of clearance errors in these mechanisms much more critical. It would be interesting to apply similar techniques to those presented in this thesis, both for error analysis and for optimal pose selection, with the focus exclusively on micro-machined mechanisms.

- **Extension of pose-selection technique to consider other objectives:** The optimal pose has been defined as that for which the mechanism output errors are (stochastically) at a minimum. However, there are many reasons why the optimal pose from minimization-of-error perspective would be otherwise sub-optimal. For example, the optimization algorithm presented in this thesis does not consider branching, feature-overlap, space conservation and many other practical issues (see Section 4.3). There are also interesting research questions regarding the optimal fabrication pose of mechanisms which have dynamic or active elements (such as springs, shape-memory alloys or actuators). Furthermore, optimal structural synthesis algorithm for mechanisms

would clearly yield significantly different results if a non-homogeneous fabrication workspace was to be included in the synthesis problem. Future work could unify all these considerations into a single framework.

- **Experimental characterization of *in-situ* processes:** It is routine in the field of stochastic analysis to use Monte-Carlo simulation as the primary validation technique. This is not without reason. It is not an easy task to experimentally validate results that are stochastic in nature. All error factors that are unique to the specific experimental laboratory, and not endemic of the general *in-situ* process need to be controlled for. Furthermore, several thousands, and even tens of thousands, of identical parts may need to be fabricated and measured in order to obtain statistically significant results. Since the values of error are very small compared to the dimensions of the parts, the measurement equipment needs to be very accurate (e.g. a Coordinate Measuring Machine, or CMM). However, a rigorous experimental validation is undoubtedly more compelling, and would add more credibility to results of this thesis. One possible option is to use commercial manufacturing process control data as *in-situ* mechanisms start to be fabricated in large quantities (e.g. commercial fabrication of DLP projector arrays).

- **Implementation in a CAD infrastructure:** The real value of the results of this thesis would only be realized with its widespread adoption. However, most designers are loathe to adopt a technique that is not tightly integrated with their existing (legacy) tools. The importance of a good interface to the end-user of a technology is often underestimated, especially in scientific and engineering applications. For this reason, the implementation of this analysis technique as an error-analysis and manufacturability assessment module built upon a "standard" CAD platform is essential for it to see be useful outside academia. However, this project is best undertaken not by University researchers, but by the vendors of CAD products.

Appendix A

Estimation of Mean and Variance

Here, we are concerned with the approximate estimation of the mean and variance of an output $\mathbf{y}$, described in terms of its output function $f(\cdot)$ and a set of n random parameters $\mathbf{\Phi} \equiv [\phi_1, \phi_2, \ldots, \phi_n]$ as follows:

$$\mathbf{y} = f(\mathbf{\Phi}) \tag{A.1}$$

where $f(\cdot)$ is, in general, a continuous and differentiable non-linear mapping, and the parameters $\mathbf{\Phi}$ are random variables with no assumptions made about their distributions, correlations or independence. It is assumed, however, that the function $f(\cdot)$ is only weakly non-linear (i.e. high-order terms in it's Taylor Series expansion can be neglected) and that the mean and variance of the parameters ϕ_i are known, and denoted as $(\mu_{\phi_i}, \sigma^2_{\phi_i})$.

We begin by expanding the output function in its Taylor Series, about the mean values of the parameters, as follows:

$$\begin{aligned} \mathbf{y} \;=\; & f(\mu_{\phi_i}; i = 1, 2, \ldots, n) + \sum_{i=1}^{n} \frac{\partial f}{\partial \phi_i}]_{\mu}(\phi_i - \mu_{\phi_i}) + \frac{1}{2!}\sum_{i=1}^{n} \frac{\partial^2 f}{\partial \phi_i^2}]_{\mu}(\phi_i - \mu_{\phi_i})^2 \\ & + \sum_{i>j} \frac{\partial^2 f}{\partial \phi_i \partial \phi_j}]_{\mu}(\phi_i - \mu_{\phi_i})(\phi_j - \mu_{\phi_j}) + \cdots \end{aligned} \tag{A.2}$$

With a little bit of rearrangement, the above equation can be re-written in terms of

proxy variables Δ_{ϕ_i} as:

$$\mathbf{y} = f(\mu_i; i = 1, 2, \ldots, n) + \sum_{i=1}^{n} \frac{\partial f}{\partial \phi_i}]_{\mu} \Delta_{\phi_i} + \sum_i \sum_j \frac{\partial^2 f}{\partial \phi_i \partial \phi_j}]_{\mu} \Delta_{\phi_i} \Delta_{\phi_j} + \mathcal{O}_3 \qquad \text{(A.3)}$$

where $\Delta_{\phi_i} = \phi_i - \mu_{\phi_i}$ are zero-mean random variables, with all higher order moments identical with ϕ_i. The term $\mathcal{O}_3$ stands for all terms in the Taylor Series expansion that are of third degree or more, and are usually negligible.

We now go about the task of estimating the mean and variance of the output (the LHS term), using the above equation. In this regard, we make use of the following results, which are based on elementary applications of theorems in the area of Mathematical Statistics (Feller, 1957):

$$\begin{aligned} E\{f(\Phi)\} &= f(\mu_{\phi_i}) \\ E\{\Delta_{\phi_i}\} &= 0 \\ Var\{\mathbf{y}\} &= E\{(\mathbf{y} - \mu_{\mathbf{y}})^2\} \\ Cov\{\Delta_{\phi_i}, \Delta_{\phi_j}\} &= E\{\Delta_{\phi_i} \Delta_{\phi_j}\} - E\{\Delta_{\phi_i}\} E\{\Delta_{\phi_j}\} \end{aligned} \qquad \text{(A.4)}$$

where $E\{\cdot\}$ stands for the expected value, $Var\{\cdot\}$ stands for the variance and $Cov\{\cdot\}$ stands for the covariance. For notational simplicity, we denote the expected value, or mean, by the symbol μ (with the appropriate subscript), and the variance by the symbol σ^2. In addition, we use the covariance coefficient (ρ_{ij}), which is defined as follows:

$$\rho_{ij} \equiv \frac{Cov\{\Delta_{\phi_i}, \Delta_{\phi_j}\}}{\sigma_{\phi_i} \sigma_{\phi_j}} \qquad \text{(A.5)}$$

Note that $-1 \leq \rho_{ij} \leq 1$, and that $\rho_{ij} = 1$ when $i = j$ amd $\rho_{ij} = 0$ for independent or uncorrelated ϕ_i and ϕ_j. From the above equations, it is also apparent that:

$$\begin{aligned} Cov\{\Delta_{\phi_i}, \Delta_{\phi_j}\} &= E\{\Delta_{\phi_i} \Delta_{\phi_j}\}, \quad and \\ E\{\Delta_{\phi_i} \Delta_{\phi_j}\} &= \rho_{ij} \sigma_{\phi_i} \sigma_{\phi_j} \end{aligned} \qquad \text{(A.6)}$$

Returning to the output expansion in Equation A.3, and using the results detailed above, we are able to write the expression for the expected value of the output

function as follows:

$$E\{\mathbf{y}\} \equiv \mu_{\mathbf{y}} \approx f(\mu_{\phi_i}) + 0 + \sum_i \sum_j \frac{\partial^2 f}{\partial \phi_i \partial \phi_j}]_\mu E\{\Delta_{\phi_i}\Delta_{\phi_j}\} \tag{A.7}$$

or, using Equation A.6:

$$E\{\mathbf{y}\} \equiv \mu_{\mathbf{y}} \approx f(\mu_{\phi_i}) + \sum_i \sum_j \frac{\partial^2 f}{\partial \phi_i \partial \phi_j}]_\mu \rho_{ij}\sigma_{\phi_i}\sigma_{\phi_j} \tag{A.8}$$

Equation A.8 is a general expression for the approximation of the mean of a function $f(\cdot)$ of random variables, which are - in general - correlated.

In a manner similar to the earlier analysis, we can use Equation A.3 to write an expression for the output variance as follows:

$$\begin{aligned} Var\{\mathbf{y}\} \equiv \sigma_{\mathbf{y}}^2 &= E\{(\mathbf{y} - \mu_{\mathbf{y}})^2\} \\ &= E\{(\sum_{i=1}^{n} \frac{\partial f}{\partial \phi_i}]_\mu \Delta_{\phi_i} + \sum_i \sum_j \frac{\partial^2 f}{\partial \phi_i \partial \phi_j}]_\mu \Delta_{\phi_i}\Delta_{\phi_j})^2\} \\ &= \sum_i \sum_j \frac{\partial f}{\partial \phi_i}]_\mu \frac{\partial f}{\partial \phi_j}]_\mu E\{\Delta_{\phi_i}\Delta_{\phi_j}\} + \mathcal{O}_3 \end{aligned} \tag{A.9}$$

Combining Equation A.9 with Equation A.6,

$$\sigma_{\mathbf{y}}^2 \approx \sum_{i=1}^{n} (\frac{\partial f}{\partial \phi_i})_\mu^2 \sigma_{\phi_i}^2 + 2\sum_i \sum_j \frac{\partial f}{\partial \phi_i}]_\mu \frac{\partial f}{\partial \phi_j}]_\mu \rho_{ij}\sigma_{\phi_i}\sigma_{\phi_j}, \;\; i \neq j \tag{A.10}$$

Equation A.10 is a general expression for the approximation of the variance of a function of correlated random variables. The first term in the RHS expression is the variance assuming independent and uncorrelated parameters. The second term applies an adjustment to the variance estimate from the first term, accounting for any correlative effects.

Appendix B

Assembly and Non-Assembly Tolerances

In this section, it is shown how *in-situ* processes are able to control gap geometry more accurately than conventional fabrication processes which require assembly of individual components. The processes are illustrated with the example of a simple, isolated hole and shaft pair. An arbitrary axial clearance is assumed and the manufacturing precision required to obtain a given diametrical clearance is derived, with and without the assemblability constraint. We assume that the following two parameters are given, and remain invariant in the two methodologies (assembly and non-assembly):

- The desired bearing clearance (Δ_d): this will depend upon the performance requirements of the joint (i.e. the desired fit-type and task tolerance).
- The best achievable precision on the size of the hole and shaft (ϵ_H^{size} and ϵ_S^{size}). These will depend upon the capability of a given process. Alternately, if the size-precision on both the hole and shaft are assumed to be the same, then we denote the precision as ϵ_C^{size}.

We further assume that the worst-case *form* distortions (roundness, cylindricity etc.) are subsumed within the tolerance zone defined by the size tolerances. This is a valid assumption because size tolerances on hole/shaft features implicitly restrict maximum form tolerances, and similarly, position tolerances restrict size tolerances (Requicha, 1983). Form errors that remain within these bounds are assumed to not

have an effect on joint behavior that is worse than that of the worst-case limiting material condition (LMC or MMC).

B.1 Method 1: Parts Individually Fabricated And Assembled

We use the ANSI Y14.5M (ANSI, 1994) specified tolerancing method to ensure interference-free assembly. The parts that contain the hole and the shaft are assumed to be manufactured separately, using machines with similar capability.

We choose the nominal shaft diameter to be φ_S^{nom}. The nominal hole diameter, subsequently, depends upon the desired clearance:

$$\varphi_H^{nom} = \varphi_S^{nom} - \Delta_d \tag{B.1}$$

The maximum material sizes of the hole and the shaft depend upon the circular size precision of the process:

$$\begin{aligned} \varphi_H^{min} &= \varphi_H^{nom} - \epsilon_H^{size} \\ \varphi_S^{max} &= \varphi_S^{nom} + \epsilon_S^{size} \end{aligned} \tag{B.2}$$

Next, we fabricate the shaft at some nominal location (d_S^{nom}), with location precision ϵ_S^{loc} for the position of the shaft axis with respect to a global datum frame. The worst-case assemblability constraint is expressed in terms of the required location precision on the position of the hole axis at the maximum-material condition (MMC):

$$\epsilon_H^{loc} = \varphi_H^{min} - (\varphi_S^{max} - \epsilon_S^{loc}) \tag{B.3}$$

Substituting from Equation B.1 and Equation B.2, it can be shown that:

$$\epsilon_H^{loc} = \Delta_d - (\epsilon_S^{loc} + \epsilon_S^{size} + \epsilon_H^{size}) \tag{B.4}$$

If we assume that the achievable size precision on the shaft and hole are the same, then Equation B.4:

$$\epsilon_H^{loc} = \Delta_d - (\epsilon_S^{loc} + 2\epsilon_C^{size}) \tag{B.5}$$

We can also write the least material condition (LMC) sizes of the shaft and the hole as follows:

$$\begin{aligned} \varphi_H^{max} &= \varphi_H^{nom} + \epsilon_H^{size} \\ \varphi_S^{min} &= \varphi_S^{nom} + \epsilon_S^{size} \end{aligned} \tag{B.6}$$

Noting that the maximum and minimum clearances occur when the features are at LMC and MMC respectively, we can derive expressions for the extrema of the clearance:

$$\begin{aligned} \Delta_{max} &= \Delta_d + \epsilon_H^{size} + \epsilon_S^{size} \\ \Delta_{min} &= \Delta_d - \epsilon_H^{size} - \epsilon_S^{size} \end{aligned} \tag{B.7}$$

Again, if we assume the same achievable size precision for both the hole and the shaft, we get:

$$\begin{aligned} \Delta_{max} &= \Delta_d + 2\epsilon_C^{size} \\ \Delta_{min} &= \Delta_d - 2\epsilon_C^{size} \end{aligned} \tag{B.8}$$

B.2 Method 2: Building The Parts *In-Situ*

In building a hole-shaft pair using *in-situ* fabrication techniques, it is possible to reference the geometry of the second-built feature (hole or shaft) directly from a best-fit surface on the actual geometry of the first-built feature. Since assemblability is no longer a constraint in the layered paradigm, looser location precision requirements (sufficient only to ensure that there is no material interference) will result. Additionally, if we assume the same process capability (in terms of the best possible hole and shaft size tolerances), better control over the clearance geometry is achieved using this method. These results are demonstrated below.

In a manner similar to the earlier section, we choose the nominal shaft diameter to be φ_S^{nom}. We build the shaft at some nominal location (d_S^{nom}), with a location precision given by ϵ_S^{loc}. Alternately, we could choose to build the hole first, with similar results.

We measure the resulting shaft using a touch probe and fit an appropriate approximating cylinder to it. Either the Least Square or Chebychev fits could be used, depending upon the reliability of our measuring instrument (Feng and Hopp, 1991). The resulting fit cylinder has a known axis location and diameter, given as φ_S^{actual}. Note that the worst case shaft diameters are given by:

$$\begin{aligned} \varphi_S^{max} &= \varphi_S^{nom} + \epsilon_S^{size} \\ \varphi_S^{min} &= \varphi_S^{nom} - \epsilon_S^{size} \end{aligned} \tag{B.9}$$

Next, we choose the nominal diameter of the hole based upon the clearance we need (similar to Method 1):

$$\varphi_H^{nom} = \varphi_S^{actual} + \Delta_d \tag{B.10}$$

Instead of building the hole, we now build the gap out of sacrificial support material. This is done by depositing the sacrificial support in near-net shape around the shaft that has already been built, and machining the excess material. This is equivalent to building another shaft with diameter φ_H^{nom} . Once this step is complete, the "hole" is deposited around the gap, and the sacrificial support is removed. The worst-case outer diameter of the support shaft is assumed equal to the worst-case inner diameter of the final hole and can be estimated as:

$$\begin{aligned} \varphi_H^{max} &= \varphi_H^{nom} + \epsilon_S^{size} \\ \varphi_H^{min} &= \varphi_H^{nom} - \epsilon_S^{size} \end{aligned} \tag{B.11}$$

We now note that the axis location of the sacrificial shaft just built could be off from the location of the original shaft axis by the *amount of the designed clearance* without any occurrence of interference (i.e. without undercutting into the actual shaft). Furthermore, the most conservative estimate of the location precision requirement would be obtained when the sacrificial shaft is in its MMC. i.e.:

$$\epsilon_H^{loc} = \varphi_H^{min} - \varphi_S^{actual} \tag{B.12}$$

Substituting from Equation B.10 and B.11, it can be shown that:

$$\epsilon_H^{loc} = \Delta_d - \epsilon_S^{size} \tag{B.13}$$

An equivalent result would be attained if the hole were built first. If the achievable hole and shaft size precision are assumed to be the same (i.e. ϵ_C^{size}), then Equation B.13 can be re-written as:

$$\epsilon_H^{loc} = \Delta_d - 2\epsilon_C^{size} \tag{B.14}$$

We can derive the expressions for the maximum and minimum clearances achieved using this methodology as follows:

$$\begin{aligned} \Delta_{max} &= \varphi_H^{max} - \varphi_S^{actual} \\ \Delta_{min} &= \varphi_H^{min} - \varphi_S^{actual} \end{aligned} \tag{B.15}$$

Substituting again from Equations B.10 and B.11, and assuming identical hole and shaft size precision:

$$\begin{aligned} \Delta_{max} &= \Delta_d + \epsilon_C^{size} \\ \Delta_{min} &= \Delta_d - \epsilon_C^{size} \end{aligned} \tag{B.16}$$

Figure B.1 graphically illustrates the relationships derived in Equations B.4 and B.14. Comparisons of the two methods can readily be made using Equations B.4, B.8, B.14 and B.16. A smaller value for the location precision implies a tighter constraint (and superior process control), and is therefore undesirable. Note that the required precision for the hole location using the second method is indifferent to the achievable precision on the shaft location.

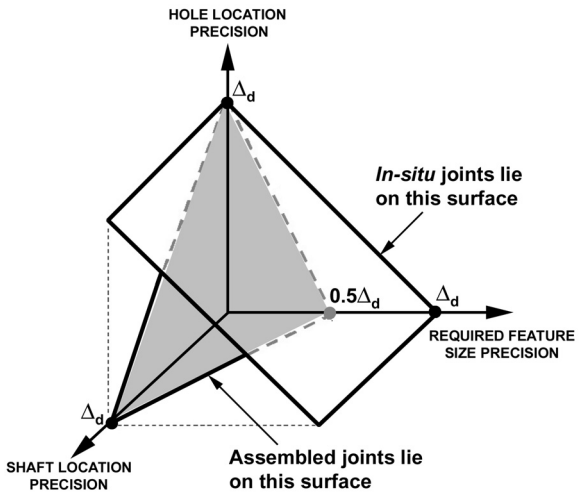

Figure B.1: Comparison of assembly and non-assembly methods: required precision in order to satisfy manufacturing and functional constraints.

Appendix C

Additional Data and Results

C.1 Achievable Manufacturing Tolerances

The accuracy with which a part can be manufactured typically depends upon the size of the part dimension that is being controlled. For example, it may be more difficult to hold a thousandth inch tolerance on a 10 inch dimension, as compared to a 1 inch dimension. This trend is codified in the form of International Tolerance Grades, which is an integral part of many national standards, including those of the United States, Canada and Great Britain (Fortini, 1967).

International Tolerance Grades are designated using the notation IT1, IT2, ..., IT16 - with IT1 being the most stringent, and IT16 the most loose. Figures C.1 and C.2 graphically illustrate how the tolerances specified in these grades vary as a function of part feature size for IT1 and IT16. The international standard also defines the concept of a *fundamental tolerance unit* (or FTU, denoted as i) as follows:

$$i \equiv 0.052D^{\frac{1}{3}} + 0.001D \tag{C.1}$$

where D is the controlled dimension in inches, and i is in thousandth of an inch. Table C.1 shows how the actual achievable tolerance is defined in terms of the FTU.

Grade	IT6	IT8	IT10	IT12	IT14	IT16
t	$10i$	$25i$	$64i$	$160i$	$400i$	$1000i$

Table C.1: Tolerance grades related to the Fundamental Tolerance Unit i (Fortini, 1967).

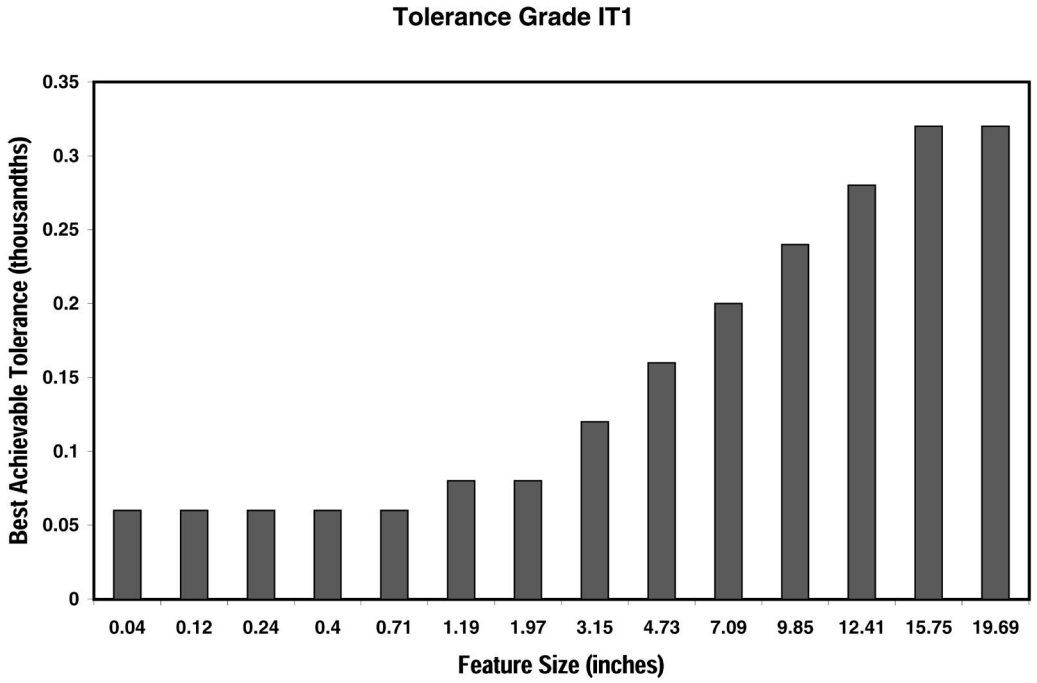

Figure C.1: Empirical estimates for the best achievable manufacturing tolerances versus feature size with conventional machining, International Tolearance Grade IT1 (Fortini, 1967).

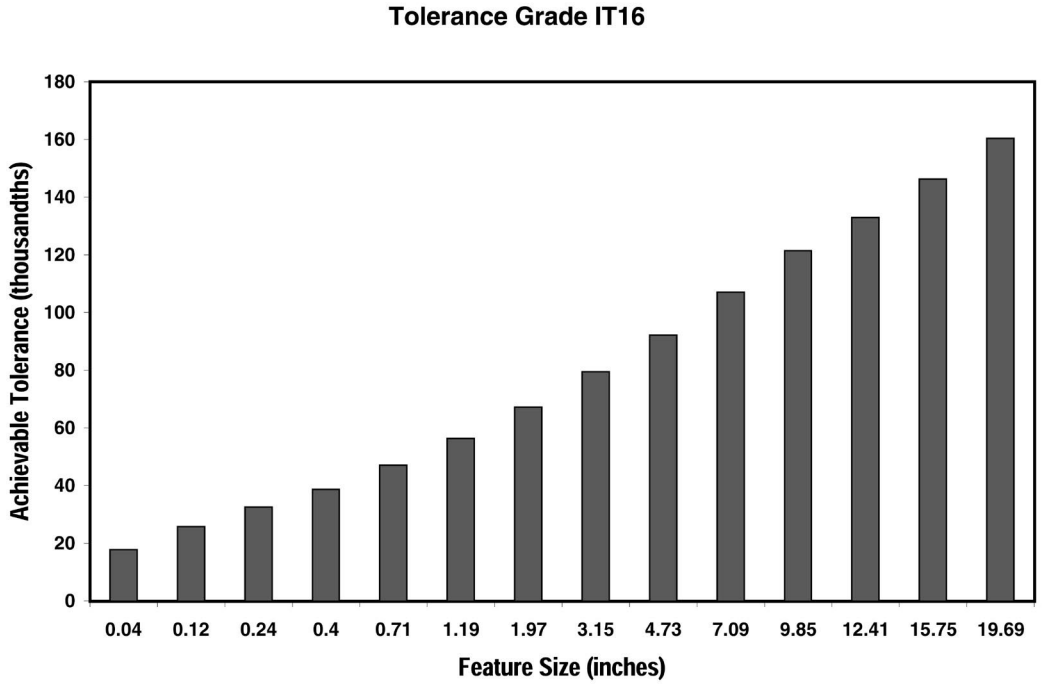

Figure C.2: Manufacturing tolerance versus feature size for the International Tolerance Grade IT16 (Fortini, 1967).

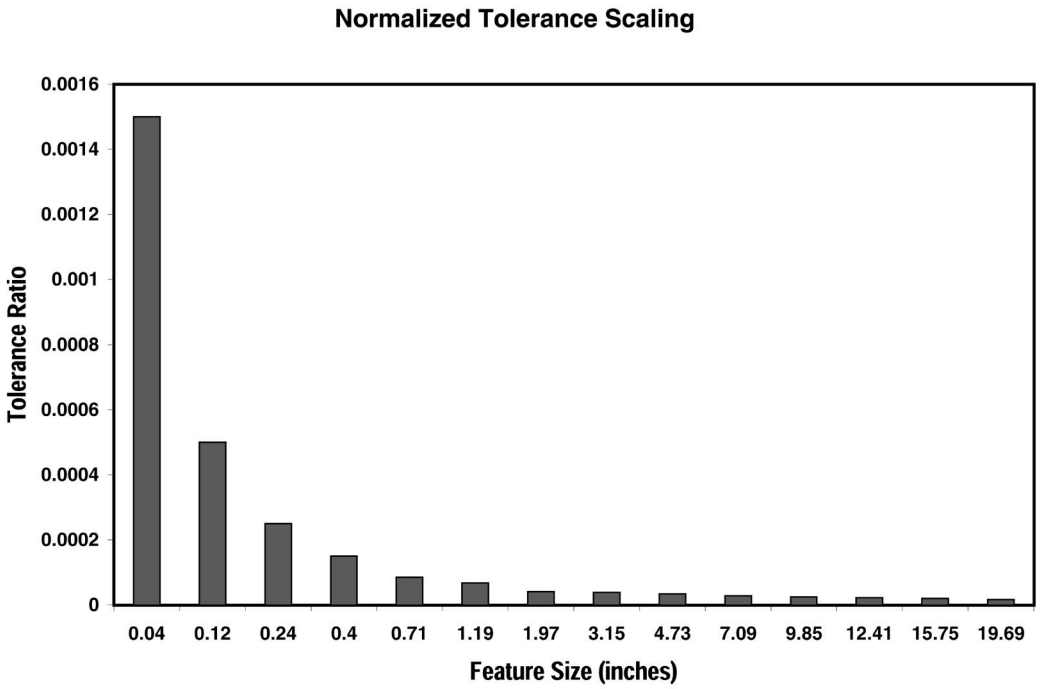

Figure C.3: Best achievable manufacturing tolerance as a ratio of the feature size, plotted against the feature size.

While smaller dimensions can typically be held to tighter tolerances in the absolute sense, in fact, they are looser in a relative sense. As a ratio of the feature dimension, smaller parts are more difficult to manufacture accurately. Figure C.3 plots the ratio of the best achievable dimensional tolerance and the feature dimension versus the feature dimension. Thus, accuracy and tolerance scale unfavorably to meso-scale and micro-scale mechanisms - with the achievable accuracy being roughly equal to the feature size itself at the smallest scales.

Another interesting issue is the comparison of the achievable accuracy of SFF processes with respect to conventional machining processes. A comprehensive experimental determination of this measure is beyond the scope of this thesis, but a preliminary set of measurements were performed on polyurethane test structures fabricated using the Shape Deposition Manufacturing process at Stanford. The result of this test is shown in Figure C.4.

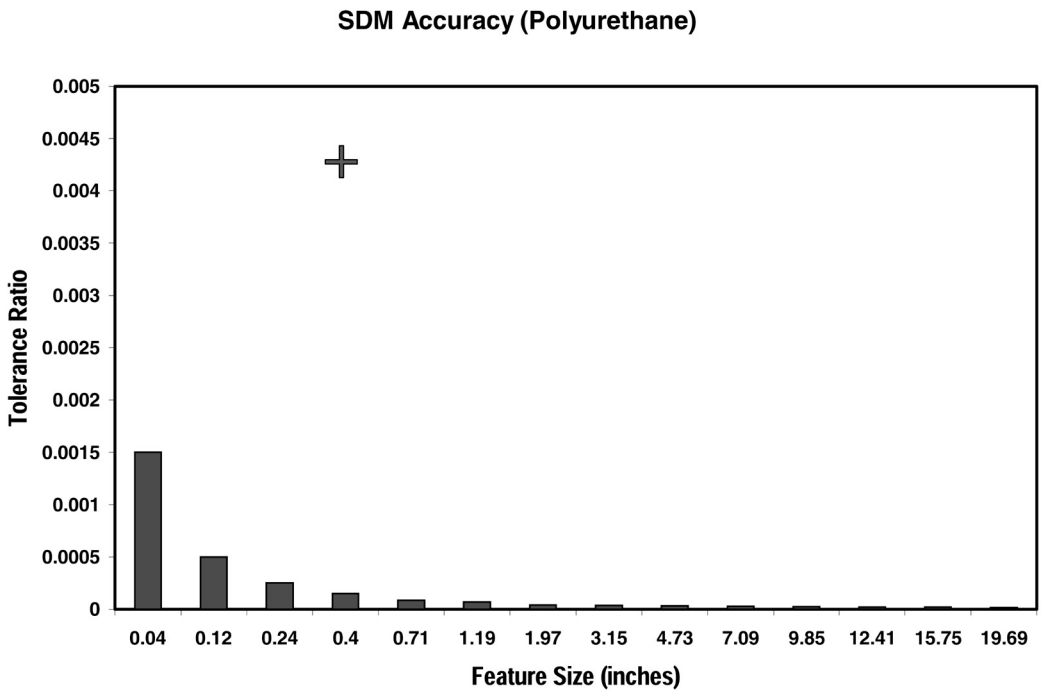

Figure C.4: Achievable positioning accuracy for polyurethane parts using the Stanford Shape Deposition Manufacturing process, compared to the best achievable accuracy via conventional manufacturing.

C.2 Comparison of Conventional and *In-Situ* Performance

In this section, the coupler point positional error of the example 4-bar crank rocker mechanism built *in-situ* is compared to the error in one that is built using conventional techniques. The link-length variance in both cases is identical. However, the output variance is different due to the correlative effects of joint position variability, and that *in-situ* techniques offer the opportunity to optimize the build pose in order to reduce error. Figure C.5 compares the error in the mechanism built using conventional techniques to the best-case and worst-case build poses for *in-situ* fabrication at each operational angle. Figure C.6 graphically illustrates the percentage improvement of the *in-situ* mechanism performance over that of the conventional mechanism. It should be noted that the improvement in performance even for the worst-case build pose is an artifact of the particular example, and it does not hold in general. However, significant improvement in performance clearly results when the best-case build pose is chosen.

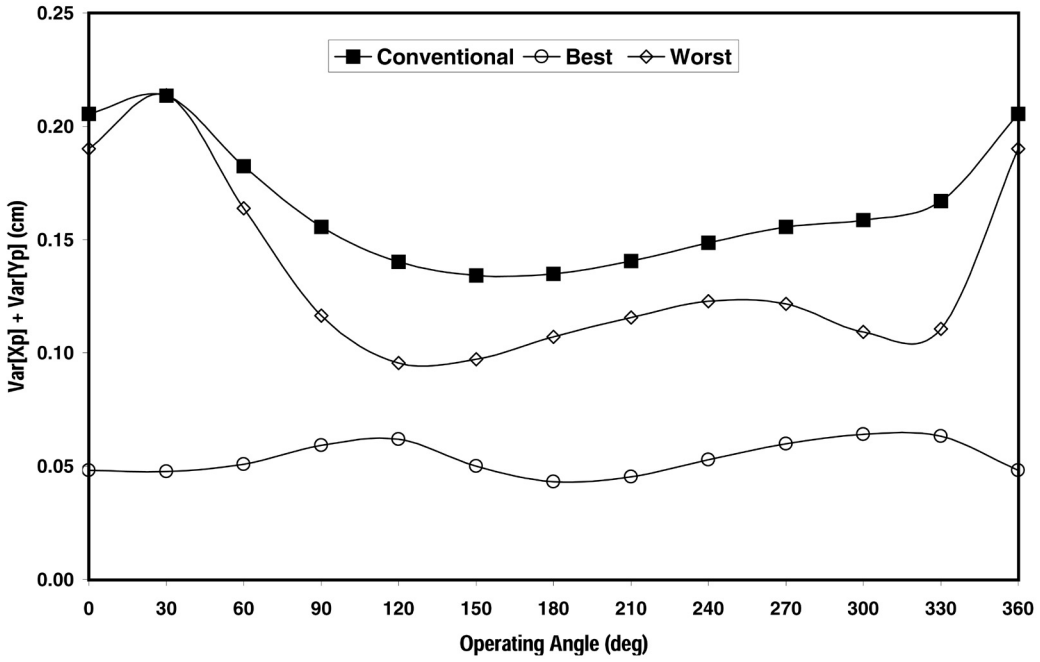

Figure C.5: *In-situ* coupler point error for the example 4-bar crank rocker mechanism compared with a mechanism built using conventional techniques. Both the best-case and worst-case build positions at each operating angle are shown.

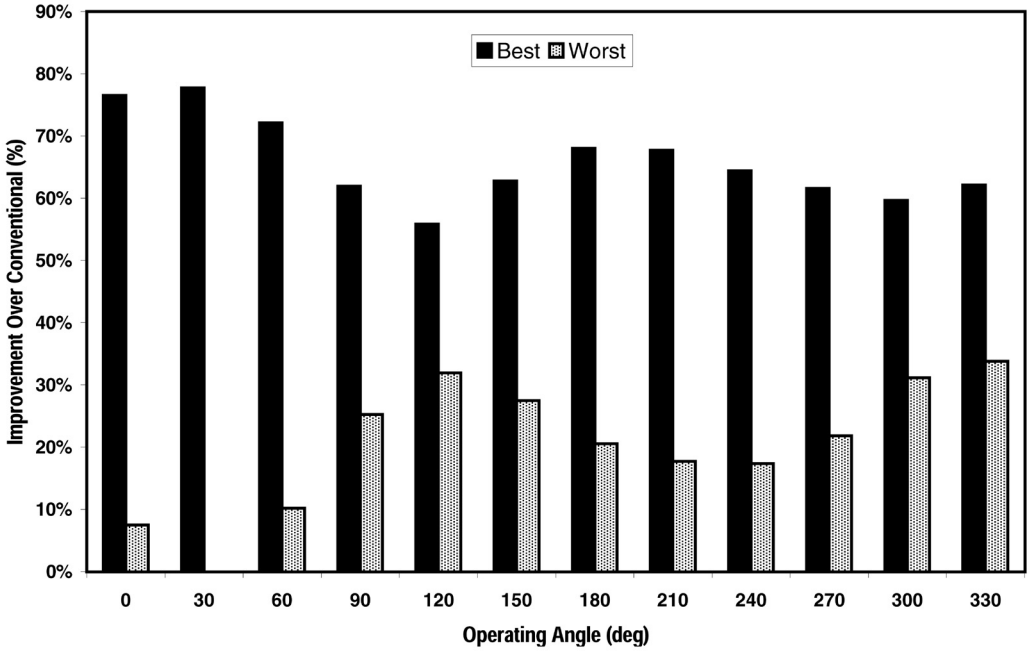

Figure C.6: Best-case and worst-case improvement in coupler point accuracy (over a mechanism built using conventional techniques) for the 4-bar crank rocker mechanism.

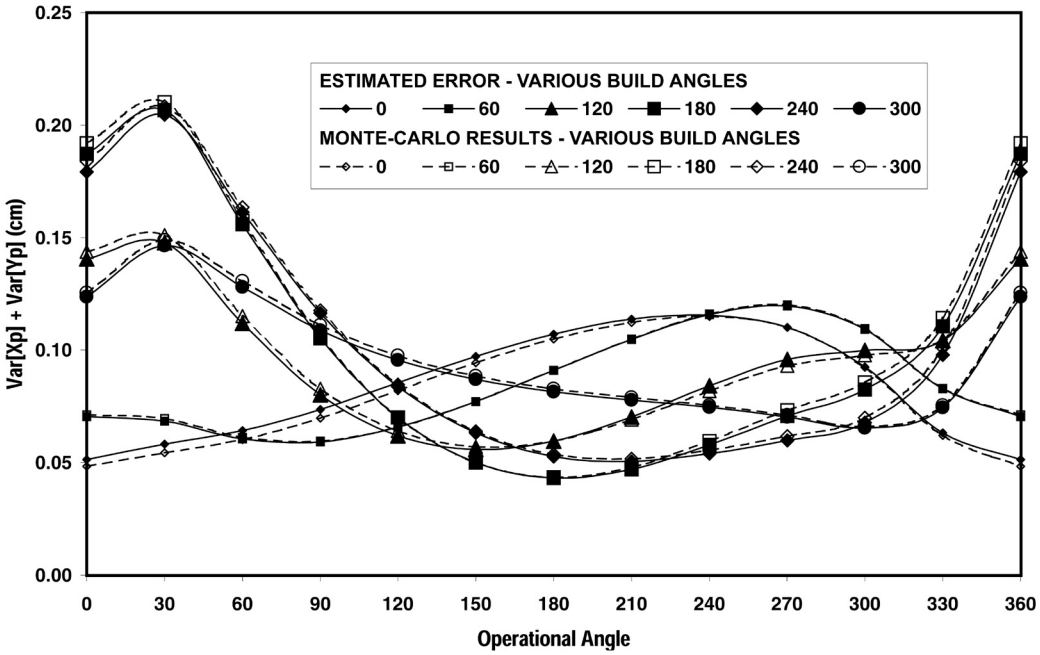

Figure C.7: First-order error estimates compared to the Monte Carlo simulation results for additional build angles.

C.3 Additional Monte-Carlo Simulation results

Figure C.7 compares the first-order estimates of output error (see Equation 3.29) at each operational configuration to the Monte Carlo simulation of the same quantity - for various build positions. These results complement those that were presented in Figure 3.19.

Bibliography

Alam, M., Mavroidis, C., Langrana, N., and Bidaud, P., Mechanism design using rapid prototyping, In *Proceedings of the 10th World Congress on the Theory of Machines and Mechanisms*, Oulu, Finland, 1999.

ANSI Y14.5M, Geometric dimensioning and tolerancing, *American National Standard #Y14.5M*, 1994.

Beaman, J.J., Solid freeform fabrication : a new direction in manufacturing - with research and applications in thermal laser processing, Kluwer Academic Publishers, Boston, 1997.

Bellman, R., Dynamic Programming, Princeton University Press, Princeton, NJ, 1957.

Bhattacharya, B.K. and Toussaint, G.T., Efficient algorithms for computing the maximum distance between two finite planar sets, *Journal Of Algorithms*, 4(2):121-136, 1983.

Binnard, M., Design by composition for rapid prototyping, Ph.D. Thesis, Stanford University, February, 1999.

Blumenthal, L.M., *Theory and Applications of Distance Geometry*, Oxford, Clarendon Press, 1953.

Bottema, O., and Roth, B., Theoretical kinematics, Dover Publications, New York, NY, 1979.

Breyfogle, F.W., *Implementing six sigma*, John Wiley & Sons, New York, NY, 1999.

Burgett, S.R., Pister, K.S.J., and Fearing, R.S., Three dimensional structures

made with microfabricated hinges, In *Proceedings of the Symposium on Micromechanical Systems*, DSC-Vol 40, ASME Winter Annual Meeting, Annaheim, CA, pp. 1-11, Nov. 1992.

Chakraborty, J., Synthesis of mechanical error in linkages, *Mechanism and Machine Theory*, v. 10, 155-165, 1975.

Cham, J., Pruitt, B.L., Cutkosky, M.R., Binnard, M., Weiss, L., and Neplotnik, G., Layered manufacturing of embedded components: process planning considerations. In *Proceedings of the 1999 ASME DETC/DFM Conference*, Las Vegas, NV, September 12-15, 1999.

Choi, J.-H., Lee, S.J., and Choi, D., -H., Stochastic linkage modeling for mechanical error analysis of planar mechanisms, *Mechanics of Structures and Machines*, 26(3), 257-276, 1998.

Chua, C.K. and Fai, L.K., Rapid prototyping : principles and applictions in manufacturing, Wiley, New York, NY, 1997.

Denavit, J., and Hartenberg, R.S., A kinematic notation for lower-pair mechanisms based on matrices, *Journal of Applied Mechanics*, 215-221, June, 1955.

Dhande, S., and Chakraborty, J., Analysis and synthesis of mechanical error in linkages - A stochastic approach, *ASME Journal of Engineering for Industry*, Series B, 95, 677-680, 1973.

Evans, D.H., Statistical tolerances: the state of the art, Part I and II, *Journal of Quality Technology*, Vol. 6-7, 1975.

Feller, W., An introduction to probability theory and its applications, Vol. 2, Wiley & Sons, New York, NY, 1957.

Feng, C.F., and Hopp, T.H., A Review of Current Geometric Tolerancing Theories and Inspection Data Analysis Algorithms, *NIST Internal Report*, NISTIR 4509, 1991.

Fenton, R.G., Cleghorn, W.L., and Fu, J., Allocation of dimensional tolerances for multiple loop planar mechanisms, *Journal of Mechanisms, Transmissions and Automation in Design*, v. 111, 465-470, December 1989.

Fortini, E.T., Dimensioning for interchageable manufacture, Industrial Press, Inc., New York, NY, 1967.

Fox, R.L., Optimization methods for engineering design, *Addison-Wesley*, Mass., 1971.

Freudenstein, F., Structural error analysis in plane kinematic synthesis, *ASME Journal of Engineering for Industry*, Serial E, vol. 81, n 1, pp. 15-22, 1959.

Furuhashi, T., Morita, N., and Matsuura, M., Research on dynamics of four-bar linkage with clearances at turning pairs (1st report), *Bulletin of JSME*, v. 21, n. 153, pp. 518-523, March 1978.

Gadh, R., and Prinz, F.B., Automatic determination of feature interactions in design-for-manufacturing analysis, *Journal of Mechanical Design*, Transactions of the ASME, Vol. 117, No. 1, pp. 2-9, March 1995.

Garrett, R.E., and Hall, A.S., Effects of tolerance and clearance in linkage design, *ASME Journal of Engineering for Industry*, Series B, 91, 198-202, 1969.

Hammersley, J.M., and Handscomb, D.C., Monte Carlo methods, Chapman & Hall, London, U.K., 1964.

Hartenberg, R.S., and Denavit, J., *Kinematic synthesis of linkages*, McGraw Hill, New York, 1964.

Hayati, S., and Mirmirani, M., Improving the absolute positioning accuracy of robot manipulators, *Journal of Robotic Systems*, **2**(4), 397-413, 1985.

Hounshell, D. A., From the American system to mass production, 1800-1932 : the development of manufacturing technology in the United States, Johns Hopkins University Press, Baltimore, MD, 1984.

Huttenlocher, D.P., Kedem, K., and Kleinberg, J.M., On dynamic voronoi diagrams and the minimum Hausdorff distance for point-sets under Euclidean motion in the plane, In *Eighth Annual Symposium On Computational Geometry*, pages 110-119, ACM, New York, N.Y., 1994.

ISO 10303-1, Industrial automation systems and integration - Product data representation and exchange - Part 1: Overview and fundamental principles, *US Product Data Association*, ANS US PRO/IPO-200-001-1994, 1994.

Jayaraman, R. and Srinivasan, V., Geometric tolerancing: Parts 1 and 2, *IBM Journal of Research and Development*, 33(2):90-124, 1989.

Joskowicz, L. and Neville, D., Representation language for mechanical behavior, *Artificial Intelligence in Engineering*, 10(2):109-116, 1996.

Joscowicz, L., Sacks, E. and Srinivasan, V., Kinematic tolerance analysis, *Computer-Aided Design*, 29(2), 1997.

Kazmer, D.O., Dynamic feed control: A new method for injection molding of high quality plastic parts, Ph.D. Thesis, Stanford University, 1995.

Knappe, L.F., Technique for analysing mechanism tolerances, *Machine Design*, 155-157, April 25, 1963.

Kothalkar, S.A. and Yajnik, K.S., The effect of play in the joints of a function-generating mechanism, *Journal of Mechanisms*, v. 5, 521-532, 1970.

Kovacs, G., Micromachined transducers sourcebook, WCB/McGraw Hill, New York, NY, 1998.

Lakshminarayana, K., and Ramaiyan, G., Analysis of the effects of errors and clearances in mechanisms as a problem in statics, ASME publication 76-DET-67, In *Proceedings of the ASME DETC*, Montreal, Quebec, Canada, September 1976.

Laliberte, T., Gosselin, C., and Cote, G., Rapid prototyping of mechanisms, In *Proceedings of the 10th World Congress on the Theory of Machines and Mechanisms*, Oulu, Finland, 1999.

Latombe, J-C., *Robot Motion Planning*, Boston: Kluwer Academic Publishers, 1991.

Lee, S.J., and Gilmore, B.J., The determination of the probabilistic properties of velocites and accelerations in kinematic chains with uncertainty, *ASME Journal of Mechanical Design*, v. 113, 84-90, 1991.

Liang, X. W-., and Xian, Z., Q-., Probabilistic analysis and monte carlo simulation of the kinematic error in a spatial linkage, *Mechanisms and Machine Theory*, vol. 24, no. 1, pp. 19-27, 1989.

Lin, P.D., and Chen, J.F., Analysis of errors in precision for closed loop mechanisms, *Journal of Mechanical Design*, v. 116, 197-203, March, 1994.

Mallik, A.K., and Dhande, S.G., Analysis and synthesis of mechanical error in path generating linkages using a stochastic approach, *Mechanism and Machine Theory*, v. 22, no. 2, 115-123, 1987.

Maluf, N., An introduction to microelectromechanical systems engineering, Artech House, Boston, 2000.

Merz, R., Prinz, F.B., Ramaswami, K., Terk, M. and Weiss, L., Shape Deposition Manufacturing, In *Proceedings of the Solid Freeform Fabrication Symposium*, pages 1-8, The University of Texas at Austin, August 8-10, 1994.

Morrison, P., and Morrison, E., Charles Babbage and his calculating engines, Dover Publications, Inc., New York, NY, 1961.

Mukherjee, A., and Hilibrand, J., Group 1 report: workshop on new paradigms in manufacturing, In *National Science Foundation Report NSF 94-123*, Mukherjee, A. and Hilibrand, J. eds., pp. 9-16, Arlington, VA, 1994.

Nahvi, A., Hollerbach, J.M. and Hayward, V., Calibration of a parallel robot using multiple kinematic closed loops, In *Proceedings of the 1994 IEEE International Conference on Robotics and Automation*, San Diego, CA, USA, 1994.

Park, S.H., *Robust design and analysis for quality engineering*, Chapman & Hall, London, UK, 1996.

Preparata, F.P., *Computational Geometry: an Introduction*, Springer-Verlag, New York, N.Y., 1985.

Rajagopalan, S. and Cutkosky, M.R., Tolerance representation for mechanism assemblies in layered manufacturing, In *Proceedings of the 1998 ASME DETC/DFM Conference*, Atlanta, GA, September 13-16, 1998.

Rajagopalan, S., Pinilla, J.M., Losleben, P., Tian, Q., and Gupta, S.K., Integrated design and rapid manufacturing over the Internet, In *Proceedings of the 1998 ASME DETC/CIE Conference*, Atlanta, GA, September 13-16, 1998.

Rajagopalan, S., Goldman, R., Shin, K.H., Kumar, V., Cutkosky, M., and Dutta, D., Representation of heterogeneous objects during design, processing and freeform fabrication, accepted for publication, *Materials and Design*, 2000.

Requicha, A.A., Towards a theory of geometric tolerancing, *The International Journal of Robotics Research*, 2(4):45-60, 1983.

Requicha, A.A., Representation of tolerances in solid modeling: issues and alternative approaches, General Motors Solid Modeling Symposium, 1984.

Requicha, A.A., and Chan, S.C., Representation of geometric features, tolerances, and attributes in solid modelers, based on constructive geometry, *IEEE Journal of Robotics and Automation*, RA2(3), pp. 156-165, 1986.

Requicha, A.A., Mathematical definition of tolerance specifications, *ASME Manufacturing Review*, 6(4):269-274, 1993.

Roy, U. and Liu, C.R., Feature based representational scheme of a solid modeler for providing dimensioning and tolerancing information, *Journal of Robotics and Computer Integrated Manufacturing*, v. 4, no. 3, pp. 335-345, 1988.

Sachs, E., Three dimensional printing - rapid tooling and prototypes directly from CAD model, *Journal of Engineering for Industry*, Transactions of the ASME, 114(4):481-488, 1992.

Sequin, C., Position paper: Can the VLSI CAD revolution be repeated in Mechanical Engineering?, Workshop on new paradigms in manufacturing, In *National Science Foundation Report NSF 94-123*, pp. 41-42, Mukherjee, A. and Hilibrand, J. eds., 1994.

Shigley, J.E., Kinematic analysis of mechanisms, McGraw Hill, New York, NY, 1959.

Shigley, J.E., and Uicker, J.J., Theory of machines and mechanisms, McGraw Hill, New York, NY, 1995.

Sommerville, D.M.Y, Analytical geometry of three dimensions, Cambridge University Press, London, 1959.

Srinivasan, R.S. and Wood, K.L., Geometric tolerancing in mechanical design using fractal-based parameters, *ASME Journal of Mechanical Design*, 117(1):203-205, 1995.

Stampfl, J., Leitgeb, R., Cheng, Y. -L., Prinz, F.B., Electro-discharge machining of mesoscopic parts with electroplated copper and hot-pressed silver tungsten electrodes, accepted for publication, *Journal of Micromechanics and Microengineering*, 1999.

Stolfi, J., Oriented projective geometry: a framework for geometric computations, Academic Press, Boston, MA, 1991.

Suh C.H., and Radcliffe C.W., Kinematics and mechanism design, *Wiley and Co.*, New York, 1978.

Taguchi, G., *Introduction to quality engineering*, Tokyo, Asian Productivity Organization, 1986.

Taguchi, G., *Taguchi on robust technology development: bringing quality engineering upstream*, ASME Press, New York, NY, 1993.

Tischler C.R., and Samuel, A.E., Prediction of slop in general spatial linkages, *The International Journal of Robotics Research*, v. 18, no. 8, 845-858, August 1999.

Toussaint, G.T., Optimal algorithm for computing the minimum vertex distance between two crossing convex polygons, In *Proceedings - Seventh International Conference on Pattern Recognition*, pages 465-467, Montreal, Quebec, Canada, 1984.

Tsai, J.C. and Cutkosky, M.R., Representation and reasoning of geometric tolerances in design, Chapter In *Artificial Intelligence for Engineering Design, Analysis and Manufacturing II*, pages 325-341, 1997.

Turner, J.U., Tolerances in computer-aided geometric design, *Ph.D. Dissertation*, Rensselaer Polytechnic Institute, 1987.

Tuttle, S.B., Error analysis, *Machine Design*, v.32, no. 12, 1960.

Voelker, H.B., A current perspective on tolerancing and metrology, In *Proceedings of the 1993 International Forum on Dimensional Tolerancing and Metrology*, Dearborn, MI. Vijay Srinivasan and Herbert B. Voelker, eds., pp 49-60, 1993.

Waldron, K.J., and Kumar, A., Development of a theory of errors in manipulators, In *Proceedings of the 5th World Congress on Theory of Machines and Mechanisms*, New York, pp. 821-826, 1979.

Walker, R.K., and Srinivasan, V., Creating a standard: Y14.5.1, *Quality*, Vol. 32, pp. 24-28, 1993.

Wang, H.H.S., and Roth, B., Position errors due to clearances in journal bearings, *Journal of Mechanisms, Transmissions and Automation in Design*, vol. 111, n 3, pp. 315-320, 1989.

Weiss, L.E., Prinz, F.B., Neplotnik, G., Padmanabhan, P., Schultz, L., and Mertz, R., Shape Deposition Manufacturing of wearable computers. In *Proceedings of the Solid Freeform Fabrication Symposium*. University of Texas at Austin, August 10-12, 1996.

Whitney, D.E., and Gilbert, O.L., Representation of geometric variations using matrix transforms for statistical tolerance analysis in assemblies, In *Proceedings*

of the IEEE International Conference on Robotics and Automation, v. 2, pp. 314-321, 1993.

Wohlers, T., Rapid prototyping and tooling: state of the industry, *1999 Progress Report*, Wohlers Associates, Inc., Fort Collins, Colorado, USA, 1999.

Wright, P.K. and Dornfeld, D.A., CyberCut: A Networked Manufacturing Service, In *transactions of NAMRC/SME*, Vol. XXVI, 1998.